

Total Retinal Blood Flow and Retinal Oxygen Saturation
in the Major Retinal Vessels of Healthy Participants

by

Afua Oteng-Amoako

A thesis
presented to the University of Waterloo
in fulfillment of the
thesis requirement for the degree of
Master of Science
in
Vision Science

Waterloo, Ontario, Canada, 2013

© Afua Oteng-Amoako 2013

I hereby declare that I am the sole author of this thesis. This is a true copy of the thesis, including any required final revisions, as accepted by my examiners.

I understand that my thesis may be made electronically available to the public.

ABSTRACT

Introduction: Oxygen delivery, or utilization, is a function of retinal blood flow and blood oxygen saturation. The retinal pigment epithelium (RPE), in particular, has been shown to have the highest levels of metabolic activity within the human body. Oxygen delivery is therefore of extreme importance to the maintenance of the health and integrity of the retina.

Animal models presuppose that the oxygen tension in the retina is highest in the innermost layers at the level of the choriocapillaris, less in the photoreceptors and further decreases throughout the outer retinal structures. The choroid provides by far the largest component of the oxygen for consumption by the photoreceptors. A lack of oxygen stores in the inner retina therefore makes a constant supply crucial for its normal functioning. Blood flow dysfunction and subsequent hypoxia are both a feature in the pathogenesis of several major ocular diseases such as retinopathy of prematurity (ROP), age-related macular degeneration (ARMD), diabetic retinopathy (DR) and glaucoma. The development of methods to measure retinal blood flow and blood oxygen saturation is crucial to improve understanding of the pathophysiology of major ocular diseases.

Purpose: The aims of this work were, firstly, to determine the least variable (range \pm standard deviation) wavelength combination (610/548, 600/569 and 605/586) and subsequent ODR with the prototype HRC device. Secondly, using the ODR with the lowest measurement variability, we sought to quantify retinal blood SO_2 in arterioles and venules and investigate the relationship between retinal blood SO_2 and total retinal blood flow (TRBF) in response to stepwise changes in $P_{ET}O_2$ in healthy participants. Retinal blood SO_2 and TRBF were assessed using the IRIS HRC (Photon etc. Inc. Montreal, Canada) and the RTvue Doppler Fourier Domain OCT (Optovue Inc, Fremont, CA) instruments, respectively.

Methods: Ten healthy participants between the ages of 23 and 37, with an average age of 28.3 years were evaluated in two descriptive cross-sectional studies. Two gas provocation protocols; hyperoxia (end-tidal oxygen; $P_{ET}O_2$ of 100, 200, 300, 400mmHg) and hypoxia ($P_{ET}O_2$ of 100, 80, 60, 50mmHg) were

administered in a fixed sequential order. In each phase of gas provocation (via modulation of $P_{ET}O_2$), retinal blood SO_2 and TRBF measurements were acquired with the HRC and Doppler FD-OCT. The precise and repeated control of the partial end tidal pressures of oxygen ($P_{ET}O_2$) and carbon dioxide ($P_{ET}CO_2$) over the pre-determined phase duration, irrespective of the individuals' respiratory rate, was made possible with the RespirAct (Thornhill Research Inc., Toronto, Canada); a sequential re-breathing gas delivery

Results: In arterioles, the group range (\pm SD) of ODR values for baseline measurements ($P_{ET}O_2$ of 100mmHg) was 0.169 ± 0.061 for the 605/586 wavelength combination, 0.371 ± 0.099 for the 600/569 wavelength combination and 0.340 ± 0.104 for the 610/548 wavelength combination. In venules, the group range (\pm SD) of ODR values was 0.600 ± 0.198 for the 605/586 wavelength combination, 0.569 ± 0.169 for the 600/569 wavelength combination and 0.819 ± 0.274 for the 610/548 wavelength combination. With the 605/586 combination at baseline 1 and 2 in arterioles, the group range (\pm SD) of ODR values was 0.607 ± 0.224 and 0.619 ± 0.158 , respectively ($p = 0.370$), while in venules the group range (\pm SD) of ODR at baseline 1 and 2 was 0.289 ± 0.750 and 0.284 ± 0.729 , respectively ($p = 0.714$). For the 600/569 combination at baseline 1 and 2 in arterioles, the group range (\pm SD) of ODR values was 0.747 ± 0.350 and 0.761 ± 0.391 , respectively ($p = 0.424$) while in venules the group range (\pm SD) of ODR at baseline 1 and 2 was 0.329 ± 0.675 and 0.366 ± 0.659 , respectively ($p = 0.372$). For the 610/548 combination at baseline 1 and 2 in arterioles, the group range (\pm SD) of ODR values was 0.604 ± 0.263 and 0.685 ± 0.450 , respectively ($p = 0.056$) while in venules, the group range (\pm SD) of ODR at baseline 1 and 2 was 0.292 ± 0.746 and 0.285 ± 1.009 , respectively ($p = 0.131$). There was no statistical difference found between baseline ODR values (baseline 1 and 2) across all three wavelength combinations in both arterioles and venules.

The mean retinal blood SO_2 value at baseline in arterioles for 4 participants was $95.19\% \pm 31.04\%$ and venules was $53.89\% \pm 17.24\%$ ($p = 0.115$). There was a negative linear relationship between group retinal blood SO_2 and TRBF values in the 10 participants studied, although the results of any of the 10

individuals did not show evidence of such a relationship using the described methodology. The Pearson's correlation coefficient (r) between TRBF and SaO₂ was $r = -0.354$ and $p = 0.001$ and between TRBF and SvO₂ was $r = -0.295$, $p = 0.008$

Conclusion: Of the three wavelength combinations investigated (605/586, 600/569 and 610/548), the 605/586 combination was shown to have the overall least variability. It would be unwise at this stage to adopt this wavelength combination for clinical usage, however, since it is presupposed that the 605/586 combination is also the most reliable combination to detect change in retinal blood SO₂ i.e. lower variability of the 605/586 combination may be irrelevant if this combination proves to be insensitive to change in retinal blood SO₂. The absolute mean \pm SD retinal blood SO₂ in the arterioles (SaO₂) was $95.19\% \pm 31.04\%$ and in the venules (SvO₂) was $53.89\% \pm 17.24\%$. These values fell within the range expected and described in the literature. The magnitude of the difference between the SaO₂ and SvO₂ was also consistent with the literature. These findings were all appropriate for a low flow, high oxygen exchange vascular network typical of the inner retinal vascular system. Using group rather than individual data, TRBF was found in this study to relate inversely with SaO₂ ($r = -0.354$ and $p = 0.001$) and SvO₂ ($r = -0.295$ and $p = 0.008$), respectively. This relationship between TRBF and SaO₂ and SvO₂, was as expected based upon data derived primarily from animal models. This study is ground-breaking and unique, in that, it is the first study to concomitantly measure both retinal blood SO₂ and TRBF in human participants. Individual data showed extensive variability and noise, thus limiting the strength of the association between TRBF and SaO₂ and SvO₂.

ACKNOWLEDGEMENTS

My thanks go first and foremost to the Creator of this Universe - Almighty God from whom I draw my strength from day to day and without whom none of this would have ever been possible.

I would like to sincerely thank my supervisors Dr. John Flanagan and Dr. Christopher Hudson for their guidance, support and encouragement throughout my program.

I would also like to express my gratitude to my committee members, Dr. Natalie Hutchings and Dr. Trefford Simpson for their guidance, support and valuable suggestions.

Additional thanks also goes to Ms. Krista Parsons (Graduate Coordinator, Fac. of Science) and especially Dr. Vivian Cho (Graduate officer) whose presence, support and advice kept me going in the dying days leading up to the defense.

I would also like to thank dear friends, fellow graduate students and members of the Hudson lab at the School of Optometry and Vision Science at the University of Waterloo and Department of Ophthalmology, University of Toronto; most especially, Dr. Sunni Patel (Toronto), Michal Vymyslicky, Firdaus Yusof, Kalpana Rose, Faryan Tayyari, Dr. Susith Kulasekara (Toronto), Richard Cheng (Toronto), Dr. Emmanuel Alabi and Bolarinwa Amoye for their support and help in various ways with the collection of data, and writing of the thesis.

Sincere thanks also go to the Ontario Research Fund for the financial support.

Finally, my sincere gratitude goes to my dear parents; Mrs Cecilia Agyei-Amoako and Dr. Andrew Oteng-Amoako for their immeasurable support, suggestions and to whom I owe most of my success and achievements to this day.

DEDICATION

This thesis is dedicated to my loving father, Dr. Andrew Oteng-Amoako whose love, dedication, sacrifice and support have made me what I am today. I am blessed to have such a wonderful father like you.

“Dada, Meda Wo Ase! (*Dad, Thank you*)”

Table of Contents

List of Figures.....	xi
List of Tables.....	xiii
List of Abbreviations.....	xiv
1 Introduction.....	1
1.1 The Vascular Systems of the Human Retina	2
1.1.1 Anatomy of Retinal Vessels.....	2
1.1.2 The Retinal Vascular System.....	3
1.1.3 The Choroidal/Uveal Vascular System.....	4
1.1.4 Differences in the Choroidal & Retinal Vascular Systems.....	4
1.1.5 Venular Drainage.....	5
1.2 Regulation of Ocular Blood Flow in the Human Retina	5
1.2.1 The Rate of Blood Flow	5
1.2.2 Ocular Perfusion Pressure (OPP).....	6
1.2.3 Vascular Resistance (R)	7
1.2.4 Autoregulation.....	8
1.2.5 Blood Gases	9
1.2.6 Endothelial Derived Factors.....	10
1.2.7 Other Influences on Retinal Blood Flow	12
1.3 Optical Coherence Tomography.....	14
1.3.1 Overview of OCT.....	14
1.3.2 Types of OCT.....	15
1.4 Quantification of Retinal Hemodynamics	17
1.4.1 Retinal vessel analyzer (RVA).....	18
1.4.2 Fluorescein Angiography.....	18
1.4.3 Blue Field Entoptic Technique	19
1.4.4 Laser Speckle Technique	20
1.4.5 Laser Doppler Velocimetry.....	20
1.4.6 Color Doppler Imaging (CDI).....	23
1.4.7 Doppler Fourier Domain Optical Coherence Tomography (FD-OCT)	24

1.4.8	Laser Doppler Flowmeter (LDF)	25
1.5	Partial Pressures of Oxygen, Nitrogen and Carbon Dioxide (PO ₂ , PN ₂ and PCO ₂)	26
1.5.1	Diffusion of Gases Between the Gas and the Dissolved Phase.....	27
1.6	Oxygen Loading & Transport	27
1.6.1	Oxygen-Hemoglobin Dissociation Curve (OHDC).....	28
1.6.2	Arteriovenous Oxygen Difference	28
1.7	Retinal Oximetry	29
1.7.1	Principle of Retinal Oximetry & The Beer-Lambert Law.....	30
1.8	Historical Approaches of Measuring Retinal Oxygen Saturation	31
1.8.1	Digital Multispectral and Hyperspectral Imaging of the Retina.....	31
1.8.2	Fundus Reflectance Oximetry.....	33
1.8.3	Hickam Photographic Two Wavelength Technique	33
1.8.4	Photoelectric Oximeter with Three Wavelengths.....	33
1.8.5	Image Replicating Imaging Spectrometer (IRIS) Hyperspectral Retinal Camera (Photon etc. Inc. Montreal).....	34
1.9	Summary.....	35
2	Rationale, Hypotheses and Aims	37
2.1	Hypotheses.....	39
2.2	Aims	40
3	Optical Density Ratio (ODR) Variability with a Novel Hyperspectral Retinal Camera (Photon etc. Inc. Montreal).....	41
3.1	Introduction.....	41
3.2	Materials and Methods	47
3.2.1	Sample.....	47
3.2.2	Study Visits.....	48
3.2.3	Study Procedure.....	50
3.2.4	Statistical Analysis	50
3.3	Results.....	53
3.3.1	ODR Variation in Arterioles for All Participants Comparing All Three Wavelength Combinations.....	53
3.3.2	ODR Variation in Venules for All Participants Comparing All Three Wavelength Combinations.....	55

3.3.3	Comparison of Variation Between Baseline Measurements for All Participants and Wavelength Combinations.....	58
3.4	Discussion and Conclusion	69
3.4.1	Summary	71
4	The Effect of Change in Oxygen Tension on Total Retinal Blood Flow and Retinal Oxygen Saturation in Healthy Participants.....	72
4.1	Introduction.....	72
4.2	Materials and Methods	75
4.2.1	Sample.....	75
4.2.2	Study Visits.....	76
4.2.3	Novel Hyperspectral Retinal Camera.....	76
4.2.4	Gas Delivery System (RespirAct™, Thornhill Research Inc., Toronto, Canada).....	76
4.2.5	RTVue Doppler FD-OCT.....	78
4.2.3	Study Procedure.....	78
4.2.4	Statistical Analysis	79
4.3	Results	82
4.3.1	HRC Systemic SO ₂ Data for n=9.....	82
4.3.1	RtVue Systemic SO ₂ Data for n=9.....	83
4.3.2	Quantification of Retinal Blood SO ₂ at baseline with 605/586 Wavelength Combination .	84
4.3.2	Relationship between Retinal Blood SO ₂ and Retinal Blood Flow.....	85
4.4.0	Discussion and Conclusion	89
4.4.1	Quantification of retinal blood SO ₂ at baseline	89
4.4.2	Relationship between Retinal SO ₂ and Retinal Blood Flow	90
4.3.3	Summary	91
5	Conclusion.....	93
	Letters of Copyright Permission.....	96
	Nature	96
	References.....	101
	Appendix A: Optical Density Ratio (ODR) Variability with the Image Replicating Imaging Spectrometer (IRIS) Hyperspectral Retinal Camera (Photon etc. Inc. Montreal). Flow Chart of Procedures	125
	Appendix B: Total Retinal Blood Flow and ODR with Gas Provocation Challenge in Healthy Participants. Flow Chart of Procedures.....	126
	Appendix C: Hyperoxia and Hypoxia Protocols.....	128

List of Figures

Figure 1.1 Basic OCT system, based on Michelson interferometer 15

Figure 1.2 Schematics of time-domain OCT. The reference mirror (upper right) is moveable over a distance that corresponds to the axial (depth) range of interest in the sample. Reproduced with Permission. 16

Figure 1.3 Schematic diagram of a spectrometer-based Fourier-domain OCT system. It contains a stationary reference mirror and a spectral interferogram (spectrum of the combined reference and sample reflections). Spectral modulations of difference periodicities are formed from reflections from different depths of the sample. A Fourier Transform converts spectral modulations into an A-scan. Reproduced with Permission. 17

Figure 1.4.0 Diagrammatic representation of the Doppler shift effect. The frequency, f_i of an incident wave of light changes by Δf_m when reflected from a moving RBC. 21

Figure 1.5 Doppler method of measuring blood flow (f =non shifted light ray, f_i =shifted ray)..... 22

Figure 1.6 En face view of 3D OCT image showing DCSP with two concentric rings of radii 3.75 and 3.40mm. The retinal vessels are labelled from 1 to 15. The red and blue colour represents software identified vessel type as blood flowing away from the ON..... 25

Figure 1.7 Oxygen-Hemoglobin Dissociation Curve. 28

Figure 1.8 Graph displaying the absorption spectra of Hb and HbO₂..... 29

Figure 3.1 The intensity of light reflected from the vessel is compared to that of the adjacent retina for both arterioles and venules 51

Figure 3.2 Baseline ODR in arterioles for all three wavelength combinations (605/586, 600/569, 610/548) for n=10..... 55

Figure 3.3 Baseline ODR in arterioles for all three wavelength combinations (605/586, 600/569, 610/548) for n=10..... 57

Figure 3.4 Boxplots representing repeat baseline measurements of ODR in Arterioles with 605/586 60

Figure 3.5 Boxplots representing repeat baseline measurement of ODR in venules with 605/586	60
Figure 3.6 Boxplots representing repeat baseline measurements of ODR in Arterioles with 600/569	62
Figure 3.7 Boxplots representing repeat baseline measurements of ODR in venules with 600/569.....	63
Figure 3.8 Boxplots representing baseline measurement of ODR in arterioles with 610/548.....	65
Figure 3.9 ODR (610/548) Boxplots representing baseline measurement of ODR in venules with 610/548	66
Figure 4.4.1 The intensity of light reflected from the vessel is compared to that of the adjacent retina for both arterioles and venules	80
Figure 4.2 Box plots representing baseline retinal SO ₂ values for 4 participants.....	85
Figure 4.3 Scatter plot of TRBF against SaO ₂ across all 8 provocation steps (n=10)	87
Figure 4.4 Scatter plot of TRBF against SaO ₂ across all 8 provocation steps (n=10)	88

List of Tables

Table 3.1 Wavelength Combinations Used by Various Investigators	45
Table 3.2 Arteriolar ODR at mean baseline for 605/586, 600/569 and 610/548 for n=10	54
Table 3.3 Venular ODR at Mean Baseline for 605/586, 600/569 and 610/548 for n=10	57
Table 3.4 Variation in Baseline ODR with 605/586 (n=10) in arterioles and venules	59
Table 3.5 Variation in Baseline ODR with 600/569 (n=10)	62
Table 3.6 Variation in Baseline ODR with 610/548 (n=10)	65
Table 3.7 Total Variation in Mean ODR for three Wavelength Combinations \pm SD in Arterioles	67
Table 3.8 Total Variation in Mean ODR for three Wavelength Combinations \pm SD in Venules	67
Table 3.9 Differences between baseline measurements for all 3 wavelength combinations (600/586, 600/569, 610/548)	68
Table 4.1 Systemic SO ₂ per PETO ₂ for n=9 during HRC measurements	83
Table 4.2 Systemic SO ₂ per PETO ₂ for n=9 during Rtvue measurements	83
Table 4.3 ODR and retinal SO ₂ baseline measurements for 4 participants in venules and arterioles	84
Table 4.4 Table showing mean \pm SD TRBF and retinal SO ₂ values in arterioles and venules for each of 10 participants	86

LIST OF ABBREVIATIONS

ACA	Anterior Ciliary Artery
ANS	Autonomic Nervous System
AVD	Arteriovenous Oxygen Difference
AVP	Arteriovenous passage time
BRB	Blood Retinal Barrier
BLDV	Bidirectional Laser Doppler Velocimetry
CDI	Color Doppler Imaging
CRA	Central Retinal Artery
DOCTORC	Doppler Optical Coherence of Retinal Circulation
DSPS	Doppler Shift Power Spectrum
EDCF	Endothelial Derived Contracting Factors
EDRF	Endothelial Derived Relaxing Factors
ET1	Endothelin-1
F	Blood flow
FAZ	Foveal Avascular Zone

FD-OCT	Fourier Domain Optical Coherence Tomography
FiO ₂	Fraction of Inspired Oxygen
FWHM	Full Width Half Maximum
Hb	Hemoglobin
HbO ₂	Oxy-dehemoglobin
HRC	Hyperspectral Retinal Camera
IRIS	Image Replicating Imaging Spectrometer
LDF	Laser Doppler Flowmeter
LDV	Laser Doppler Velocimetry
MCT	Mean Circulation Time
MTT	Mean Transit Time
NO	Nitric Oxide
OA	Ophthalmic Artery
OCT	Optical Coherence Tomography
ODR	Optical Density Ratio
ODRA	Optical Density Ratio in Arteries

ODRV	Optical Density Ratio in Veins
OHDC	Oxygen-Hemoglobin Dissociation Curve
ONH	Optic Nerve Head
OPP	Ocular Perfusion Pressure
PaCO ₂	Partial pressure of Carbon Dioxide
PaO ₂	Partial pressure of Oxygen
PCA	Posterior Ciliary Artery
PCO ₂	Carbon dioxide tension
P _{ET} O ₂	End Tidal Pressures of Oxygen
PO ₂	Oxygen tension
PP	Perfusion Pressure
R	Resistance to flow
RBC	Red Blood Cells
RBF	Retinal Blood Flow
RER	Respiratory Exchange Ratio
RVA	Retinal Vessel Analyzer

SaO₂ Oxygen Saturation in Arteries

SO₂ Oxygen Saturation

SvO₂ Oxygen Saturation in Veins

TLS Tunable Laser Source

TRBF Total Retinal Blood Flow

VR Vascular Reactivity

1 Introduction

Vascular reactivity (VR) is the magnitude of change of the diameter of blood vessels, velocity or blood flow to provocative stimuli, such as the partial arterial pressures of carbon dioxide (PaCO_2) or oxygen (PaO_2) in the blood. VR data provides the opportunity to look at more parameters regarding our blood flow information and the magnitude of changes observed do not require large sample sizes. Several studies have demonstrated the disturbance of VR due to disease with various provocative stimuli including such as CO_2 , O_2 and flicker¹⁻⁴.

Oxygen saturation (SO_2) is the measure of the percent amount of hemoglobin (Hb) bound to oxygen in blood. Oximetry; the method of measuring SO_2 , is measured in our lab with spectroscopic techniques such as pulse oximetry (finger and ear oximeters) which measures the absorbances due to the pulsatile nature of arterial blood alone in systemic SO_2 . Retinal SO_2 on the other hand is measured with a two wavelength oximetry method, using a prototype digital hyperspectral device for imaging the retina. This method was first developed by Beach and co-workers (1999)⁵ in the late 90's.

Several noninvasive methods of measuring retinal blood flow (RBF) have been developed over the years such as color doppler imaging, fluorescein angiography and laser doppler velocimetry and flowmetry techniques among others. The Doppler Fourier Domain OCT (FD-OCT) allows for the quantification of Total Retinal Blood Flow by applying bidirectional laser doppler velocimetry methods. Retinal blood flow is related to SO_2 in that hemoglobin is carried by the blood.

The measurement of retinal blood SO_2 is plagued with several difficulties such as the scattering of light in retinal tissues due to the discontinuities in the refractive indices between the plasma, red blood cells and other components of whole blood; and the variation in fundus pigmentation with ethnicity⁶⁻⁹. Despite the numerous challenges faced by retinal oximetry, several methods have been developed over the decades that compare the absorbance spectra of oxyhemoglobin (HbO_2) to that of deoxyhemoglobin (Hb) and then

derive the optical density ratio (ODR) and retinal blood SO_2 . These technologies devised for the measurement of retinal SO_2 show promise in the earlier detection of hemodynamic changes in the retina which has been shown to be affected in several major ocular diseases such as glaucoma, diabetic retinopathy and age-related macular degeneration ¹⁰⁻¹³. Indeed, methods of measuring retinal SO_2 bring scientists significantly closer to a fuller understanding of the processes involved in retinal diseases with hemodynamic components.

1.1 The Vascular Systems of the Human Retina

The human ocular circulation is multifaceted and unique. This uniqueness is primarily due to the presence of a dual vascular system; the retinal and choroidal systems. Since the middle of the 19th century, several non-invasive methods have been developed for studying various aspects of ocular hemodynamics and its response to stimuli of a physiological and pharmacologic nature. These methods have enabled advances into understanding the physiology of ocular blood flow and also greater awareness of its disturbance in several systemic and ocular diseases.

1.1.1 Anatomy of Retinal Vessels

Retinal arterioles and venules are made up of 3 layers; adventitia, smooth muscle cells, and endothelial cells. The adventitia forms the outermost layer of the vessel and the endothelium the innermost. Retinal capillaries on the other hand, are composed of only endothelial cells which are surrounded by a basement membrane which contains pericytes arranged in a laminar fashion.

Arterioles, termed “resistance” vessels, together with the central retinal artery (CRA) are thought to be responsible for the major regulation of the flow of blood to the capillaries ¹⁴. The capillaries are responsible for the exchange of metabolites (“exchange” vessels) with the tissues and, via the contractile properties of the pericytes, are thought to play a minor role in the fine tuning of retinal perfusion ¹⁴⁻¹⁶. The inner blood retina barrier (BRB) is made up of numerous tight junctions between the endothelial cells

lining the retinal blood vessel lumen. At the level of the capillaries, the BRB prevents leakage of blood constituents into the retinal tissue but does allow transfer of oxygen across the vessel wall. The endothelium and its associated tight junctions are often collectively termed the inner BRB.

Blood vessels of both the choroid and retina of human ocular circulation take their source from the first branch of the internal carotid artery known as the ophthalmic artery (OA) which has several branches including the CRA, the short and long posterior ciliary arteries (PCA), and the anterior ciliary arteries (ACA). Choroidal and retinal vessels differ both morphologically and in their purposes from each other. Retinal vessels are non-fenestrated and have a narrower lumen than choroidal ones which provide less resistance to blood flow. The flow of blood is low in the retina, subsequently allowing for a higher extraction of oxygen with an arteriovenous saturation difference of about 40%^{17,18}. The choroidal system on the other hand has a high blood flow rate, representing 85% of the total ocular blood flow¹⁹ and a low oxygen extraction of 3%²⁰. Fenestrations in the choroidal capillaries facilitate the high rate of blood flow and the exit of retinol-binding protein which allows retinol (vitamin A) to reach the retinal pigment epithelium (RPE)²¹. The choroidal capillaries also provide the RPE with all the building blocks of phototransduction such as amino acids, proteins and oxygen and are responsible for the removal of waste products from the RPE. Choroidal vessels, unlike retinal capillaries also leak plasma proteins. The RPE forms the outer BRB through its role of selectively transferring retinol from its carrier protein to the retina while preventing the diffusion of plasma proteins²². In addition, the tight junctions of the RPE cells and the selectively permeable cell membrane determine the exchange features of the outer BRB.

1.1.2 The Retinal Vascular System

The inner two-thirds of the retina receive its supply of oxygen and metabolites from the terminal arterioles without anastomoses. After emerging from the optic disc 10-15mm behind the globe, the CRA divides into two major branches and then into arterioles which each supply a quadrant of the inner retina (layers closest to the vitreous compartment). The arterioles form an anastomotic capillary plexus which

supply the nerve fiber, ganglion cell and inner nuclear layers of the retina. The single layered capillaries extend to the periphery of the retina. At the extremes of the peripheral retina, there is a noticeable avascular, capillary free zone either side of the arterioles that runs parallel with the vessel course and can be up to approximately 1.5mm wide ²³. The foveal avascular zone (FAZ) is supplied primarily by the underlying choroidal and to a lesser extent the surrounding retinal capillary network of vessels. In about 25% of human eyes the macular region of the retina will also be perfused by the cilioretinal artery emerging from the temporal margin of the optic disk ²⁴. Inner RBF constitutes only about 4% of total ocular blood flow ²³.

1.1.3 The Choroidal/Uveal Vascular System

The PCAs and ACA form the vessels of the choroid and supply the uvea and outer and middle layers of the retina after entering the globe around the optic nerve, forming paraoptic and perimacular patterns ²⁵. The major arterioles of the choroid are formed from the subsequent branches of the short PCAs ^{26,27}.

1.1.4 Differences in the Choroidal & Retinal Vascular Systems

It has been demonstrated previously that retinal blood flow (RBF) is significantly slower with subsequent increased oxygen exchange than choroidal blood flow in the outer retina ²⁸. The low rate of flow of blood in the inner retina makes it much more susceptible to interruptions in blood supply as compared to the choroidal system ^{29, 30}. The arteriovenous difference in blood oxygenation extraction in the retina is 35% as compared to only ~4% in the choroid ³¹. The retinal circulation lacks sympathetic innervation, unlike the choroid, and it is influenced by intrinsically released local factors ²². A further difference between the choroidal and retinal systems is the thermoregulatory property of the choroidal vessel network which in effect cools the metabolically active pigment epithelium- photoreceptor complex.

1.1.5 Venular Drainage

After running its course in the globe, deoxygenated blood drains from the eye through the venules and veins primarily via the vortex veins, the central retinal vein and finally the ophthalmic vein. The central retinal vein exits the globe with the optic nerve parallel and against the flow of the CRA³².

1.2 Regulation of Ocular Blood Flow in the Human Retina

Local and systemic factors play a role in the rather complex regulation of blood flow in the eye. Generally, local factors such as O₂ tension (PO₂), CO₂ tension (pCO₂) and pH adjust the flow based on local needs, while systemic factors such as circulating hormones and the autonomic nervous system (ANS) adapt the distribution of the cardiac output over the different vascular beds depending on the general blood flow needs of the body²².

The cardiac cycle consists of the period from the end of one heart contraction to the end of the next. With a period of relaxation called diastole, followed by a period of contraction called systole. Arterial pressure has a pulsatile nature due to the intermittent pumping of blood by the heart. Cardiac output is the quantity of blood pumped by the heart in a unit period of time and is about 5 liters/minute²⁰.

Chocolate³³, dynamic and isometric exercise³⁴⁻³⁷, smoking^{1,38,39}, alcohol (ethanol)^{40,41} caffeine⁴², high fat diets⁴³, hyperglycemia^{42,44-46} and vitamin C⁴⁷ intake have been shown to alter retinal hemodynamics of humans.

1.2.1 The Rate of Blood Flow

The rate of blood flow (F) is the volume of blood that passes a given point in the vasculature at a given point in time. Blood flow is normally expressed in microlitres per minute ($\mu\text{l}/\text{min}$)²⁰. The rate of blood flow in a vascular bed depends on two main factors; the perfusion pressure gradient (ΔP) over the vascular bed and the resistance to flow (R) within the vascular bed (Ohm's/Darcy's Law)²².

$$F = \frac{\Delta P}{R} \dots\dots\dots 1$$

Where, R depends on blood viscosity (η), the vessel length (L) and diameter (2r) of the blood vessels.

Using steady blood flow conditions through a cylindrical rigid tube, R is directionally proportional to blood viscosity (η) and the length (L) and inversely proportional to the fourth power of the radius (r) of the vessel;

$$R = 8\eta L / \pi r^4 \dots\dots\dots 2$$

Or as stated in the Law of Poiseuille:

$$F = \Delta P \pi r^4 / 8\eta L \dots\dots\dots 3$$

The contraction and relaxation of the arterioles modifies the blood resistance, R.

Poiseuille’s equation serves as a useful approximation for blood flow calculation; however, it possesses a few limitations for use in the cardiovascular system. Unlike the rigid tubes used by Poiseuille, the elasticity and tapering structure of the human vessels, lack of laminar flow in some larger vessels, pulsatile flow resulting from heart contractions and the variability of blood viscosity with velocity (deviation from a perfect Newtonian fluid) all serve as departures from the standards used to derive Poiseuille’s equation ⁴⁸.

1.2.2 Ocular Perfusion Pressure (OPP)

OPP is the pressure that drives blood through a vessel and is calculated as the difference between the local arterial blood pressure and the venous pressure. Venous pressure is not easily calculated however, it has been shown to be only slightly higher than intraocular pressure (IOP). IOP therefore serves as a good

surrogate for venous pressure and has since been widely accepted as the standard ⁴⁹. OPP is thus calculated as follows:

$$OPP = \frac{2}{3}BP_{mean} - IOP \dots\dots\dots 4$$

Where, BP_{mean} is the mean arterial blood pressure and IOP is the intraocular pressure ^{50,51}.

1.2.3 Vascular Resistance (R)

Vascular resistance generated by friction between the moving blood and vessel wall cannot be measured directly. Increases in arterial pressure have been shown to not only increase the force that tends to push blood through the vessels, but to also distend the vessels concurrently, which decreases their resistance ²⁰. However, vascular resistance is influenced by a number of factors such as the blood viscosity, length and diameter of the vessels.

1.2.3.1 Blood Viscosity (μ)

Blood viscosity is the measure of the resistance of blood to flow and is the major determinant of the shear stress imparted by blood flow ⁵². The viscosity of blood plays an important role in maintaining vascular homeostasis and varies as a function of the shear rate; increasing at low shear rate due to the ‘Rouleaux’ effect of the red blood cells (RBCs) and diminishing to an almost constant rate at high shear rate. Shear rate can be described as a force or pressure acting on the blood which may cause blood layers to slide past each other at a certain velocity altering its shear rate. An increase in shear stress acting against vessel walls increases the shear rate. The ‘Rouleaux’ effect describes stacks of RBCs formed as a result of the large surface area of the cells which allows adhesion to each other due to the unique discoid shape of the cells in vertebrates. In certain diseased states, substantial changes occur in the blood velocity ⁵³.

1.2.3.2 Vessel Length (L)

Changes in the length of vessels appear to be of little significance in the regulation of ocular circulation. This is due to the constant state of perfusion of the ocular capillaries compared to capillaries found in other parts of the body e.g. capillaries of the pulmonary circulation ²².

1.2.3.3 Vessel Diameter (2r)

Variation in diameter is the main regulatory mechanism of ocular circulation. Slight changes to the diameter of a vessel cause substantial changes to resistance and blood flow as vascular resistance, R is inversely proportional to the fourth power of the radius of a blood vessel. Both systemic and local factors can trigger a change in vessel diameter ²². The change in diameter of the vessels is also directly related to the blood velocity. This relationship applies to arterioles and venules. Blood flow touching the wall of large vessels (laminar flow) is extremely slow compared to that near the center of the same vessel due to its adherence of RBCs to the vascular endothelium. This is not the case in vessels of smaller diameter, where essentially all of the blood flow is in contact with the wall. The blood velocity therefore remains relatively constant throughout the vessel. For a specific vessel diameter, the blood flow rate and velocity in a retinal arteriole is greater than in the retinal venule ²⁰. The rate of blood flow, F, that flows through a vessel in a given period of time is equal to the velocity of flow times the cross-sectional area ⁵⁴;

$$F = v\pi r^2 \dots\dots\dots 5$$

Where F is the rate of blood flow ($\mu\text{l/s}$) and πr^2 is the cross-sectional area (cm^2)

1.2.4 Autoregulation

Myogenic autoregulation is “the ability of a vascular bed to keep blood flow constant despite changes in perfusion pressure (PP)”. Alternatively, metabolic autoregulation is “the ability of a vascular bed to change blood flow to meet metabolic needs” by the constriction or dilation of retinal vessels ⁵⁵.

Myogenic, metabolic stimuli and endothelium-derived vasoactive factors regulate RBF by influencing the tone of the muscles in the retina and choroid. Vasoconstriction is promoted by calcium ion movement into the smooth muscle cells which reduces blood flow in order to avoid hyper-perfusion, capillary damage and edema ⁵⁶. The opposite is also true with vasodilation as a result of potassium ions producing a reduction in perfusion pressure (PP). The myogenic regulation of blood flow alters blood flow resistance so that the blood supply maintains the concentrations of certain metabolites and waste-products within narrow limits (principally the PO₂ and PCO₂) ¹¹. An increase in PP results in an increase in transmural pressure which leads to a distension of the blood vessel wall and the myogenic contraction of retinal arteries ⁵⁷. The autoregulatory process of the retinal and optic nerve head (ONH) blood flow holds only if PP is not reduced by more than 50 percent ^{58,59}.

1.2.5 Blood Gases

When otherwise healthy individuals inhale mixtures of 100% oxygen or co-administered 90% oxygen and 5% CO₂, it leads to an increase in partial pressures of oxygen (PO₂) in the arteries resulting in hyperoxia ^{60, 61}. Hyperoxia elicits a vasoconstriction of retinal blood vessels and significant decrease in RBF in the macular and peripheral retinal regions of the retina ⁶²⁻⁶⁵. A full, vasoconstrictor response to hyperoxia stabilizes after 6 minutes ⁶², Vasoconstriction of the retinal arterioles serves as a regulatory response for keeping the PO₂ in retinal blood constant. Reduced retinal capillary and ONH blood flow has been seen in smokers, secondary to hyperoxia ⁶⁶. During breathing of 100% O₂, the retina receives added O₂ from the choroid due to a reduction in blood flow in the retina.

Hypoxia is a state of abnormally low PO₂, resulting in an increase in RBF to maintain a stable PO₂ environment and vasodilation in the inner retina which may be due the secretion of retinal lactate ^{67, 68}. Lactate is believed to be mediated by endothelium-derived Nitric Oxide (NO) ⁶⁹. Hypoxia of the retina causes vasodilation of the retinal arterioles beginning at hemoglobin (Hb) SO₂ below 90% and can be measured clearly below 65mmHg ^{61,70}.

In conditions of normoxia (baseline) in healthy participants, PaO₂ and PaCO₂ values vary depending on a number of biological factors such as gender, height, weight, age and medical history. Generally speaking, however, PaO₂ values vary between about 75-100mmHg (10-13kPa)⁷¹ and PaCO₂ about 34-45mmHg (4.5-6.0kPa)⁷². Isocapnia is a state in which the arterial carbon dioxide pressure remains constant or unchanged.

1.2.6 Endothelial Derived Factors

The vascular endothelium produces various vasodilating and vasoconstricting mediators under basal conditions and in response to stimuli from mechanical sources in the form of stretch receptors within the smooth muscle cells that respond to changes in trans-luminal pressure⁷³ and chemical (e.g. acetylcholine - ACh, histamine and calcium ionophores). Endothelial locally derived factors can be divided into two groups; endothelial derived relaxing factors (EDRF) and endothelial-derived contracting factors (EDCF). Prostaglandins are also vasoactive factors released by the endothelium which may elicit both vasoconstriction and vasodilation. Prostaglandins have been shown to disrupt the internal BRB thus causing an increase in the permeability of retinal capillaries and may have a significant role in the regulation of choroidal and retinal circulation²². Blood flow is locally regulated by these vasoactive factors derived from the endothelium when they act upon the smooth muscle cells (surrounding the endothelial cells) and the pericytes (that surround the capillaries). The hemodynamic regulatory property of the endothelium may be disrupted by many vascular diseases such as ischemia and reperfusion, hypertension, hypercholesterolemia and diabetes. Therapeutic agents can be used to trigger the secretion of vasoactive substances by the endothelium⁷⁴.

1.2.6.1 Endothelium Derived Relaxing Factors (EDRF)

Nitric oxide (NO) is one of the most important endothelial relaxing factors⁷⁵. It is formed from *L*-arginine by NO-synthase and has been shown to be released continuously by the endothelium of the ophthalmic⁷⁶ and retinal arteries⁷⁷. NO release can be stimulated by a variety of endogenous substances such as

acetylcholine, bradykinin, noradrenaline and histamine⁷⁷⁻⁸⁰, in response to an increase in shear stress⁸¹ and platelet-derived products such as adenosine diphosphate, serotonin, thrombin⁸⁰. This relation to shear stress is more likely however in larger conduit arteries²². NO is produced also in response to changes in trans-luminal pressure and shear stress. NO induces vasodilation by increasing cyclic guanine monophosphate that in turn reduces calcium ion concentration (Ca^{2+}) in smooth muscle cells resulting in relaxation and subsequent dilation⁸². NO also inhibits platelet function Vasoconstriction results when NO is inhibited.

Prostacyclin (PGI_2 , ecoprostenol) is also an endothelium secreting vasodilator. It also inhibits platelet aggregation⁸³ and is produced from arachidonic acid via the activation of the enzyme cyclooxygenase⁸⁴

1.2.6.2 Endothelium Derived Constricting Factors (EDCF)

Endothelin-1 is a large 21 amino acid peptide present in almost all blood vessels²⁰. The endothelin family is comprised of 3 polypeptides that are all important in vascular regulation; endothelin-1 (ET1), endothelin 2 (ET2) and endothelin 3 (ET3). ET1 is the most potent vasoconstrictor secreted by the endothelial cells⁸⁵ which at higher concentrations causes vasoconstriction and vasodilation at low concentrations⁸⁶. The vasodilatory response to endothelin involves the activation of endothelial receptors (ET_B -type) linked to NO and/or prostacyclin released by the endothelial cells⁸⁷. On the other hand, vasoconstriction results from the activation by endothelin of specific membrane receptors (ie. ET_A and ET_B receptors) on the smooth muscle cells⁸⁸. Receptors for endothelin-1 have also been reported on choroidal and retinal arteries²². Vasoconstriction results in a reduction of RBF after intravenous administration of ET1 and occurs secondary to increased intracellular Ca^{2+} ^{23,89}. NO inhibits the release of ET-1⁹⁰ while ET-1 impairs NO bioavailability resulting in a self-limiting mechanism that inherently limits the vasoactive properties of ET-1 and NO. Shear stress down-regulates endothelin synthesis⁹¹. Endothelin-1 and the endothelin-A receptor have been reported to play a role in the retinal hemodynamic

responses to hyperoxia⁹². Other EDCFs such as thromboxane A₂, prostaglandin H₂ or superoxide anions are produced by the cyclooxygenase pathway of the endothelium

1.2.6.3 The Interaction of EDRFs and EDCFs in the Regulation of Ophthalmic Circulation

The ophthalmic circulation is maintained in a constant state of vasodilation due to the constant basal release of NO in the ophthalmic vascular bed. Stimulated release of NO occurs as a result of agonists such as bradykinin, acetylcholine and histamine mediated by receptors^{74,79,92}. Inhibitors of NO formation such as L-NMMA or L-NAME reduce the responses to these agonists. EDRFs are essential especially in small vessels and possibly in the microcirculation. This has been demonstrated in vitro in extraocular pig vessels in which the sensitivity to the agonist bradykinin increases as the diameter of vessels reduces⁹³. In addition, both constriction and dilation of the vessels occur with certain agonists such as histamine (e.g. histamine interacting with H₁-histaminergic receptors inducing both NO mediated relaxation and a contraction when acting on smooth muscle cells) when it activates the endothelial or smooth muscle cells.

Endothelin-1 and 3 at lower doses elicits the release of prostacyclin – causing vasodilation at lower doses and reduced flow and vasoconstriction at higher concentrations of endothelin-1. ET_B-receptor is activated at very low doses of endothelin-1. On the other hand, the ET_B-receptor is activated predominantly at higher doses of endothelin-1 on smooth muscle cells^{70,94}.

The inner retinal blood flow system may be influenced by a number of systemic regulatory systems and factors in various organs such as hormonal, pharmaceutical, ions and other chemical factors.

1.2.7 Other Influences on Retinal Blood Flow

1.2.7.1 Hormonal Influences

Vasoactive hormones influence blood flow through two main mechanisms; the mediation of the endothelial cells and directly on the smooth cells and pericytes of blood vessels⁹⁵.

1.2.7.1.1 Renin/Angiotensin

Angiotensin II, a highly active octapeptide is a potent vasoconstrictor of ocular vessels formed by angiotensin-I which is activated by the angiotensin-converting enzyme (ACE) ^{20,96}

1.2.7.1.2 Norepinephrine and Epinephrine

Norepinephrine and Epinephrine are vasoconstrictors; with norepinephrine being more powerful than the latter. Epinephrine can cause mild vasodilation. Norepinephrine is released by sympathetic nerve endings in individual tissues when the sympathetic system of the body is stimulated during stress or exercise which stimulates α -receptors and β -receptors (in the case of vasodilation in certain vascular beds) and contracts veins and arterioles ^{20,96}. The adrenal glands also secrete norepinephrine and epinephrine by the sympathetic nerves to the adrenal medulla. Choroidal vessels are constricted by catecholamines found circulating in the blood ^{1499 96}.

1.2.7.1.3 Vasopressin

One of the body's most potent vascular constrictor substances is vasopressin (also called antidiuretic hormone). It is a more powerful vasoconstrictor than angiotensin II. Vasopressin is formed in the nerve cells in the hypothalamus of the brain and transported downwards to the pituitary gland by nerve axons where it is secreted into the blood ²⁰.

1.2.7.1.4 Natriuretic Peptide

Natriuretic peptides (atrial natriuretic peptide, C-type natriuretic peptide and brain natriuretic peptide) are produced in cardiocytes and vascular endothelial cells and may be considered a part of the renin-angiotensin system. Natriuretic peptides have a vasodilatory effect on vessels.

1.2.7.1.5 Ions and Other Chemical Factors

1.2.7.1.5.1 Vasodilatory Effects

An increase in potassium, magnesium (inhibits smooth muscle contraction) and hydrogen ions (decrease in pH), acetate and citrate anions and carbon dioxide (marked vasodilation in the brain, moderate vasodilation in the tissues) concentration causes vasodilation ²⁰.

1.2.7.1.5.2 Vasoconstrictor Effects

An increase in calcium ion (stimulates smooth muscle) and decrease in hydrogen ion concentration causes arteriolar constriction ²⁰.

1.3 Optical Coherence Tomography

Optical Coherence Tomography (OCT) ⁹⁷ provides a non-invasive, non-contact method of providing high-resolution cross-sectional imaging of human tissues such as the retina ⁹⁸⁻¹⁰¹ and is commonly used in the diagnosis and management of retinal diseases and glaucoma ¹⁰²⁻¹⁰⁶. The optical configuration of OCT is that of a low coherence (white light) interferometer ¹⁰⁷. OCT technology emerged from in vivo optical length measurements of the eye with low coherence interferometry ¹⁰⁸.

1.3.1 Overview of OCT

OCT relies on the interference between a split and subsequently re-combined broadband optical field. The split field travels in the reference arm of the system, reflecting from a reference mirror, and also in a sample arm where it is reflected from several layers within a sample tissue. Interference between the optical fields is only detected when the reference and sample arm optical path lengths are coordinated to within the coherence length of the light, due to the broadband nature of the light used. The depth or axial resolution of the OCT therefore is determined by the temporal coherence of the light source. Differences

in refractive index between layers in the sample tissue of interest manifest themselves as consistent peaks in the interference pattern ¹⁰⁹. A schematic of a typical OCT system is shown in figure 1.1.

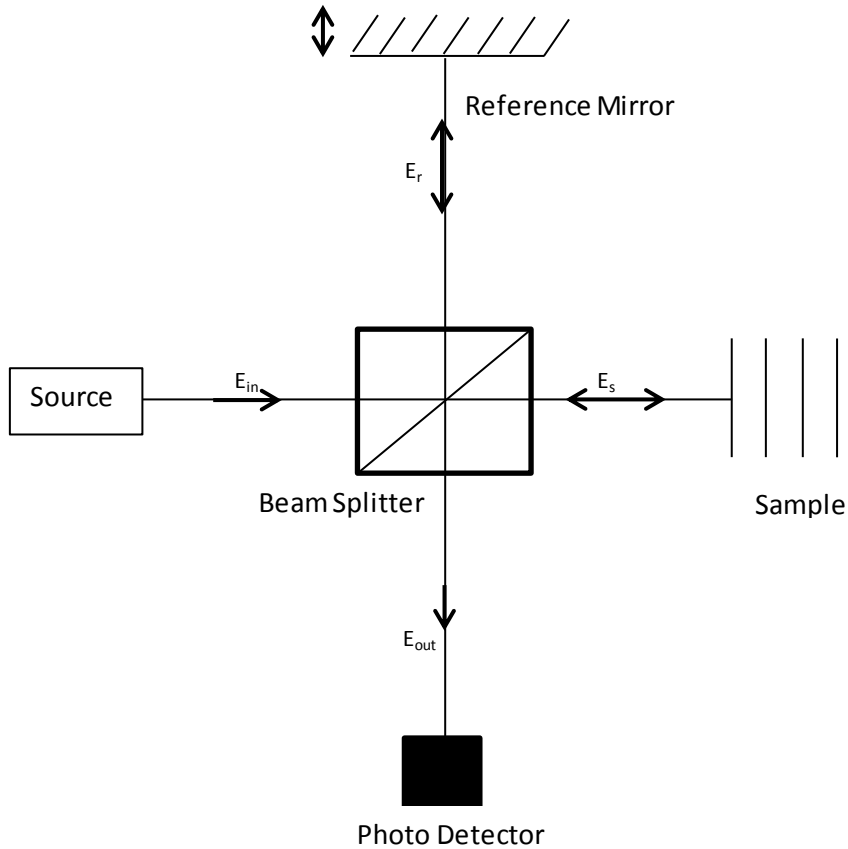


Figure 1.1 Basic OCT system, based on Michelson interferometer

1.3.2 Types of OCT

OCT can be classified into two broad groups based on its design components. These are the time domain OCT (TD-OCT) and frequency domain OCT (FD-OCT) systems.

1.3.2.1 Time-Domain OCT

The TD-OCT system has a reference mirror which is scanned along the z-axis to match the optical path from reflections within the sample. Light that carries a signal returning from the eye interferes with light that has travelled a known path length. The moveable nature of the reference mirror is the most essential

and unique feature of the TD-OCT ^{110, 111}. A time-domain interference pattern formed displays a reflectivity profile (with spatial dimension details of the tissue) in the form of axial scans (A-scans) which is then further combined to form a cross-sectional tomograph. Commercial OCT instruments have been developed for ophthalmology based on the TD-OCT system ^{109,111}.

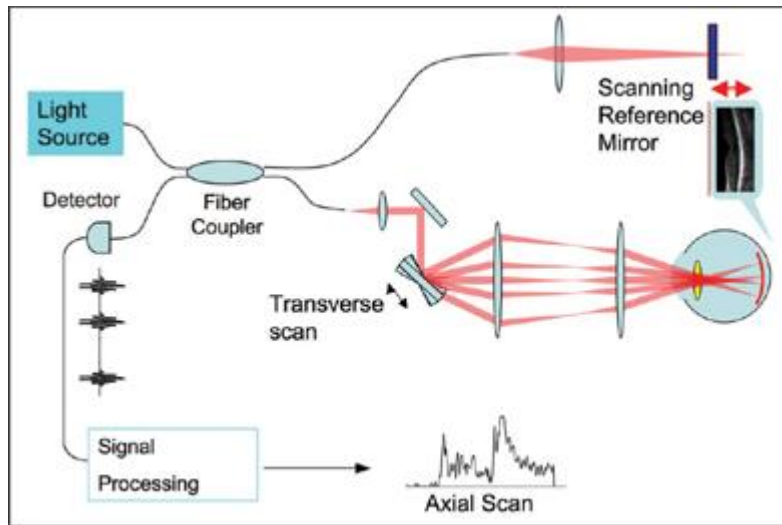


Figure 1.2 Schematics of time-domain OCT. The reference mirror (upper right) is moveable over a distance that corresponds to the axial (depth) range of interest in the sample. Reproduced with Permission. ¹¹²

1.3.2.2 Frequency Domain OCT

The reference optical path length remains fixed with the FD-OCT system and component frequencies of the OCT output are detected with a spectrometer ^{109, 113}. The lack of moving parts in the system are an advantage of the system in that it allows for rapid image acquisition and a greater signal to noise ratio ^{108, 113, 114}. The presence of a fixed mirror is one of the major advantages and differences that FD-OCT has over the TD-OCT which has an adjustable mirror. The intensity spectrum determined is converted by Fourier techniques into the time domain to recreate the depth resolved sample optical structure ¹⁰⁹.

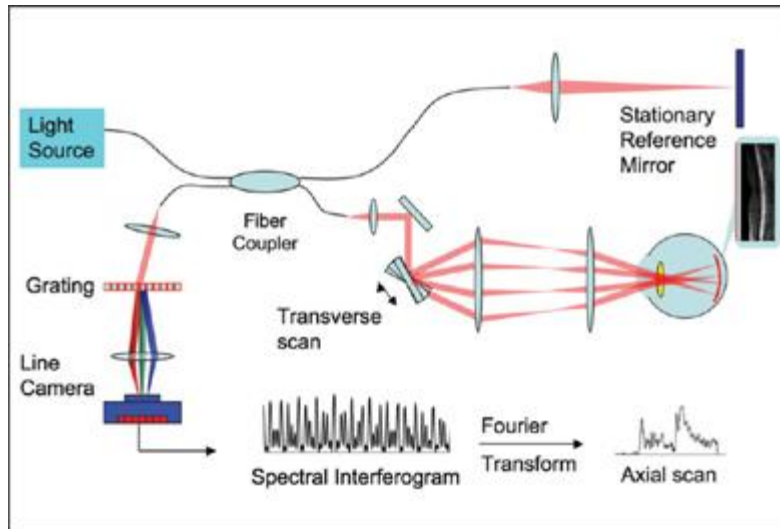


Figure 1.3 Schematic diagram of a spectrometer-based Fourier-domain OCT system. It contains a stationary reference mirror and a spectral interferogram (spectrum of the combined reference and sample reflections). Spectral modulations of difference periodicities are formed from reflections from different depths of the sample. A Fourier Transform converts spectral modulations into an A-scan. Reproduced with Permission.¹¹²

1.4 Quantification of Retinal Hemodynamics

The first attempt at quantifying hemodynamics in humans in response to alterations in PO_2 in the retina was made by Hickman and Frayser in the 80's with the bidirectional laser Doppler velocimetry methodology¹¹⁵. Since then, the development of methods of quantifying ocular hemodynamics in humans and animals has been ongoing over several decades and has led to several technologies of varying efficacy. Initial methods carried out experimentally were of an invasive nature and tested on animals. These invasive methods included the cannulation of uveal veins in rabbits and cats¹¹⁶ to directly measure blood flow and labelling microspheres radioactively¹⁹. In more recent years however, non-invasive methods have been advanced that are applicable and safe for use on humans. These methods focus on the measurement of retinal hemodynamic parameters such as the diameter (D) of retinal vessels, mean circulation or transit time (MCT or MTT) of fluorescein injected intravenously through a retinal segment from entry to exit of microvascular segment¹¹⁷, arteriovenous passage time (AVP); the time difference between the first appearance of the dye at a reference point at the temporal artery and that at the adjacent vein¹¹⁸. For several years, the bidirectional laser Doppler velocimetry (BLDV) methodology was the only

technology that was capable of measuring absolute blood flow velocities, prior to the introduction of Doppler FDOCT. However, the high costs involved with purchasing BLDV systems for routine use by practitioners has prevented the method from being introduced on a large scale for routine clinical use and as a gold standard for the quantification of blood flow.

1.4.1 **Retinal vessel analyzer (RVA)**

Diameter has been measured in the past with the use of magnified fundus photographs using a caliper or scanning across the vessels^{119, 120}. This technique however was improved and simplified by the use of the Retinal Vessel Analyzer (RVA) allowing the additional possibility for dynamic measurements of diameter¹²¹⁻¹²³. Making use of the brightness profile of the vessel, RVA measures the diameter of vessels. The basic principle of the RVA is based on the fact that RBCs within the retinal vessels absorb light at a maximum wavelength of 400–620 nm, whereas the background and surrounding fundus mostly reflects it. The differences between the brightness profile of the RBC column within the vessel compared with that of the surrounding fundus are then used for further analysis. To achieve an optimum contrast for vessel visualization, a green filter is inserted into the illumination pathway of the fundus camera. Thus, the RVA therefore measures mainly the width of the RBC column within selected vessels^{117, 123}

This technique however is complicated due to shadowing of structures and reflections from vessel surfaces. The RVA measures change in diameter in relative units, but is incapable of quantifying blood velocity or flow.

1.4.2 **Fluorescein Angiography**

Fluorescein angiograms have been used to measure MCT and AVP with the use of fluorescein dye injected intravenously through a retinal segment, assuming that the segment being investigated has a single inflow (feeding artery) and single outflow (draining vein)¹¹⁷. Dilution curves are used to determine MCT¹²⁴⁻¹²⁶. Several complications related to the properties of the dye, mode of its injection, method of

recording dilution curves, etc. make it difficult and imprecise to apply this technique to the eye; especially in the case of retinal vascular pathologies. MCT in this scenario is therefore considered only an estimation of true MCT¹¹⁸. Fluorescence intensity emitted by the dye is measured and recorded when the fundus is illuminated with blue light which excites the fluorescein spectrum photographically or by video¹¹⁷. Other parameters such as mean velocity of the dye (MVD) in a retinal artery and AVP have been derived from the time course of the fluorescein intensity using scanning laser ophthalmoscopy¹²⁷. AVP strongly favors the measurement of passage times of the dye through the shortest segment between an arteriole and a venule close to the papilla¹¹⁸. Additional limitations of this method to those previously mentioned include the assumptions that an arteriole is completely drained by a corresponding vein, the sum of vessel diameters is directly related to blood volume, no leakage of fluorescein occurs during measurements¹²⁸, the generally invasive nature of the procedure and anaphylactic reactions in response to the fluorescein chemical used.

1.4.3 Blue Field Entoptic Technique

The velocity, number and pulsatility of leukocytes in the macular of the retina can be determined using the Blue Field Entoptic Technique. The blue-field entoptic phenomena or “flying corpuscles” can be perceived using a deep-blue field of light with a narrow spectrum centered at a 430nm wavelength. This visual perception originates from within the terminal arterioles and capillaries in the inner retina surrounding the foveal avascular zone but can only be perceived when illuminated in a specific manner. The moving RBCs are seen in an area of 10-15 degrees of arc radius centered at the fovea¹²⁹. Participants are asked to make comparisons between a standard of moving computerized motion of leukocytes (at a known velocity) with their observations of movement of corpuscles¹¹⁷. Measurements are therefore subjectively made based on the participant’s observation of the phenomena and highly dependent on the participant’s visual abilities requiring a visual acuity better than 20/50 for a reliable measurement¹³⁰. The objective scanning laser ophthalmoscope-adaptive optics imaging technique has been used to confirm measurements obtained with the blue-field technique¹³¹. Limitations of this technique lie in its poor

reproducibility of results, subjectivity, individual variation and need for participants to have good visual acuity.

1.4.4 Laser Speckle Technique

The speckle effect is an interference pattern phenomenon that makes use of laser light sources or other coherent light sources¹³². A speckle pattern is produced when there is a scattering of light upon illumination of the fundus. The pattern varies significantly dependent on the vascular blood flow velocity within the retinal vessels¹³³. The speckle patterns produces images with low contrast and blur when there is blood flow; the blur increasing with increased blood velocity and exposure time of the photo. In areas of no flow however, the image remains in high contrast with minimal blurring¹³⁴. This method provides an immediate overall map of blood velocities, as compared to other techniques such as Doppler velocimetry which gives measurements only at one point in time¹³⁴. Limitations of only providing semi quantitative estimations (non-absolute) of retinal microcirculation and the inability to follow time course changes however exist with this technique^{134,135}.

1.4.5 Laser Doppler Velocimetry

1.4.5.1 Doppler Shift Theory

The frequency, f of a beam of laser light scattered by a moving red blood cell (RBC) (moving at a speed V_{max} ; shifts by an amount Δf_{max} from the frequency of the incident light (f_i) or from the frequency of reflected light from a stationary neighbouring object.

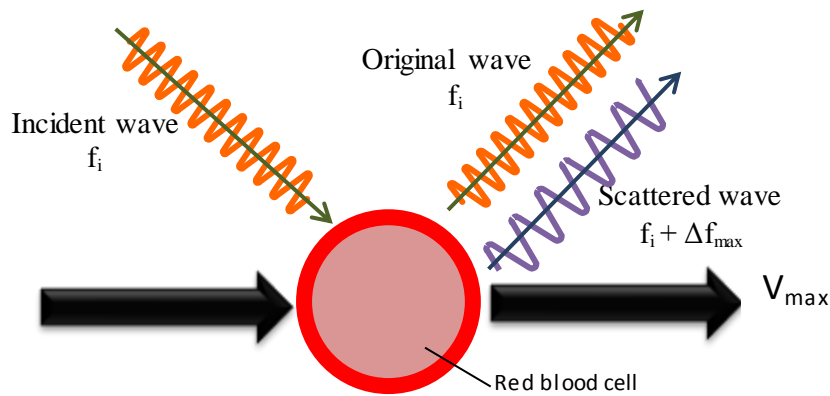


Figure 1.4.0: Diagrammatic representation of the Doppler shift effect. The frequency, f_i of an incident wave of light changes by Δf_{ma} when reflected from a moving RBC.

This theory is utilized in laser Doppler velocimetry (LDV). Here, scattered light reflected from moving RBCs in a blood vessel is spread out to form a spectrum called the Doppler Shift Power Spectrum (DSPPS)¹³⁶ which contains both the original (f_i , scattering from the vessel wall) and shifted frequency (f , scattering from moving RBCs) with a difference in frequencies, Δf . The direction of light waves is incorporated with angle α being the angle between the direction vector of V_{max} and the reflected light wave and β , the angle between the incident beam and resultant direction vector of V_{max} ¹³⁷. Δf is related to the velocity of RBCs by the equation:

$$\Delta f = \frac{\cos\alpha + \cos\beta v}{\lambda} \dots\dots\dots 6$$

Where, V = velocity and λ is the wavelength of the incident light.

1.4.5.2 Bidirectional Laser Doppler Velocimetry (BLDV)

BLDV allows the quantification of absolute blood velocity in major retinal vessels with the use of a single laser and two laser photodetectors scattered by RBCs, with the application of the Doppler shift principle. RBF ($\mu\text{l}/\text{min}$) is calculated from the measurement of vessel diameter and of centreline blood velocity, V_{max} . Using bi-directional laser Doppler velocimetry, the measurement of V_{max} is independent of the angle of incident light¹³⁷ since the use of the two photodetectors separated by a known angle of separation

results in frequency shift in two directions (K_1 and K_2 , with frequencies f_s^1 and f_s^2 respectively) (Figure 1.2)¹¹⁵. The difference in frequency shift between the two photodetectors can be used to calculate absolute velocity irrespective of the angle, α according to the equation:

$$V_{max} = \frac{\lambda \Delta f}{\Delta \alpha \cos \beta} \dots \dots \dots 8$$

where, $\Delta f = (\alpha_1 - \alpha_2)v/\lambda \dots \dots \dots 9$

α_1 and α_2 are the associated angles to the frequencies of the original wave, f_i and the scattered wave, $(f_i + \Delta f_{max})$ respectively. $\Delta \alpha$ is the angle between f_s^1 and f_s^2 ($\alpha_1 - \alpha_2$) and β is the angle between direction of the velocity and the incident beam.

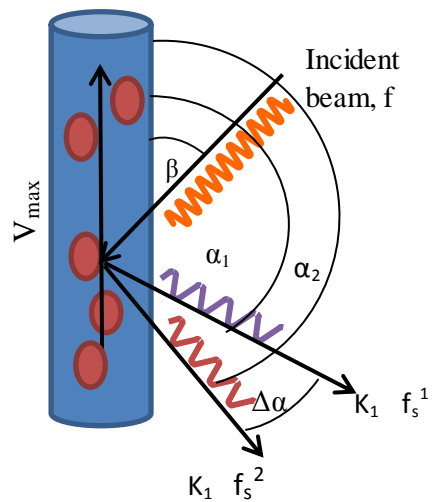


Figure 1.5 Doppler method of measuring blood flow (f=non shifted light ray, fi=shifted ray)

With V_{max} , the known angle of separation between the two laser lights ($\Delta \alpha$) (which is used to determine the frequency shift in the two directions - f_s^1 and f_s^2) and angle β (angle between the vessel plane at the measurement site and the direction of the velocity), RBF can be calculated with the knowledge of diameter, D , as well as velocity. Diameter is calculated using a green laser which is orientated

perpendicular to the vessel wall and a densitometry methodology is then utilised to determine vessel diameter. (Figure 1.1) ^{115,138}.

Total retinal blood flow (TRBF) ranges from about 40.8 to 52.9 µl/min in humans using BLDV ^{115,139}. RBF measurements from BLDV are larger in the temporal human retina than in the nasal region; this is believed to be due to the larger size (20-25%) and higher metabolic rate in the temporal retina. However, there appears to be no difference between RBF values in the superior and inferior hemispheres of the retina ¹³⁹⁻¹⁴²

1.4.6 Color Doppler Imaging (CDI)

Ultrasonography is utilized in the technique of CDI. CDI is used to image vessels behind the eyeball and acquire blood flow information by simultaneously combining B-scans of tissue structure, color-coded representation of blood flow and pulse-Doppler measurements of blood velocities ¹⁴³. The color-coding varies in proportion to the velocity, with red-to-white for motion toward the probe and blue-to-white for motion away from the probe. CDI systems are unique because they use a single, multifunction probe to perform all functions. Parameters of blood flow that can be measured with CDI are peak-systolic velocity (PSV), the end-diastolic velocity (EDV), and the resistivity index ⁵⁰.

$$RI = (PSV - EDV) / PSV \dots\dots\dots 7$$

Changes in hemodynamics have been shown with the use of CDI in a variety of ocular disease conditions such as retinal artery and vein occlusions, and glaucoma. It has also been used to detect vascularization of orbital and ocular tumors ¹⁴³. CDI cannot be used to measure the diameter, and as such RBF cannot be quantified. Additionally, if excessive pressure is applied to the eyelid, this can lead to significant changes in intraocular pressure and thus, perfusion pressure and blood flow. Acquiring hemodynamic parameters has also been shown to be very subjective which may lead to measures that are not reproducible. There

appears to exist a learning effect curve with the use of CDI and thus operator experience becomes an essential factor⁵⁰.

1.4.7 Doppler Fourier Domain Optical Coherence Tomography (FD-OCT)

The RTVue Doppler FD-OCT (Optovue Inc., Fremont, CA) used in this study contains a superluminescent diode with a center wavelength of 841nm and a bandwidth of 49nm. The axial resolution is 5.6 μm in tissue and the transverse resolution is 20 μm since it is limited by optical properties of the eye. The technique utilizes a custom spectrometer, consisting of 1024-pixel high speed line-scan camera.

In addition to obtaining morphological images, the FD-OCT can detect a Doppler shift of reflected light from RBCs which provides information about blood flow^{144, 145}. The differences in phase between sequential axial scans at each pixel are calculated to determine the Doppler shift. The Doppler shift is proportional to the velocity component parallel to the axis of the probing beam and introduces a phase shift in the spectral interference pattern that is captured by the line camera¹³⁹. The quantification of TRBF requires the knowledge of the incident angle between the OCT light beam and the resultant direction of movement in a given blood vessel, which cannot be acquired from a single OCT cross-sectional scan. 3-D imaging of the vessel using more than one cross-sectional scan is required to determine the incident angle. This can be acquired with the Doppler Circular Scan Pattern (DCSP) of the RTVue Doppler FD-OCT which makes measurement of TRBF several times within a cardiac cycle (4 times per second)¹⁴⁶. The DCSP consist of two concentric circles of 3.4 and 3.75mm diameters respectively which transect all retinal vessels entering and exiting the ONH in two locations. In a single acquisition, a total of six dual circular scan frames are obtained and averaged for each ring; with 5 to 6 repeated measurements to ensure high quality scans. The Doppler angle is estimated from among other things the difference in vessel center depth between the two concentric rings in a single scan. This Doppler angle, together with the measured Doppler shift is used to calculate blood velocity, which when

combined with the vessel diameter volumetric flow can be derived. The methodology used in this study to derive retinal blood flow is a semi-automated software algorithm; Doppler Optical Coherence of Retinal Circulation (DOCTORC) ¹⁴⁷. The sum of the flows from all branch venules at one time is computed as TRBF ¹³⁹.

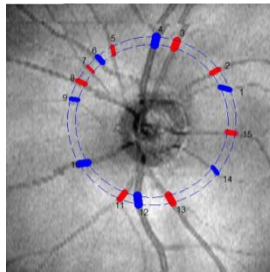


Figure 1.6: En face view of 3D OCT image showing DCSP with two concentric rings of radii 3.75 and 3.40mm. The retinal vessels are labelled from 1 to 15. The red and blue colour represents software identified vessel type as blood flowing away from the ON

1.4.8 Laser Doppler Flowmeter (LDF)

LDF can be used to measure BF in the ONH using two main methods; dynamic and scanning ^{118,148}. The dynamic method occurs when the light scattered by a tissue when a laser beam of light is focused on it forms a DSPS due to RBCs in motion. Blood flow is then calculated as,

$$BF = k \times Velocity \times Volume \quad 11$$

Where, Velocity (Hertz) and Volume are the mean speed of the RBCs moving in the sampling volume and the number of moving RBCs respectively. K, is a constant of proportionality. In the scanning mode on the other hand, a laser beam is used across a two-dimensional area of the fundus providing an image of the RBC flow in the capillaries of the optic disk and peri-papillary retina, as well as a perfused image of the neuroretinal rim of the ONH ¹⁴⁹.

1.5 Partial Pressures of Oxygen, Nitrogen and Carbon Dioxide (PO_2 , PN_2 and PCO_2)

The partial pressure of a gas (PP) in a mixture of other gases is the pressure exerted by that gas alone and is directly proportional to the rate of diffusion of the gas. The pressure of the gas in humans acts initially on the surface of the respiratory passages and alveoli and is directly proportional to the concentration of the gas molecules. Inspired air is made up of three main gases, approximately; 21% oxygen (O_2), ~0.03% carbon dioxide (CO_2) and 79% nitrogen (N_2). The total pressure of inspired air at sea level is about 760mmHg, which is termed the ‘atmospheric pressure’. PO_2 , PN_2 , and PCO_2 is thus 160mmHg (21% of 760mmHg), 600mmHg (79% of 760mmHg) and 22.8mmHg (0.03% of 760mmHg) respectively. At the level of the alveolus, PO_2 is 100mmHg. This measure is termed ‘normoxia’ or ‘baseline’.

Gases dissolved in tissues of the body move randomly and have kinetic energy; therefore, they exert a partial pressure just as they do in the gas state when it comes into contact with a surface such as a cell membrane. Besides the concentration, the solubility coefficient of the gas also determines its partial pressure. According to Henry’s law some molecules are more attracted to water molecules than others e.g. CO_2 , this makes them easily dissolved without building up excess partial pressure within a solution and vice versa in the case of molecules that are repelled by water molecules ²⁰. This is according to the equation:

$$PP = \frac{\text{Concentration of dissolved gas}}{\text{Solubility coefficient}} \dots\dots\dots 12$$

When partial pressure is expressed in atmospheres (1 atmosphere pressure = 760 mmHg) and concentration is expressed in volume of gas dissolved in each volume of water, the solubility coefficients for the three major components of inspired air are 0.024, 0.57 and 0.012 for oxygen, carbon dioxide and nitrogen ²⁰.

The change in PaO_2 and $PaCO_2$ is reflected by the change of $P_{ET}O_2$ and $P_{ET}CO_2$ respectively ¹⁵⁰. $P_{ET}O_2$ is the maximum concentration of O_2 present at the end of an exhaled breath; that is, ‘the tension of a gas in a

mixture of gases from all ventilated alveoli, including alveolar dead space, i.e. at functional residual capacity' ¹⁵¹.

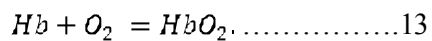
1.5.1 Diffusion of Gases Between the Gas and the Dissolved Phase

The gas present in the alveolar respiratory gas mixture is forced by its partial pressure into blood solutions of the alveolar capillaries. Dissolved gas molecules are also capable of diffusing out of the blood. The net diffusion of the gas is determined by the difference between the two partial pressures; this is usually higher in the gas phase of the alveoli for oxygen, thus resulting in oxygen molecules diffusing into the blood more than in the other direction.

1.6 Oxygen Loading & Transport

The bulk (~98%) of oxygen is carried in the body to the tissues combined with hemoglobin (Hb), while the remaining 2% is dissolved in blood plasma after diffusing from the alveoli into the pulmonary blood.

Hb consists of a protein (globin) molecule attached to four iron-porphyrin (heme) groups. Each heme group is able to carry only a single molecule of O₂; suggesting that one Hb molecule can bind a total of 4 molecules of oxygen. Oxygen binds loosely and reversibly to the heme group; the higher the PO₂ the more affinity it has for Hb. This facilitates the loading of oxygen in the lungs and the release of oxygen to the tissues:



Oxygen saturation (SO₂) is the measure of the percent amount of Hb bound to oxygen:

$$SO_2 = \frac{HbO_2}{(Hb+HbO_2)} \times 100 \dots\dots\dots 14$$

1.6.1 Oxygen-Hemoglobin Dissociation Curve (OHDC)

The relationship between PO_2 and SO_2 is graphically illustrated in the OHDC (Fig 4). Oxygen loading in the lungs and oxygen release to the tissues is facilitated by the sigmoid shape of the OHDC curve. Generally, as PO_2 increases there is a steady increase in the SO_2 . The SO_2 of systemic arterial blood is about 97% on average and 57% in the venous blood ²⁰.

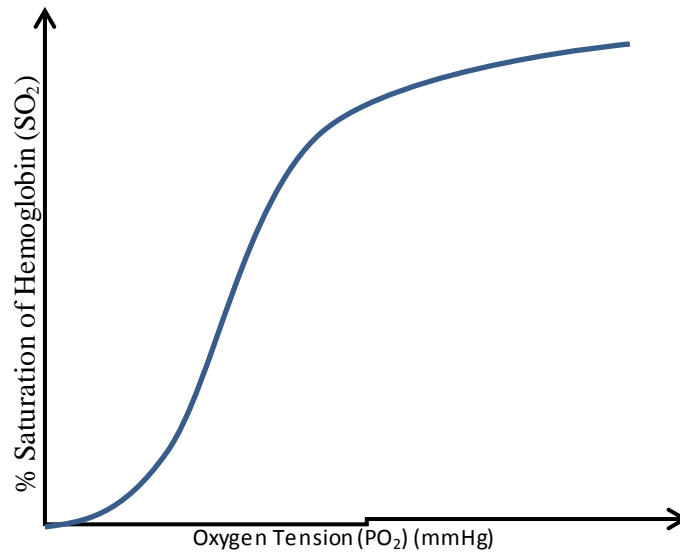


Figure 1.7 Oxygen-Hemoglobin Dissociation Curve.

1.6.2 Arteriovenous Oxygen Difference

The extent to which oxygen is consumed and subsequently removed from the blood as it passes through the body is characterized by the arteriovenous oxygen difference (AVD). AVD is the difference between the oxygen content of arterial blood and that of venous blood. It may be expressed as millilitres of oxygen per 100mL of blood ¹⁵².

Oxygen Delivery

Oxygen delivery by the retinal blood (FO_2), is the sum total of oxygen delivered to the retina from the retinal circulation. FO_2 is the product of the AVD, the RBF and the oxygen capacity of arterial blood, $0.201 \mu\text{l}/\text{min}$ ^{153,154}.

$$F O_2 = RBF * AVD * 0.201 \dots \dots \dots 15$$

1.7 Retinal Oximetry

Oximetry is the quantification of the amount of oxygen saturated within the blood of the vessels in the body tissues mostly with the use of spectral analysis techniques. In retinal oximetry, the different absorbance spectra of oxyhemoglobin (HbO₂) and deoxyhemoglobin (Hb) is quantified using light of specific wavelengths (oxygen sensitive and oxygen insensitive wavelengths) from a narrow band light source. The absorption characteristics of HbO₂ and Hb can be expressed by the extinction coefficients of Hb (Fig 1.5) ¹⁵⁵. Light penetrates to different depths of the retina depending on the wavelength of illuminating light and is generally more easily transmitted through human tissue at wavelengths between 660nm and 940nm, than it is at wavelengths below 660nm where blood significantly absorbs the light and transmits little (Fig. 1.5). 530-580nm light illuminates the retinal background and retinal vessels while wavelengths above 600nm penetrate the retinal vessels and background to the level of the choroid at 640nm ¹⁵⁶. Scattering of light occurs due to changes in the refractive index between RBCs and the blood plasma in which they are contained.

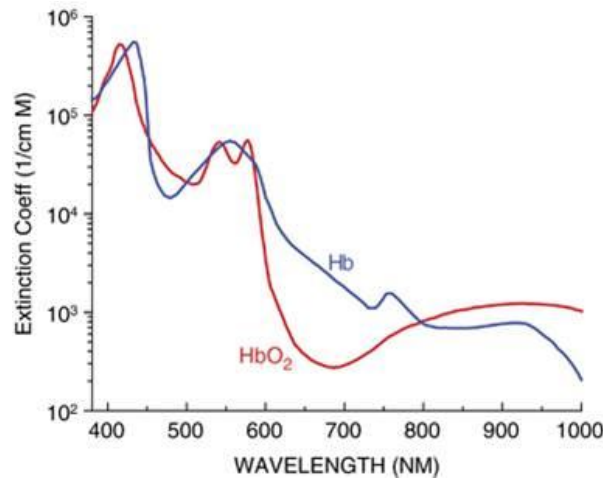


Figure 1.8 Graph displaying the absorption spectra of Hb and HbO₂

1.7.1 Principle of Retinal Oximetry & The Beer-Lambert Law

Assuming that blood is comprised entirely of HbO₂ and Hb, SO₂ can be defined as:

$$SO_2 = \frac{C_{HbO_2}}{(C_{Hb} + C_{HbO_2})} \dots\dots\dots 16$$

Where, C_{HbO₂} and C_{Hb} are the molar concentrations of oxygenated and deoxygenated haemoglobin respectively.

The Beer-Lambert law represents; the basis of spectral analysis and it explains that “the concentration of an absorbing substance in solution can be determined from the intensity of light transmitted through that solution, given the intensity and wavelength of incident light, the transmission path length, and the characteristic absorbance of that substance at a specific wavelength (extinction coefficient)” ¹⁵⁸. The attenuation of light by a sample of blood can be described as the linear sum of the attenuation of each component:

$$A_{\lambda} = \sum_{i=1}^n \epsilon_{ai} \lambda \cdot c_i \cdot d_i \dots\dots\dots 16$$

Where, ε_{ai} is the extinction coefficient due to absorption at wavelength λ, c is the concentration of the retinal chromophores (Hb and HbO₂), d is the path length travelled by the photon through the sample, and i denotes the individual chemical species in which the light travels. Measuring the attenuation at several wavelengths equal to the number of chromophores is sufficient to calculate the concentration of each particular chromophore. Difficulties arise in quantifying, d due to the high scattering and absorption characteristics of light occurring in the retina. To overcome this, multiple optical-path parameter η, and losses resulting from scattering (S), are incorporated into the Beer-Lambert law (eqn. 17). Measuring the attenuation at numerous wavelengths is therefore necessary to estimate the concentration of

chromophores. In blood oximetry, two wavelengths are sufficient to calculate SO_2 when the scattering is assumed to be independent of wavelength ¹⁵⁶.

$$A_{\lambda} = \sum_{i=1}^n S_i(\lambda) + \epsilon_{ai} \lambda \cdot c_i \cdot \eta_i \cdot d_i(\lambda) \dots \dots \dots 17$$

1.8 Historical Approaches of Measuring Retinal Oxygen Saturation

The determination of retinal oxygen saturation has proven to be very challenging ^{50, 136, 137}. Over the years, several approaches have been devised for retinal oximetry such as spectral image analysis techniques with a fundus camera, and more recently the use of ultrahigh-resolution OCT (UHR-OCT). However, there still remains the lack of a gold standard methodology for the assessment of retinal SO_2 in humans. Regardless of the technique employed, each principle of retinal oximetry is based on the differences in the absorption spectra of oxy and deoxyhemoglobin. Typically, the data output is in the form of a spectral cube (two spatial dimensions and wavelength as the third dimension) ^{13, 156, 159}. Due to spectral properties and the spatial distribution of retinal chromophores, spectral retinal images show variation in contrast with different wavelengths due to the different amounts of light absorption of oxy and deoxyhemoglobin at each wavelength. Four major methods of measuring retinal SO_2 have been discussed below; hyperspectral imaging fundus reflectance, Hickam’s photographic two wavelength method and photoelectric oximetry with three wavelengths from Delori and co-workers (1988). However, several other methods exist such as the imaging ophthalmospectrometer ¹⁶⁰, the scanning laser eye oximeter ¹⁶¹, the computed tomographic imaging spectrometer ¹⁶², the fourier transform spectral retinal imager ¹⁶³ amongst others.

1.8.1 Digital Multispectral and Hyperspectral Imaging of the Retina

Beach & co-workers (1999) developed a two-wavelength spectral imaging system which contained a beam splitter that enables the simultaneous acquisition of two retinal images which are then filtered using narrow bandpass interference filters centered at 569nm and 600nm with 4.5nm FWHM. Optical density

ratios (ODRs) were calculated and used to determine SO_2 using the linear relationship between ODRs and SO_2 ^{9, 164, 165}. The influence of fundus pigmentation was factored into the calculation of ODRs. Mean retinal venous oxygen saturation was $55 \pm 3.38\%$ in normoxia and $19.2 \pm 2.9\%$ during hyperoxia (100% inspired oxygen). This system was developed to measure SO_2 in the retinal vasculature of diabetic subjects.

More recently, Khoobei and co-workers (2004). developed a hyperspectral imaging system to evaluate relative SO_2 in the retinal vessels and ONH tissues consisting of a fundus camera with an attached prism grating prism spectrograph coupled to a CCD digital camera¹⁶⁶. A sequence of line scans across the optic disc provided spectral reflectance in the wavelength range 410-950nm. This one-dimensional information of spectral reflectance was converted into a three-dimensional data cube by moving the imaging system to obtain the second spatial dimension (Fig 1.5).

SO_2 maps were subsequently used to determine changes in SO_2 changes in retinal vessels and ONH tissues with the use of a spectral profile analysis of Hb at high and low oxygenation between 530nm and 584nm. Further improvements to this method include the inclusion of a correction factor for blood volume and variation in illumination in vessels overlying ONH and tissues¹⁶⁷. Limitations of this method include motion artifacts and the technique is poor and therefore limited to use in animals.

Simultaneous retinal images at four wavelengths have been made possible by Stefansson¹⁶⁸, an adaptation of the Beach and co-workers (1999) two-wavelength method⁹. A beam splitter allowed the replication of the original retinal image into four retinal images filtered at wavelengths of 542, 558, 586, and 605nm. Algorithms for registration and vessel detection were used to align images and detect vessels which were then subsequently used to calculate ODRs. ODRs were calculated using 586nm and 605nm retinal images based on the Beach and co-workers. technique⁹. The mean arteriolar retinal SO_2 at normoxia was $96 \pm 9\%$ and $55 \pm 14\%$ for mean venular oxygen saturation. In a state of hyperoxia, these amounts increased to $101 \pm 8\%$ and $78 \pm 15\%$. The limitations of this technique are its failure of addressing

the influence of confounding factors such as light scattering, fundus pigmentation and vessel diameter. This raises questions about validity of the method.

1.8.2 Fundus Reflectance Oximetry

One of the first studies that looked at changes in retinal SO_2 on reflectance from the fundus under monochromatic illuminations was conducted by Gloster et al. in 1967¹⁶⁹. These experiments focussed on reflectance of different colours from the choroid when the concentration and oxygenation of blood was altered. These changes to blood resulted in a change in colour to red and cyan. Incident light was filtered by three filters. The limitations of these experiments were that they were qualitative in nature and could not quantify retinal SO_2 measurements.

1.8.3 Hickam Photographic Two Wavelength Technique

In this technique of estimating SO_2 in retinal veins of humans, two-wavelength imagers (centered at 640 and 800nm, and 640 and 505nm) are utilized to illuminate the fundus¹². Absorption profiles acquired with a microdensitometer are produced with retinal images recorded on photographic film. ODRs were calculated from optical density measurements for all the wavelengths. A linear relationship between ODRs and retinal SO_2 was established with the use of isobestic (oxygen insensitive) wavelengths. The average retinal venous oxygen saturation for the 640,505nm pair was calculated as $58 \pm 10\%$ and $60 \pm 16\%$. Limitations of this technique included the influence of vessel diameter on retinal SO_2 estimation. Smaller vessels were not consistently detected in the reflectance profiles produced.

1.8.4 Photoelectric Oximeter with Three Wavelengths

Retinal SO_2 was determined in this method by utilizing a three-wavelength (558nm, 569nm and 586 nm at 7-8 FWHM) photoelectric oximeter to determine retinal SO_2 ¹⁷⁰. A fundus camera was employed with three interference filters, a photomultiplier (to enhance reflections from the fundus) and a photocathode. Light reflected from the fundus was filtered into three wavelengths centered at 558nm, 569nm and 586

nm (7-8 FWHM). This technique allows the scanning of selected retinal vessels using a slit because a small area of the fundus was illuminated at a time

1.8.5 **Image Replicating Imaging Spectrometer (IRIS) Hyperspectral Retinal Camera (Photon etc. Inc. Montreal)**

This technique allows for two-dimensional spectral and spatial information to be recorded in a single exposure ¹⁷¹. The device is a spectral demultiplexer that allows for replication of original images in multiple spectral bands onto a single detector array by employing polarizing interferometry and Wollaston prism polarizing beam splitters ¹⁵⁶. The device has a built in prototype mydriatic fundus camera with a tunable laser source (TLS) allowing for observance of the fundus at wavelengths ranging from 420 to 1,000nm with safe and comfortable illuminations. The TLS is based on the Bragg grating filtering technology allowing for rapid and accurate (<1nm) wavelength selection from the supercontinuum source. For high definition imaging, it contains a sensitive CCD camera and spectral reproducibility in time is assured with a built in calibration system ¹⁷². Two-dimensional images of the retina are recorded and registered to produce a spectral cube while assuring patient comfort and simplified calibration procedures. Other spectral cameras make use of a snapshot flash system that changes the physiology of the fundus and subsequently affects derivation of accurate retinal SO₂ ¹⁷³. The IRIS HRC however does not use a flash, thus the physiology of the retina is maintained due to its smaller bandwidth of 2nm (FWHM). The IRIS HRC has longer acquisition times compared to most other snapshot methods (80ms exposure time, 0.5s per wavelength) making it susceptible to movement artefacts and light intensity changes. This method is utilized in this study. Image cubes acquired with the HRC contain fundus reflectance profiles of nine wavelengths; 451, 540, 548, 558, 569, 586, 600, 605 and 610 for each of the two baseline phases per participant. Image cubes centered on the optic disk were acquired with the PHySpec V1.17.0 (Photon etc. Inc. Montreal, Canada) custom designed software.

1.9 Summary

The retina, unlike the choroid is autoregulated⁵⁵. The arterioles of the retina are resistance vessels that are believed to be primarily involved in perfusion processes in the retina, and the regulation of blood flow to the capillaries¹⁴, where nutrients and gases are exchanged with the tissues¹⁴⁻¹⁶. There are major structural and functional differences between the choroidal and retinal vascular systems^{21,22}.

Ocular blood flow follows Poiseuille's Law, and is affected by a number of local and systemic factors such as oxygen and carbon dioxide tension, circulating hormones, endothelial derived factors and the ANS. NO and Endothelin-1 are believed to be the most important endothelial derived relaxing and constricting factors respectively²². Over the years, several noninvasive methods of quantifying ocular hemodynamics have developed and have then been applied to determine the magnitude of response to external biologic stimuli. The RTVue Doppler FD-OCT (Optovue Inc. Fremont, CA) is unique in that it provides the capability of quantifying TRBF non-invasively through the detection of Doppler shift of reflected light from RBCs with the DCSP and semi-automated DOCTORC software.

Like RBF, several approaches have been devised for the measurement of retinal blood SO_2 in the scientific literature^{3, 64, 65}. These methods were spearheaded by Hickam and co-workers in the 1960s¹², but is yet to be mastered as a technique that is reliable and useful clinically. The IRISTM Hyperspectral imaging device (Photon etc. Inc. Montreal, Canada) (IRIS HSRC) makes possible the measurement of retinal SO_2 through the localization of structures in the retina using their specific spectral signatures through non-invasive means. At specific wavelengths in the visible spectrum (e.g. 585 nm) there is strong absorption by the hemoglobin, which enhances the contrast of blood vessels. Oxygenated (oxyhemoglobin) and deoxygenated hemoglobin (deoxyhemoglobin) show different absorption spectra, thus making it possible to distinguish between arterioles (A) and venules (V)¹⁷⁴. This process is known as retinal oximetry and is based on spectral analysis techniques according to the Beer-Lambert Law which makes use of specific oxygen sensitive and insensitive wavelengths from light-emitting diodes (LEDs).

The IRIS HSRC allows for two dimensional spectral and spatial information to be recorded in a single exposure ¹⁷¹. Unlike other oximetry snapshot systems, the IRIS HSRC does not make use of a flash, thus ensuring equi-luminance due to its smaller bandwidth of 2nm (FWHM). Retinal oximetry is a relatively novel technique which is still at 1st base in terms of practical development.

Several major ocular diseases such as retinopathy of prematurity (ROP), retinitis pigmentosa, age-related macular degeneration (ARMD), diabetic retinopathy (DR) and glaucoma ^{175,176} have been shown to have components of reduced OPP, blood flow deficits and subsequent hypoxia. Therefore, the essential role of blood flow and oxygen in maintaining ocular health cannot be underestimated. RBF varies inversely, while SO₂ varies directly with the partial pressure of arterial oxygen (PaO₂) to maintain retinal oxygenation at a relatively constant level ¹⁷⁷. Studies that provide data on TRBF and retinal SO₂ with stepwise changes in PaO₂ in conditions of hypoxia and hyperoxia would provide significant knowledge into understanding blood flow physiology and possibly the mechanism of various major ocular disease processes and their diagnosis. Additionally, it would bring us a step closer to providing a gold standard for routinely measuring oxygen and blood flow changes in human ocular disease conditions.

2 Rationale, Hypotheses and Aims

ide a greater insight into the pathophysiology of ocular disease processes and may aid diagnosis and management. FD-OCT provides the means for quantification and detection of early retinal morphometric changes associated with major retinal and systemic diseases. It also allows for the assessment of the effectiveness of new treatment regimens through the provision of non-invasive, 3-dimensional, high-resolution, histological details of the ONH and the retina of the living human eye ¹⁷⁸. The potential of FD-OCT technology to provide information on the vascular function of the retina and ONH, however, has yet to be fully exploited. Using the new and unique methodology of the Doppler FD-OCT it is possible to measure TRBF with the use of the Double Circular Scan Protocol (DCSP) which estimates the Doppler angle (incident angle between the OCT light beam and the blood vessel) unlike most other blood flow devices. Doppler FD-OCT however has yet to be fully tested and validated.

This study is further unique in its use of the combination of a computer-controlled gas sequencer that allows the implementation of precise combinations of oxygen and CO₂ concentrations as provocative stimuli that provoke blood flow change, and the quantification of retinal blood flow techniques which deliver a much improved signal-to-noise ratio compared to previous methods; this in turn provides reliable and highly reproducible data. The systemic arterial gas composition was manipulated using a sequential rebreathing circuit (HiOx-80, VIASYS Healthcare Inc.) connected to an automated gas blender (Respiract™, Thornhill Research Inc., Toronto, Canada) to provoke hyperoxic and hypoxic conditions ¹⁷⁹. This allowed the examination of the effect of the provocation on vascular beds in the retina.

Hyper-spectral retinal imaging offers the potential to non-invasively quantify retinal blood SO₂ disturbances in the retina prior to the development of clinically visible disease and potentially prior to the development of any morphometric change ¹⁸⁰. This spectral imaging technique can be used to detect and quantify various metabolic “signatures”, or molecular spectral absorbance profiles, in the retinal tissue ¹⁸⁰. The hyperspectral retinal camera (HRC) prototype used in this study is unique in that it does not employ a

flash, like other snapshot hyperspectral techniques. The use of a flash bleaches the photopigments and subsequently alters the reflective properties of the retina. Research in the area of spectral imaging of the retina, and more specifically, quantifying retinal ODRs, remains in the early stages despite methods being established as far back as the 60's. The HRC prototype device has the potential of bringing revolutionary change in this field; however, it requires further studies for validation of the technique.

RBF and retinal SO_2 are closely related hemodynamic measures, in that, the bulk of oxygen produced by the human body is carried attached to Hb molecules of the RBC's. RBF is very commonly used as a substitute measure for tissue oxygenation and metabolism, however, at this time we cannot assume that retinal blood SO_2 can be directly quantified routinely with current blood flow measuring technologies^{175, 181}. Oxygen utilisation is a function of blood SO_2 and blood flow. Optical density ratios of blood allow us to potentially measure retinal SO_2 through the relationship between ODR and SO_2 . TRBF varies inversely with $P_{ET}O_2$ to keep retinal SO_2 fairly constant^{3, 3, 177}. Normative data of TRBF and especially retinal SO_2 for novel devices such as the Doppler FD-OCT and HRC are required for validation needs. This is the first study to the best of our knowledge reporting measurements of retinal blood SO_2 and TRBF with the Doppler FD-OCT and HRC with stepwise changes in $P_{ET}O_2$ using the full range of retinal vascular reactivity on healthy participants. The results of this study will elucidate a more comprehensive understanding of retinal vascular physiology and provide further validation data for the Doppler FD-OCT device and the HRC.

In turn, the work should lead to improved understanding of the vascular pathogenesis of ocular disease.

2.1 Hypotheses

The hypothesis for Chapter 3 is that the 605/586 wavelength combination out of the three ODRs (600/569, 610/548 and 605/586) being considered, will show the least variation (range \pm standard deviation) in arterioles and venules based on previous literature and pilot studies conducted in our lab. The 605/586 wavelength combination will provide the least variable ODR for estimating retinal blood SO_2 in future studies with our prototype oximeter.

In Chapter 4, the hypothesis is that TRBF will decrease as retinal blood SO_2 is increased in healthy participants.

2.2 *Aims*

The aim of the study in Chapter 3 is to determine the least variable (range \pm standard deviation) wavelength combination (610/548, 600/569 and 605/586) and subsequent ODR with the prototype HRC device.

In Chapter 4, the specific aims of the study are to:

1. Quantify retinal blood SO_2 (in arterioles and venules) with the chosen wavelength combination in healthy participants.
2. Investigate the relationship between retinal SO_2 and retinal blood flow in healthy participants.

3 Optical Density Ratio (ODR) Variability with a Novel Hyperspectral Retinal Camera (Photon etc. Inc. Montreal)

3.1 Introduction

Oximetry methods have been used to determine the SO_2 of blood perfusing human tissues for several decades^{12, 17, 18, 30, 154, 182, 183}. In healthy individuals, the spectroscopic techniques for determining retinal blood SO_2 have been shown to produce values that are reliable, stable^{30, 168} and are able to show change in retinal vessel SO_2 in numerous eye diseases such as retinal vein occlusions¹⁸⁴, diabetic retinopathy¹⁸⁵⁻¹⁸⁷ and glaucoma^{10, 188}. Retinal oximetry has also demonstrated systemic hypoxia in Eisenmenger syndrome¹⁸⁹.

Central to retinal oximetry is the use of optical density, i.e. $\log(I_0/I)$ and subsequent ODRs of oxygen sensitive and insensitive (isobestic) wavelengths, made possible by the different absorbance spectra of HbO_2 and HbO of light reflected from the surface of the retina. Retinal oximetry is affected by several extraneous factors such as light scattering, diffusion of light resulting from the choroid, lack of uniformity in the background pigment with wavelength, corneal reflections¹⁹⁰, retinal nerve fiber bundle induced reflectance variations and the close proximity of vessels, eye movements, pupil edge light scattering and pigment clumping.

Spectral analysis techniques such as retinal oximetry require the choice of specific wavelengths, a critically important specification for reliable and optimal measurements of optical density^{170, 191, 192}. Previous studies on retinal oximetry by photographic means have made use of two wavelengths; one oxygen sensitive wavelength (large difference in the extinction coefficients) and one isobestic wavelength (oxygen insensitive wavelength) to derive the ODR (fig 1.5)³⁰.

The spectral content of reflected light depends on not only the retinal blood SO_2 , but also on the blood concentration, layer thickness and scattering of light inside the blood vessel lumen, including the number

of passes through the vessel (i.e. 1 or 2). There is strong absorption by Hb wavelengths around, for example, 585 nm (Fig 1.5), which enhances the contrast of blood vessels. The change in contrast and intensity at two wavelengths chosen enables the derivation of SO_2 ; that is, between oxygenated and non-oxygenated blood ¹⁹³.

Various studies have made use of different wavelength combinations. Hickam and co-workers (1963) employed modified fundus cameras and used two different wavelength combinations in the first retinal oximetry experiments. Broadband (>100nm FWHM) Wratten filters at 800 and 640nm in a red-infrared instrument and in later experiments wavelengths of 640 and 510nm were employed by a red-green instrument using interference filters (10nm FWHM) ¹². Manual analysis of exposed films was used to measure the optical densities of vessels ¹⁶¹. A similar device reported by Cohen and Laing employed a blue-green combination centered at 470 and 515nm, with interference filters (20nm FWHM) ¹⁹⁴. A retinal vessel oximeter was reported by Delori in 1988 that made use of three wavelengths; 558, 569, and 586nm. Tiedeman and co-workers (1998). also developed a retinal oximeter which illuminated filtered light (8nm FWHM) at 569 and 600nm. Images were acquired on a CCD camera with a high dynamic range ¹⁹⁵. Retinal vessel oximeters making use of diode lasers at 670 and 803nm as a source of light was first reported by Smith and co-workers (1998) ¹⁶¹. More recently, the Oxymap T1 (Oxymap ehf., Reykjavik, Iceland) retinal oximeter by Geirsdottir and co-workers (2012) ¹⁵³ based on the earlier approach of Beach (1999) ⁹ is able to simultaneously produce two fundus images with two different wavelengths (570 and 600nm; 5nm FWHM) of light at identical locations in the retina. This device consists of two digital cameras. Hardarson and co-workers (2006) ¹⁶⁸ using the same method of Beach and co-workers (1999), used two retinal oximeters composed of a fundus camera coupled to a digital camera with a beam splitter in further experiments. A 586 and 605nm wavelength combination was used (5nm FWHM). In this study, a novel HRC with a prototype fundus camera, a tunable laser source based on the Bragg grating filtering technology and a high definition CCD camera with a bandwidth of 2nm (FWHM) was used. Three wavelength combinations (ODRs) have been separately employed (600

and 569nm, 605 and 586nm, 610 and 548nm) for the analysis of retinal oximetry. Other spectral cameras make use of a snapshot flash system that bleaches the photopigments and therefore alters reflectance characteristics of the fundus due to uneven illuminations and subsequently affects derivation of accurate ODR readings¹⁷². The HRC does not use a flash, thus avoiding major bleaching of the photopigment during image acquisition.

Authors/Technical System	Wavelength (nm)	Calibration	Arterial SO₂	Venous SO₂	Other
<i>Hickam et al.</i> ^{1,2,3} Photographic	640,800	Hypoxia		58% ± 10%	
<i>Tiedeman et al.</i> ⁴ Digital	640,505	Hypoxia		60% ± 16%	Considered diameter and fundus pigmentation in calculations
<i>Hardarson et al.</i> ⁵	586, 605	Published arteriolar and venular SO ₂ measures from previous works**	96%±9%	55% ± 14%	
<i>Beach et al.</i> ⁶	600,569	Hypoxia		55%±3.39%	

<i>Delori et al.</i> ⁷	586,569,558	Published	98% ± 8%	45% ± 7%	Used scattering factor; considered hematocrit, diameter, and fundus pigmentation in calculation
Photoelectric		extinction coefficients			
<i>Schweitzer et al.</i> ⁸	510 to 586	Model	92.2% ± 4.1%	57.9% ± 9.9%	Multitude of wavelengths used to minimize error
Imaging spectroscopy		function separating the effects of transmission and reflection			
<i>Smith et al.</i> ^{9,10,11}	488, 635, 670, 830	In vitro model			Triggered by electrocardiogram
Multispectral confocal					
*SLO					

*Lompado et al.*¹²

*Denninghoff et al.*¹³

Heaton et al.¹⁴

<i>De Kock et al.</i> ¹⁵	660, 940	In vitro	97%
Pulse		model	

<i>Cohen and Laing</i> ¹⁶	470, 515	Rabbits	
Photographic			

*SLO – Scanning Laser Ophthalmoscope

Table 3.1 Wavelength Combinations Used by Various Investigators^{13,190}

There has not been any well-defined standard criterion reported for the determination of the best wavelength pairs for use in retinal oximetry. However, the commercial availability of sources of light that produce the desired wavelengths (red or near infrared) appears to be used as one of the selection criteria. Diode lasers are usually the light source of choice for use in retinal oximetry instruments¹⁶¹. Fundus reflectance variation is predominantly from the retinal pigment epithelium because of high choroidal absorption^{170, 191}. Wavelengths more than 640nm, show non-uniformity of fundus background reflection with poor vessel detection due to poor contrast and the colour of the fundus becomes more spatially variable and additionally, transmittance is fairly low at wavelengths longer than ~920nm¹⁹⁶. At wavelengths lower than 520nm, the measured signals are generally too small and thus too noisy for further interpretation. There is also light scattering in the ocular media especially in vessel walls, low fundus reflectance and retinal exposure limits exist at wavelengths below 450nm¹⁷⁰. Retinal surface reflections are pronounced between 450 and 580nm especially in young individuals^{170,191}. Large surface reflections result in minimal to no contribution to reflectance from deeper layers leading to errors in retinal SO₂ calculations¹³. The extinction coefficients of Hb and HbO₂ decrease drastically between 580

and 600nm¹⁵⁵ resulting in poor contrast images and subsequent difficulty in detecting retinal vessels¹⁷⁰. All things being considered, wavelengths from 450nm - 1000nm (inclusive) appear to be the most accepted and widely used range (within limits) of wavelengths for retinal oximetry¹⁶¹. The choice of wavelength combinations for our studies was largely dependent on results from preliminary studies within the lab and elsewhere.

Assumptions made in previous studies are that the contributions of numerous other Hb derivatives (e.g. methemoglobin, carboxyhemoglobin, sulphhemoglobin) present in the blood are insignificant. This same assumption will hold in this study.

The hypothesis for this study is that the 605 and 586nm wavelength combination will provide the most consistent ODR to estimate retinal SO₂ in arterioles and venules in terms of least variation (range ± standard deviation). This hypothesis is based upon previous literature and prior pilot studies conducted within our lab with the prototype HRC device. Each wavelength combination will be assessed using healthy participants over a series of stepwise changes in values.

3.2 *Materials and Methods*

3.2.1 **Sample**

Ethical clearance was obtained from the University Health Network Research Ethics Board, Toronto and the University of Waterloo Office of Research Ethics prior to the commencement of the study. After explaining the study and its possible consequences to each study participant, informed consent was obtained according to the Declaration of Helsinki. The study sample was made up of ten healthy individuals (five males and five females) between the ages of 23 and 37, with an average age 28.3 years (SD 3.90) who were recruited from the School of Optometry and Vision Science, University of Waterloo and Department of Ophthalmology and Vision Sciences, University of Toronto. Of the 10 recruited, 1 was of Middle Eastern, 3 were Black/African, 2 were Asian, 2 were White and 2 were of Indian descent. The right eye of each participant was chosen for the study for convenience of use with the prototype HRC.

Participants with distance refractive errors $> \pm 6.00$ DS and/or ± 2.50 DC, any indication or history of chronic / serious eye disease (glaucoma, diabetes, or any ocular disease permanently affecting vision or requiring surgery) in self or first degree relative or systemic disease (endocrine disorders, hypercholesterolemia, etc.), stroke or chronic obstructive/restrictive lung disease such that the volunteer is unable to walk up 2 flights of stairs or on any medications with known vascular effects (antioxidants, blood pressure medication, etc.) were excluded from the study. In addition, participants who were unable to cope with the breathing protocol e.g. due to claustrophobia, those who were habitual smokers (or quit smoking within past 6 months) or those who showed non-compliance with prescribed anti-seizure medication or who demonstrated a resting arterial SO_2 while breathing room air $< 95\%$ were also excluded. Additionally, participants were asked to abstain from vitamin C, caffeine, red meat, chocolate, alcohol and exercise for at least 12 hours prior to the study visit.

3.2.2 Study Visits

Participants attended a single visit scheduled between 9am and 11am for all participants. Retinal blood ODR measurements were taken with the HRC

3.2.2.1 Novel Hyperspectral Retinal Camera

This prototype device allows for two-dimensional spectral and spatial information to be recorded in a single exposure¹⁷³. The instrument comprises a custom-made mydriatic fundus camera with a tunable laser source (TLS) allowing for observance of the fundus at wavelengths ranging from 420 to 1,000nm at safe and comfortable illumination levels without the need for flash illumination. The TLS is based on the Bragg grating filtering technology from Photon etc. which allows for rapid and accurate (<1nm) wavelength selection from the supercontinuum source from 400 to 1000nm with a bandwidth of 2.5nm (FWHM). For high definition imaging, it contains a sensitive CCD camera and spectral reproducibility in time is assured with a built in calibration system¹⁷¹. The CCD sensor has a dynamic range of 14bits, and pixel scan rate and data rate of 12MHz/24MHz and 19.5 Mpixel/s, respectively. The spectral range of the sensor is 290nm to 1100nm. Two-dimensional images of the retina are recorded and registered to produce a spectral (i.e. third dimension is colour) cube while assuring patient comfort. The image capture time of the HRC is 80ms. A 2x2 binning mode was used with an effective pixel resolution of 696x520 pixels.

3.2.2.2 Gas Delivery System (*RespirAct™*, Thornhill Research Inc., Toronto, Canada)

The gas delivery system employed in the study was made up of a sequential re-breathing gas delivery circuit (Hi-Ox80, Viaya Healthcare, Yoruba Linda, CA). The circuit which was attached to participants via a facemask was made up of a commercial 3-valve oxygen delivery system with a rebreathing bag on the exhalation port. Participants breathed previously exhaled gas from the rebreathing bag when the contents of the fresh gas reservoir were depleted. The circuit was in turn connected to an automated gas

flow controller (RespirAct™, Thornhill Research Inc. Toronto, Canada) and blender that has been primarily developed and employed for the purposes of gas provocation by the Fisher laboratory at University of Toronto for over a decade. Similarly, Hudson laboratory have contributed to the development of the instrument from the beginning and have used it for over a decade. The device enables the precise control of the partial end tidal pressures of oxygen ($P_{ET}O_2$) and carbon dioxide ($P_{ET}CO_2$). By modulating the inspired portion of oxygen and carbon dioxide, it is possible to accurately and repeatedly generate stable controlled and safe levels of hypoxia and hyperoxia. This technique uniquely targets exact pre-determined $P_{ET}O_2$ levels and sustains them while maintaining isocapnia over the pre-determined phase duration, irrespective of the individuals' respiratory rate. $P_{ET}O_2$ and $P_{ET}CO_2$ accurately measure PaO_2 and $PaCO_2$, respectively, when breathing using the RespirAct™ sequential re-breathing gas delivery system^{197, 198}. The benefits of using this technique include the avoidance of under or overshooting the desired $P_{ET}O_2$ and $P_{ET}CO_2$, hence the consistency of data is improved. Also, safety improves since the risk of overshooting the target end tidal gases into dangerous levels are eliminated providing improved safety, sustained systemic blood gases and comfort for participants. Participants' SO_2 levels were carefully and continuously monitored while using this device. If the subject was uncomfortable or deemed at risk in any way the experiment was immediately terminated and 100% O_2 was administered.

Healthy young participants underwent spectral imaging of the retina and ONH for a series of stepped hypoxic and hyperoxic stimuli by varying the inspired portion of oxygen. For the hypoxic provocation, the study necessitated the use of a hypoxic stimulus of a $P_{ET}O_2$ of 50 mmHg to provide effective dissociation of hemoglobin, which would be detectable at the level of retina. $P_{ET}O_2$ was varied between baseline/normoxia (equivalent to sea level) and 50, 60 and 80mmHg. An end-tidal O_2 of 50 mmHg is commonly used in physiological studies. For the hyperoxic provocation, $P_{ET}O_2$ steps of 200, 300 and 400mmHg were used to provide adequate vasoconstriction of the retinal arterioles.

3.2.3 Study Procedure

Participants were seated for 15 minutes to allow stabilization of their hemodynamic parameters (heart rate and blood pressure) during which time they underwent a period of air-breathing. Medical tape (Tegaderm; 3M Health Care, St. Paul, MN) was used to seal the facemask to the participants face. The facemask was connected to the RespirAct™ sequential re-breathing gas delivery system. At the end of this stabilization period, pulse rate, resting blood pressure, retinal ODR and SPO₂ measurements were taken at normoxia/baseline. Pulse rate, SPO₂ and blood pressure were continuously monitored concurrently every 2.5 minutes using a rapid response critical care gas analyzer (Cardiicap 5, Datex-Ohmeda, Helsinki, Finland) and transmitted electronically to a data acquisition system (S5 Collect, Datex-Ohmeda, USA). Two baseline ODR measurements were taken (BL1 and BL 2). During testing, the conditions in the lab were kept stable at an absolute pressure of 101.325 kPa (14.696 psi, 1 atm) and temperature of 20 °C (293.15 K, 68 °F). The study procedure is depicted diagrammatically in Appendix A.

3.2.4 Statistical Analysis

3.2.4.1 Measuring ODR with the HRC Device

Retinal blood oximetry measurements were made in one major retinal arteriole and venule pair in the superonasal quadrant 1-2 disc diameters away from the ONH. The analysis was done by comparing the reflected light intensity within a vessel to the intensity of light in the adjacent retina at isobestic (oxygen insensitive) and oxygen sensitive wavelengths. The Image J line tool was used to accurately determine the x, y coordinate of the selected point on the retina for blood SO₂ measurements (Fig 3.1). A line (three times the width of the vessel) was drawn perpendicular to the blood vessel and with customized macros using Image J (NIH) software. The value of maximum intensity of light reflected from the adjacent retinal background and the minimum value on the vessel measurement site (vessel intensity) are used to calculate OD and ODRs. This method of calculating ODR was adopted from Beach and co-workers (1999)⁹ due to the current absence of a better algorithm.

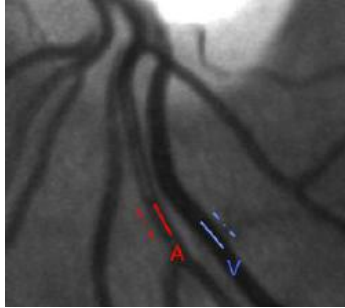


Figure 3.1 The intensity of light reflected from the vessel is compared to that of the adjacent retina for both arterioles and venules

$$OD = \log\left(\frac{I_0}{I}\right) \dots\dots\dots 18$$

Where, I_0 is the intensity of light within the vessel

I is the intensity of light of the adjacent retina

$$ODR = \frac{OD_{os}}{OD_i} \dots\dots\dots 19$$

Where, OD_{os} is the optical density at an oxygen sensitive wavelength and

OD_i is the optical density at an isobestic (oxygen insensitive) wavelength

Image processing techniques were carried out with the PHySpec V1.17.0 software on the acquired images so as to normalize and remove artifacts. The optic disk and superonasal regions of the fundus were then selected with the rectangle tool. The image cubes were then registered using a cross-correlation technique, with the 586nm image as reference. All other structures in the images were aligned to the coordinates of the reference image. Images were rotated and translated while comparing to the reference image for maximum cross-correlation. Image correction was done to stabilize and remove eye movement artifacts from image cubes.

Baseline (BL) measures of ODR were taken twice per study visit (BL 1 and BL 2). These baseline ODR measures were averaged to achieve mean baseline for each wavelength combination; 600/569nm, 605/586nm, 610/ 548nm for all 10 participants. The range and SD of mean baseline ODR for each wavelength combination was also calculated to determine the variation per participant for each of the 10 participants. In addition, the mean, range and SD of each baseline ODR measure (BL1 and BL2) were compared for each wavelength combination for all 10 participants to determine the variation. Results for arterioles and venules were computed separately for each wavelength combination. Due to the relatively small sample size, outliers (data points falling outside the 25th to 75th percentile) were maintained in the analysis. Statistica software (StatSoft, Inc., Tulsa, OK, USA) version 8.0 and Microsoft Excel 2010 was used for analysing the data.

3.3 Results

3.3.1 ODR Variation in Arterioles for All Participants Comparing All Three Wavelength Combinations

In arterioles, the group range (\pm SD) of ODR values for baseline measurements for $n=10$ ($P_{ET}O_2$ of about 100mmHg) was 0.169 ± 0.061 for the 605/586 wavelength combination, 0.371 ± 0.099 for the 600/569 wavelength combination and 0.340 ± 0.104 for the 610/548 wavelength combination (Table 3.2). The baseline ODR in arterioles for all three wavelength combinations (605/586, 600/569, 610/548) as a function of participant ID are shown in Figure 3.2.

Participant ID#	Mean Baseline ODRs in Arterioles for All Three Wavelength Combinations, 600/586, 600/569 and 610/548 (n=10)		
	600/586	600/569	610/548
01	0.549	0.613	0.597
02	0.678	0.718	0.622
03	0.665	0.792	0.746
04	0.607	0.791	0.706
05	0.530	0.682	0.548
06	0.586	0.681	0.560

07	0.549	0.741	0.529
08	0.595	0.785	0.657
09	0.671	0.752	0.612
10	0.699	0.984	0.869
Mean	0.613	0.754	0.644
Range (Max-Min)	0.169	0.371	0.340
SD	0.061	0.099	0.104

Table 3.2 Arterioler ODR at mean baseline for 605/586, 600/569 and 610/548 for n=10

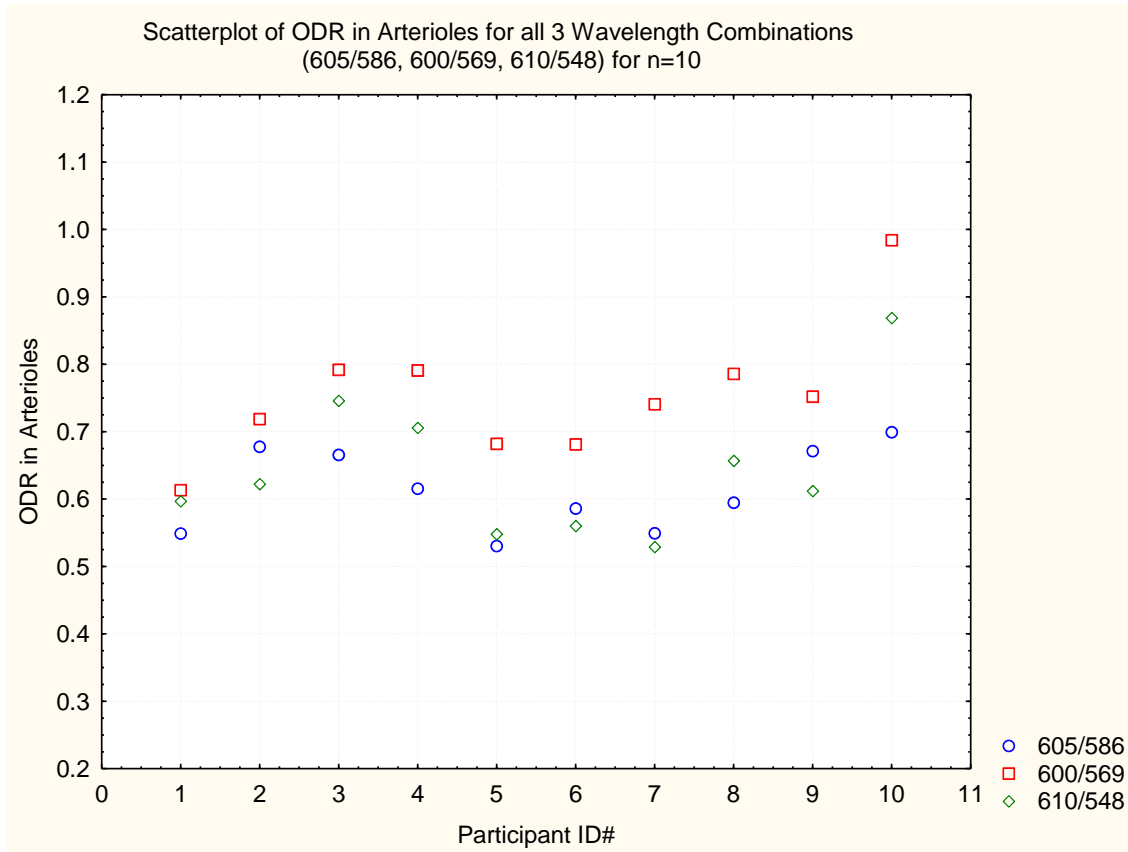


Figure 3.2 Baseline ODR in arterioles for all three wavelength combinations (605/586, 600/569, 610/548) for n=10

3.3.2 ODR Variation in Venules for All Participants Comparing All Three Wavelength Combinations

In venules, the group range (\pm SD) of ODR values for baseline measurements for n=10 ($P_{ET}O_2$ of about 100mmHg) was 0.600 ± 0.198 for the 605/586 wavelength combination, 0.569 ± 0.169 for the 600/569 wavelength combination and 0.819 ± 0.274 for the 610/548 wavelength combination (Table 3.3). The baseline ODR in venules for all three wavelength combinations (605/586, 600/569, 610/548) as a function of participant ID are shown in Figure 3.3.

Participant ID#	Mean Baseline ODRs in Venules for All Three Wavelength Combinations, 600/586, 600/569 and 610/548 (n=10)		
	600/586	600/569	610/548
01	0.286	0.347	0.289
02	0.739	0.667	0.878
03	0.867	0.833	1.100
04	0.544	0.621	0.870
05	0.515	0.544	0.486
06	0.434	0.469	0.462
07	0.268	0.281	0.281
08	0.320	0.378	0.459
09	0.481	0.637	0.691
10	0.646	0.851	0.747

Mean	0.510	0.563	0.626
Range (Max-Min)	0.600	0.569	0.819
SD	0.198	0.196	0.274

Table 3.3 Venular ODR at Mean Baseline for 605/586, 600/569 and 610/548 for n=10

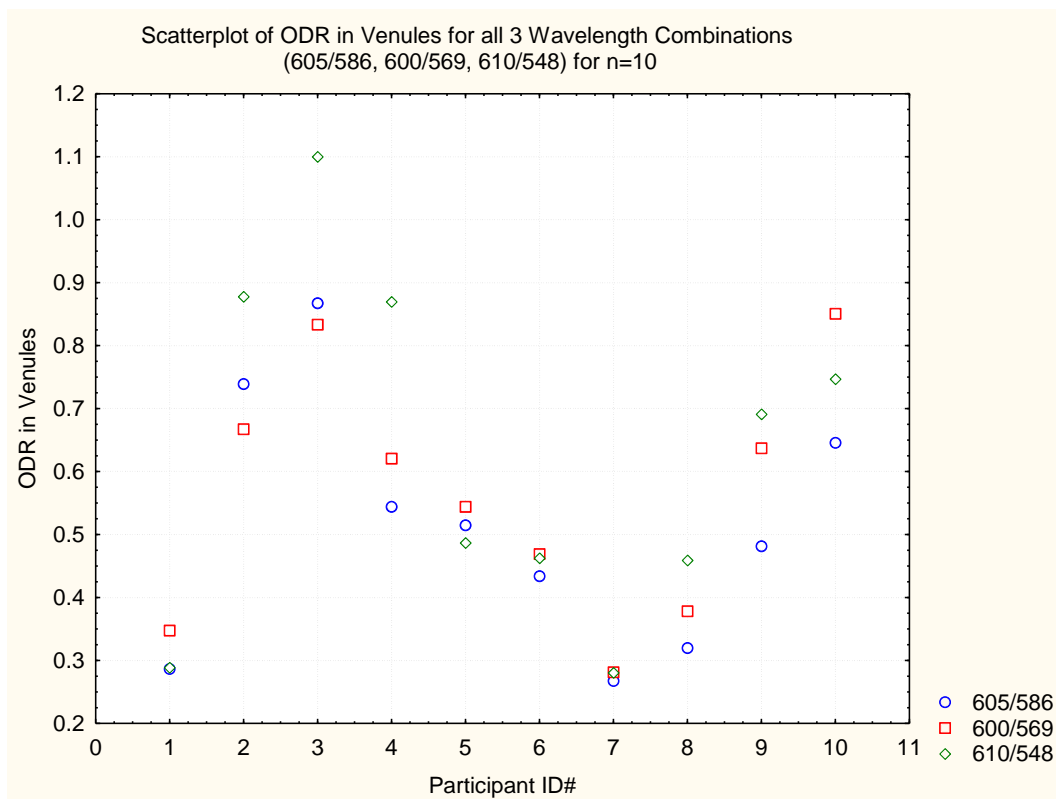


Figure 3.3 Baseline ODR in arterioles for all three wavelength combinations (605/586, 600/569, 610/548) for n=10

3.3.3 Comparison of Variation Between Baseline Measurements for All Participants and Wavelength Combinations

3.3.3.1 605/586 Wavelength Combination

In arterioles, the group range (\pm SD) of ODR values of the 605/586 wavelength combination at baseline 1 and 2 was 0.607 ± 0.224 and 0.619 ± 0.158 respectively. In venules the group range (\pm SD) of ODR at baseline 1 and 2 was 0.289 ± 0.750 and 0.284 ± 0.729 respectively (Table 3.4). The baseline 1 and 2 ODRs for the 605/586 wavelength combination as a function of participant ID are shown in Figure 3.4 and 3.5 for arterioles and venules, respectively.

	Variation in Baseline ODR with 605/586 (n=10)			
Participant ID#	Arteriole		Venule	
	BL 1	BL 2	BL 1	BL 2
01	0.532	0.565	0.289	0.284
02	0.659	0.696	0.750	0.729
03	0.635	0.696	0.845	0.889
04	0.607	0.607	0.530	0.558
05	0.488	0.572	0.514	0.516

06	0.601	0.571	0.429	0.439
07	0.560	0.539	0.252	0.283
08	0.599	0.590	0.305	0.335
09	0.677	0.665	0.494	0.469
10	0.712	0.686	0.673	0.618
Mean	0.607	0.619	0.508	0.512
Range (Max-Min)	0.224	0.158	0.593	0.606
SD	0.068	0.061	0.200	0.196

Table 3.4 Variation in Baseline ODR with 605/586 (n=10) in arterioles and venules

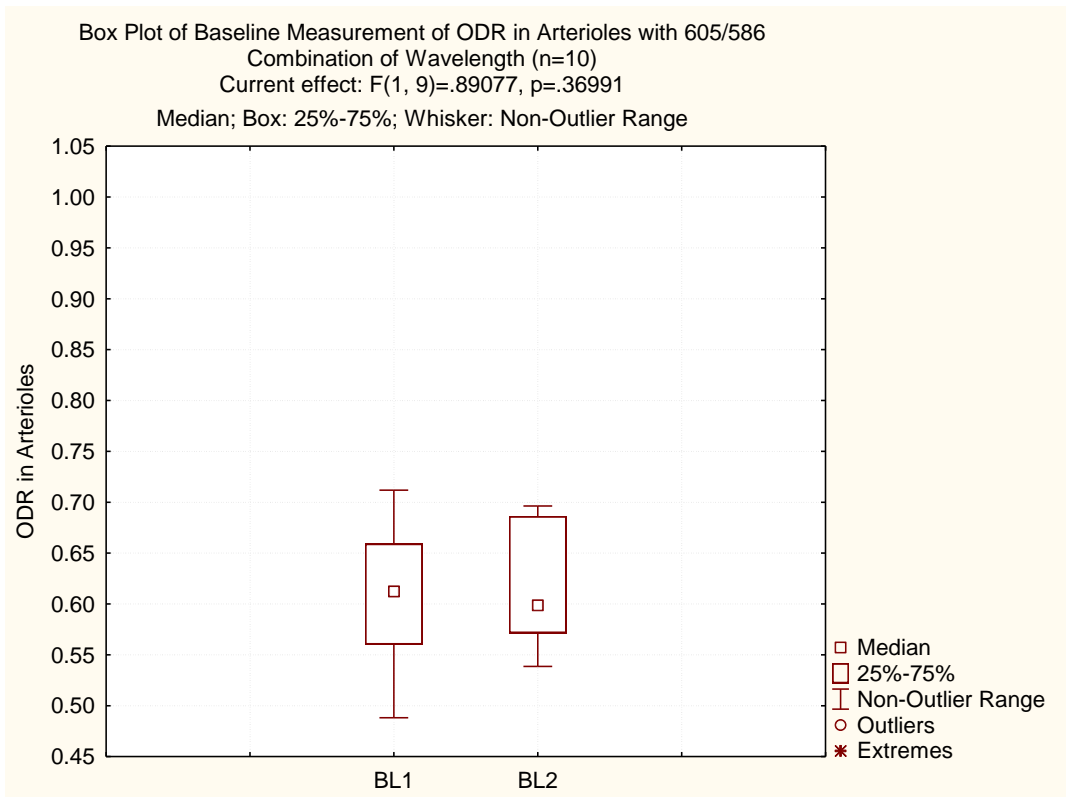


Figure 3.4 Boxplots representing repeat baseline measurements of ODR in Arterioles with 605/586

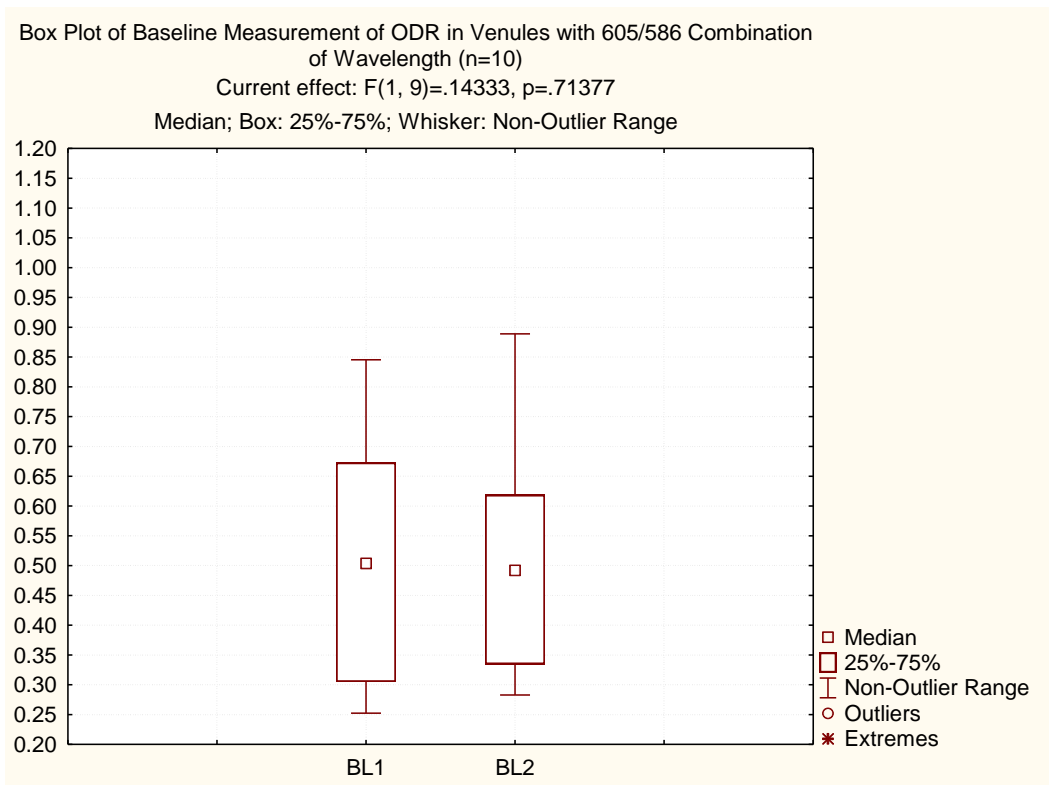


Figure 3.5 Boxplots representing repeat baseline measurement of ODR in venules with 605/586

3.3.3.2 600/569 Wavelength Combination

In arterioles, the group range (\pm SD) of ODR values with the 600/569 wavelength combination at baseline 1 and 2 was 0.747 ± 0.350 and 0.761 ± 0.391 , respectively. In venules the group range (\pm SD) of ODR at baseline 1 and 2 was 0.329 ± 0.675 and 0.366 ± 0.659 , respectively (Table 3.5). The baseline 1 and 2 ODRs for the 600/569 wavelength combination as a function of participant ID are shown in Figure 3.6 and 3.7 for arterioles and venules, respectively.

Participant ID#	Variation in Baseline ODR with 600/569 (n=10)			
	Arterioler		Venular	
	BL 1		BL 2	
01	0.607	0.619	0.329	0.366
02	0.717	0.720	0.675	0.659
03	0.825	0.759	0.843	0.823
04	0.759	0.822	0.601	0.640
05	0.667	0.697	0.573	0.514
06	0.691	0.671	0.476	0.462
07	0.769	0.713	0.284	0.279
08	0.729	0.842	0.400	0.356
09	0.746	0.758	0.665	0.609

10	0.957	1.011	0.836	0.865
Mean	0.747	0.761	0.568	0.557
Range (Max-Min)	0.350	0.391	0.559	0.586
SD	0.095	0.110	0.196	0.197

Table 3.5 Variation in Baseline ODR with 600/569 (n=10)

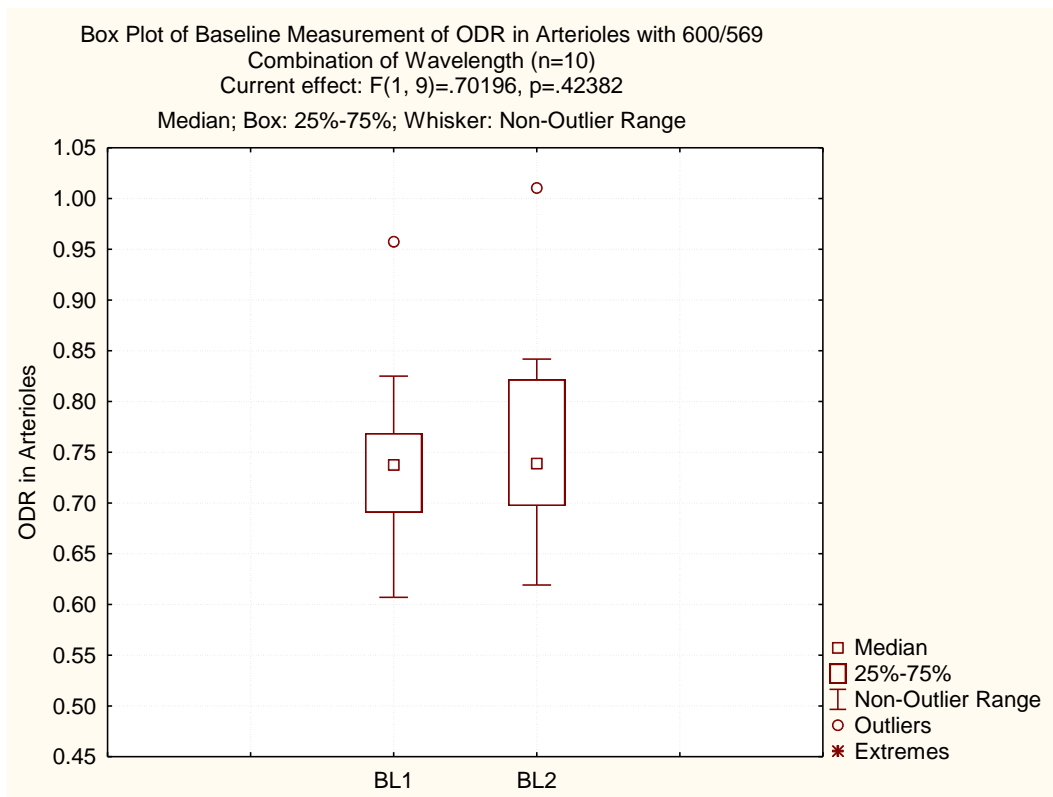


Figure 3.6 Boxplots representing repeat baseline measurements of ODR in Arterioles with 600/569

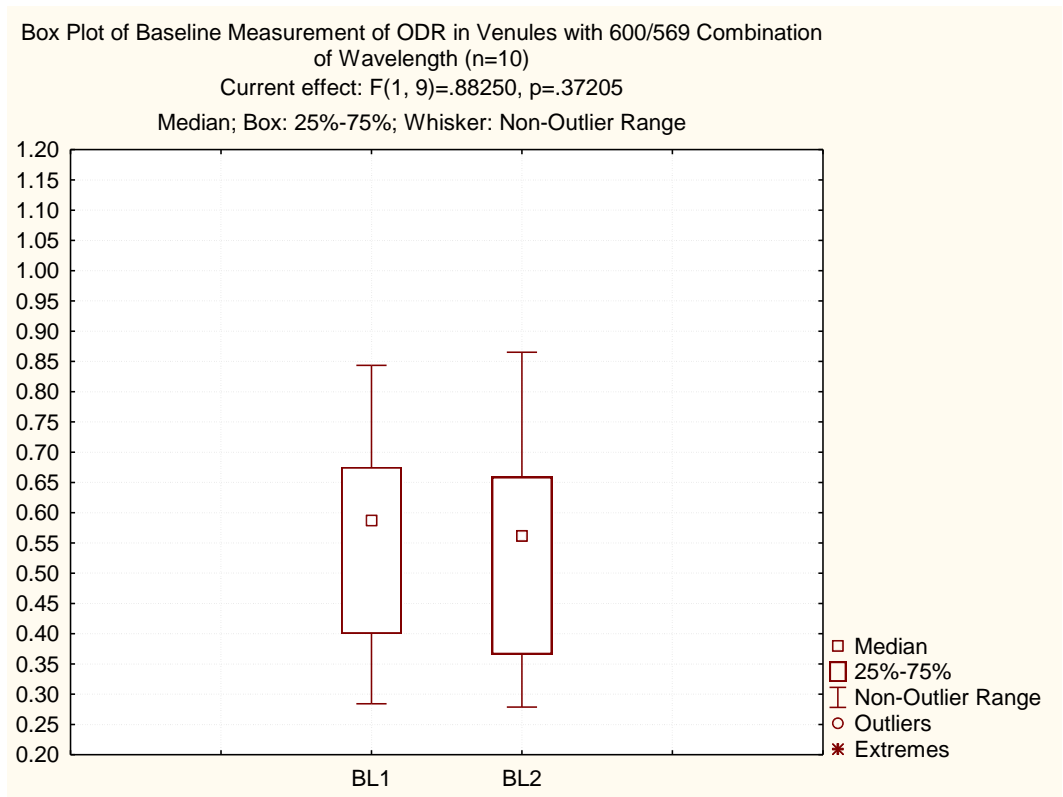


Figure 3.7 Boxplots representing repeat baseline measurements of ODR in venules with 600/569

3.3.3.3 610/548 Wavelength Combination

In arterioles, the group range (\pm SD) of ODR values with the 610/548 wavelength combination at baseline 1 and 2 was 0.604 ± 0.263 and 0.685 ± 0.450 , respectively. In venules, the group range (\pm SD) of ODR at baseline 1 and 2 was 0.292 ± 0.746 and 0.285 ± 1.009 , respectively (Table 3.6). The baseline 1 and 2 ODRs for the 610/548 wavelength combination as a function of participant ID are shown in Figure 3.8 and 3.9 for arterioles and venules, respectively.

	Vsriation in Baseline ODR with 610/548 (n=10)			
Participant ID#	Arterioler		Venular	
	BL 1	BL 2	BL 1	BL 2
01	0.558	0.635	0.292	0.285
02	0.609	0.635	0.746	1.009
03	0.649	0.843	1.062	1.138
04	0.708	0.703	0.871	0.868
05	0.491	0.605	0.489	0.484
06	0.525	0.596	0.483	0.442
07	0.505	0.553	0.256	0.305
08	0.550	0.764	0.451	0.466
09	0.691	0.533	0.654	0.728
10	0.755	0.983 64	0.732	0.761

Mean	0.604	0.685	0.604	0.649
Range (Max-Min)	0.263	0.450	0.806	0.852
SD	0.093	0.141	0.256	0.296

Table 3.6 Variation in Baseline ODR with 610/548 (n=10)

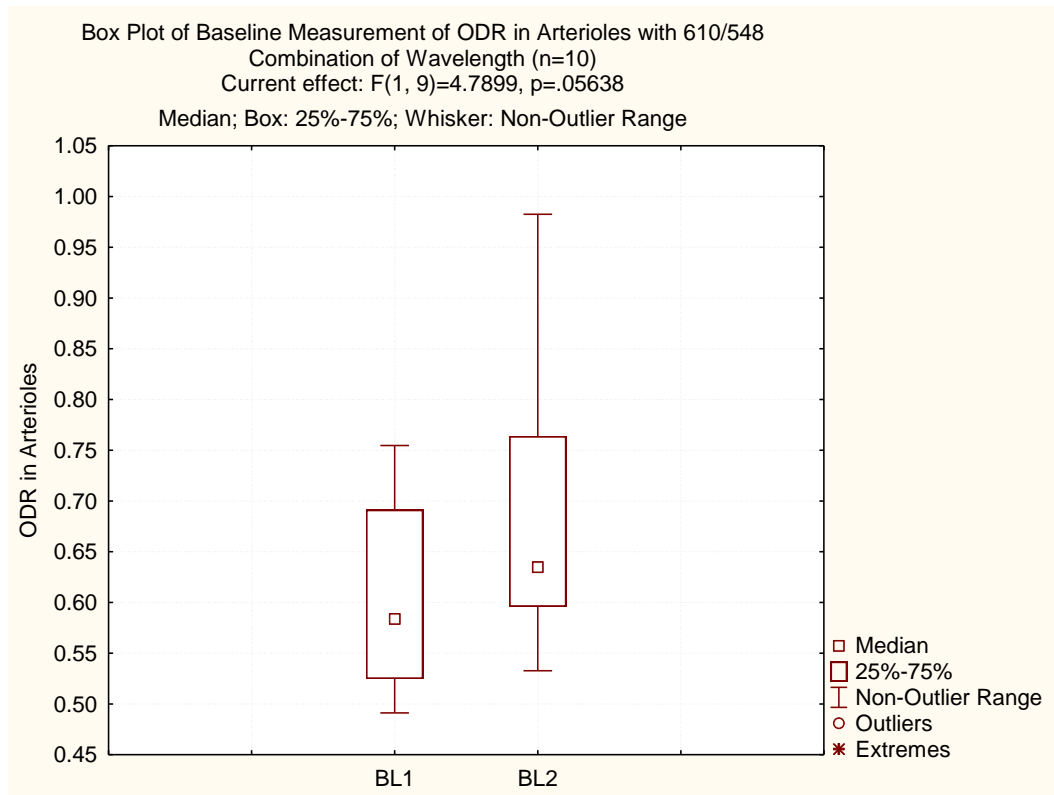


Figure 3.8 Boxplots representing baseline measurement of ODR in arterioles with 610/548

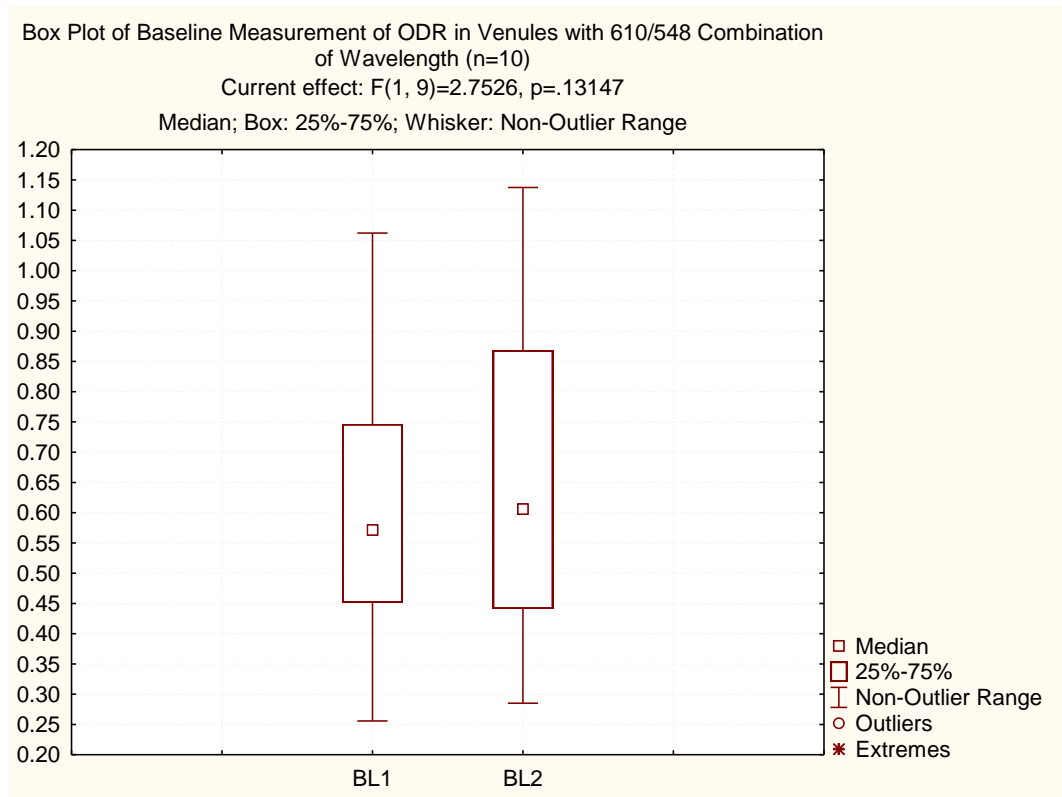


Figure 3.9 ODR (610/548) Boxplots representing baseline measurement of ODR in venules with 610/548

In summary, the total group range \pm SD of ODR values at baseline in arterioles for the 605/586 wavelength combination was 0.169 ± 0.061 , 600/569 wavelength combination was 0.371 ± 0.099 and 610/548 wavelength combination was 0.340 ± 0.104 (Table 3.7). In venules, the total group range \pm SD of ODR at baseline for the 605/586 wavelength combination was 0.600 ± 0.198 , 600/569 wavelength combination was 0.569 ± 0.196 and 610/548 wavelength combination was 0.819 ± 0.274 (Table 3.8).

	Wavelength Combinations for Calculating ODR±SD		
Total Variation in ODR (Arterioles)	605/586	600/569	610/548
Range	0.169	0.371	0.340
Standard Deviation (SD)	0.061	0.099	0.104

Table 3.7 Total Variation in Mean ODR for three Wavelength Combinations ± SD in Arterioles

	Wavelength Combinations for Calculating ODR±SD		
Total Variation in ODR (Venules)	605/586	600/569	610/548
Range	0.600	0.569	0.819
Standard Deviation (SD)	0.198	0.196	0.274

Table 3.8 Total Variation in Mean ODR for three Wavelength Combinations ± SD in Venules

There was no statistical significance reported between baseline ODR values (BL1 and BL2) for n=10 with all three wavelength combinations in arterioles and venules; for the 605/586 wavelength combination, p = 0.370 in arterioles and p = 0.714 in venules. 600/569 combination, p = 0.424 in arterioles and p = 0.372 in venules and for the 610/548 combination, p = 0.056 arterioles and p = 0.131 in venules (Table 3.9).

	Difference Between Baseline Measurements		
P-value ($\alpha=0.05$)	605/586	600/569	610/548
Arterioles	0.370	0.424	0.056
Venules	0.714	0.372	0.131

Table 3.9 Differences between baseline measurements for all 3 wavelength combinations (600/586, 600/569, 610/548)

3.4 Discussion and Conclusion

Of the three wavelength combinations selected, the 605/586 combination was shown to have the least variability in arterioles and venules with a range and SD of 0.169 ± 0.061 in arterioles and range and SD of 0.600 ± 0.198 in venules. The 600/569 combination were also found to be consistently higher across all 3 wavelength combinations in arterioles than in venules. It was also found that the variability was generally larger in measuring ODR in venules than in arterioles for all 10 participants. There was no statistical significance observed between baseline ODR values (BL1 and BL2) for $n=10$ with all three wavelength combinations in arterioles and venules. The lack of statistical significance observed was consistent with what we expected, as a healthy individual's baseline ODR does not change especially with measurements taken within minutes of each other. This range and SD in arterioles with the 605/586 combination was in comparison to 0.371 ± 0.099 for 600/569 wavelength combination and the 610/548 wavelength combination which had a range \pm SD of 0.340 ± 0.104 . In venules, the range and SD with the 605/586 combination was in comparison to 0.569 ± 0.196 for 600/569 combination and 0.819 ± 0.274 for the 610/548 combination. The least variability of the 605/586 wavelength combination in arterioles and venules presupposed that it was the most reliable in terms of measuring ODR in arterioles and venules with our prototype device. These observations were made when the three wavelength combinations were used to image primary/first degree arterioles and venules within the superonasal region of the fundus within 1-2 optic disc diameters away from the optic disk with the prototype HRC device.

The 605/586 wavelength combination has produced consistently reliable results in a number of previous studies in healthy and diseased states of the posterior fundus with noninvasive spectrophotometric oximetry^{10, 10, 168, 184, 186, 199, 200}. Hardarson and co-workers (2006) measured SO_2 in retinal vessels and tested the reproducibility and sensitivity of an automatic spectrophotometric oximeter¹⁶⁸. For repeated measurements, the mean SD was 3.7% for arterioles and 5.3% in venules, in terms of retinal blood SO_2

in first degree vessels. Measurements were inferior and superior to the ONH. All images were acquired in the dark.

The 600/570 ODR has been used by Geirsdottir and co-workers (2012) with the Oxymap T1 (Oxymap ehf., Reykjavik, Iceland) noninvasive dual-wavelength spectrophotometric retinal oximeter¹⁵³. 600 and 570 wavelengths have also been used previously to determine choroidal oximetry and to validate spectrophotometric retinal oximetry in the pig^{201,202}.

610/548 ODR has been used with some success in some systems^{173,187,188,193,203,204}. Hammer and co-workers (2008) measured the sensitivity and reproducibility of retinal SO₂ measurements in retinal vessels using a fundus camera and a semi-automated vessel recognition system. SDs of 2.52% and 3.25% SO₂ were recorded for arterioles and venules, respectively, when measurements of the identical vessel segments of five images per participant were made²⁰³. Michelson and co-workers (2006)¹⁸⁸ derived retinal SO₂ measures using the same wavelengths using a prototype spectrometer (University Jena, Germany). A single arteriole was analyzed. The Palkovits and co-workers (2013) study on the other hand measured retinal SO₂ in participants with chronic obstructive pulmonary disease with a retinal vessel analyzer (RVA) combined to an oxygen module (Imedos, Jena, Germany)¹⁹³. The modified RVA made measurements of retinal SO₂ in all vessels in a peripapillary annulus with an inner radius of 1 and an outer radius of 1.5 disc diameters and averaged over all arterioles and venules. The Lasta and co-workers (2012) study also made use of a RVA with the 610 and 548 wavelengths. This study determined the reproducibility of retinal SO₂ in healthy participants measured with the device. The intraclass correlation coefficients were between, 0.91-0.94; and between 0.84-0.88 for retinal branch arterioles and venules, respectively²⁰⁴.

The choice of the most reliable wavelengths to calculate ODR and subsequent retinal SO₂ appears to be dependent on a variety of parameters such as the specifications and/or limitations of the imaging system adopted and the choice of quadrant within the fundus for imaging. In the Geirsdottir and co-workers

(2012) study, retinal SO₂ arteriolar measures in the inferotemporal quadrant had significantly lower oxygen saturation values compared to the superotemporal, inferonasal and superonasal quadrants of the retina¹⁵³. Shahidi and co-workers (2013) also found greater retinal blood SO₂ values in the superior temporal first degree retinal arterioles and venules in young healthy individuals than in the equivalent inferior vessels²⁰⁵.

The Oxymap oximeter is generally similar to the HRC prototype device used in this study. Differences lie primarily in the Oxymap's use of a flash system and less importantly, a semi-automatic vessel detection technique and its analysis of all vessels (arterioles and venules) simultaneously. With the HRC prototype, only a single arteriole is typically analyzed for retinal SO₂, as in the Michelson and co-workers (2006) study¹⁸⁸. It therefore comes as no surprise that, like the Hardason group, our device shows almost identical SDs for both the 605/586 and 600/569 ODRs as compared to the 610/548 ODR which have both been used successfully in previous studies with the Oxymap system. It appears however that the 605/586 ODR was been used with more success and reliability; a finding that has been confirmed by this study. This study appears to be the first to look at the reliability of ODRs by comparing the variability of ODRs acquired in a specific spectrophotometric imaging system.

3.4.1 **Summary**

The 605/586 combination out of all the 3 wavelength combinations (605/586, 600/569 and 610/548) considered was shown to have the least variability in arterioles and venules with the prototype HRC used in the study.

4 The Effect of Change in Oxygen Tension on Total Retinal Blood Flow and Retinal Oxygen Saturation in Healthy Participants

4.1 Introduction

Hypoxia of the retina causes vasodilation of the retinal arterioles beginning at Hb SO₂ below 90% and can be measured clearly below 65mmHg^{61, 70}. Hyperoxia occurs as a result of an increase in P_{ET}O₂ above normal (>100mmHg) resulting in vasoconstriction of the inner retinal arteriolar vessels and a decrease in retinal blood flow^{3, 64, 65}. Vasoconstriction of the retinal arterioles serves as a regulatory response for keeping the PO₂ in retinal tissue constant, despite the fact that the hyperoxic levels required to initiate this response are not physiological. Reduced retinal capillary and ONH blood flow has been seen in smokers, secondary to hyperoxia⁶⁶.

In vivo oxygen profiles have been demonstrated and are similar in the rat, pig and cat. In the monkey, differences occur in the fovea as compared to the other animals. When the rods are fully saturated with light (light adaptation), there is a significant fall in oxygen tension of about 60mmHg from the choriocapillaris to the inner segments of the photoreceptors, with further decreases through the outer retina. This fall in oxygen tension indicates that in light adapted conditions, the choroid provides all the oxygen for consumption by the photoreceptors. On the other hand, in a dark adapted retina, retinal oxygen tension values are considerably lower than that in the light adapted retina indicating that oxygen also diffuses from the retina to the photoreceptors¹¹.

In conditions of normoxia in healthy participants, P_{ET}O₂ and P_{ET}CO₂ values vary depending on a number of biological factors such as gender, height, weight, age and medical history. Generally speaking however, P_{ET}O₂ values vary between about 75-100mmHg (10-13kPa)⁷¹ and P_{ET}CO₂ about 34-45mmHg (4.5-6.0kPa)⁷². Arterial blood oxygen saturation (SaO₂) and venous blood oxygen saturation (SvO₂) is about 95-100%⁷² and 60-80%²⁰⁶ saturation of Hb molecules in arterial and venous blood, respectively. TRBF varies inversely with P_{ET}O₂ in order to keep retinal SO₂ somewhat constant^{3,3,207}.

Very few studies have assessed both retinal SO_2 and RBF^{154,173,175,208}. In one such study by Siesky and co-workers (2010)¹⁷⁵, retinal vessel SO_2 did not change while RBF increased with the administration of dorzolamide/timolol treatment over an eight month period for each drug; suggesting an increase in oxygen delivery with an increase in blood flow. Dorzolamide had been shown in previous studies to increase optic nerve PO_2 in animal models and the same is suggested to occur in humans²⁰⁹⁻²¹¹. In a separate study by the same group on the administration of dorzolamide/brinzolamide treatment over a 3 month period per drug, it was shown that both retinal SO_2 and RBF increased in patients with primary open-angle glaucoma²¹¹. Hammer and co-workers (2011), used laser Doppler velocimetry to determine an increased blood velocity and vessel diameters during flicker stimulation. In addition, arteriolar and venular SO_2 was determined using dual wavelength (548nm and 610nm) optical oximetry fundus images¹⁷³. Another study by Sebag and co-workers (1989) looked at optic atrophy and the effects it had on retinal blood flow and SO_2 ¹⁵⁴. Retinal SaO_2 for temporal and nasal regions of affected eyes was determined by retinal vessel oximetry. Frayser and co-workers (1974) also looked at retinal blood flow and SO_2 at an altitude. Retinal blood flow was measured in otherwise normal volunteers who had been at an altitude 17,500ft for 5-9 days. Retinal blood flow was double that normally observed at sea level²⁰⁸. Several studies have focused solely on RBF measurements with the Doppler FD-OCT device²¹²⁻²¹⁹.

In this study, a novel HRC with a prototype fundus camera, a tunable laser source based on the Bragg grating filtering technology and a high definition CCD camera with a bandwidth of 2nm (FWHM) were used. Three wavelength combinations (ODR-s) were separately employed (600 and 569nm, 605 and 586nm, 610 and 548nm) for the analysis. Other spectral cameras, unlike the HRC, make use of a snapshot flash system that bleaches the photopigments and therefore alters reflectance characteristics of the fundus and subsequently affects derivation of accurate ODR readings. In addition, a Doppler FD-OCT device which enables the determination of TRBF by summing the flow of blood from all branch venules at one time is used. The study looks at the quantification of retinal blood SO_2 with the 605/586 wavelength combination and investigates the relationship between total retinal blood flow and retinal SO_2

in vessels of normal, healthy study participants under conditions of normoxia, hypoxia, and hyperoxia while maintaining isocapnia. TRBF and retinal SO_2 are expected to relate inversely with each other in hyperoxia and hypoxia.

4.2 *Materials and Methods*

4.2.1 *Sample*

Ethical clearance was obtained from the University Health Network Research Ethics Board, Toronto and the University of Waterloo, Office of Research Ethics prior to the start of the study. After explaining the study and its possible consequences to each study participant according to the Declaration of Helsinki, informed consent was obtained from each participant. The study sample of ten healthy participants (five females and five males) between the ages of 23 and 37, with an average age 28.3 years (SD 3.90) was recruited for the study from the School of Optometry and Vision Science, University of Waterloo and Department of Ophthalmology and Vision Sciences, University of Toronto. Of the 10 recruited, 1 was of Middle Eastern, 3 were of Black/African, 2 were of Asian, 2 were of White and 2 were of Indian descent. The right eye of each participant was chosen for the study for convenience of use with the prototype HRC.

Participants with distance refractive errors $> \pm 6.00$ DS and/or ± 2.50 DC, any indication or history of chronic / serious eye disease (glaucoma, diabetes, or any ocular disease permanently affecting vision or requiring surgery) in self or first degree relative or systemic disease (endocrine disorders, hypercholesterolemia, etc.), stroke or chronic obstructive/restrictive lung disease (such that the volunteer is unable to walk up 2 flights of stairs, i.e. does not include seasonal asthma) or on any medications with known vascular effects (e.g. antioxidants, blood pressure medication) were excluded from the study. In addition, participants who were unable to cope with the breathing protocol, e.g. due to claustrophobia, those who were habitual smokers (or quit smoking within past 6 months), or those who showed non-compliance with prescribed anti-seizure medication or people who demonstrated a resting arterial SO_2 while breathing room air $< 95\%$ were also excluded. Participants were asked to refrain from vitamin C, caffeine, red meat, chocolate, alcohol and exercise for at least 12 hours prior to the study visit.

4.2.2 Study Visits

Participants attended a single 140 minute study visit scheduled between 9 and 11am for all participants. Two gas provocation protocols; hyperoxia (200, 300, 400mmHg) followed by hypoxia (80, 60, 50mmHg) were administered in a fixed sequential order. Each protocol consisted of four phases of differing $P_{ET}O_2$ with three repeat measurements at each step in the order; For hyperoxia, $P_{ET}O_2$ of 100mmHg (i.e. normoxia), 200mmHg, 300mmHg, 400mmHg were utilised. For hypoxia, $P_{ET}O_2$ of 100mmHg, 80mmHg, 60mmHg and 50mmHg were utilised. Each phase was maintained for 10minutes, except for the normoxia/baseline phase which was maintained for 15 minutes. In each phase of gas provocation ($P_{ET}O_2$), retinal SO_2 and TRBF measurements were made with the HRC and Doppler FD-OCT.

4.2.3 Novel Hyperspectral Retinal Camera

This prototype device allows for two-dimensional spectral and spatial information to be recorded in a single exposure¹⁷³. The instrument comprises a custom made mydriatic fundus camera with a tunable laser source (TLS) allowing for observance of the fundus at wavelengths ranging from 420 to 1,000nm at safe and comfortable illumination levels. The TLS is based on the Bragg grating filtering technology from Photon etc. which allows for rapid and accurate (<1nm) wavelength selection from the supercontinuum source. For high definition imaging, it contains a sensitive CCD camera and spectral reproducibility in time is assured with a built in calibration system¹⁷¹. The CCD sensor has a dynamic range of 14bits, and pixel scan rate and data rate of 12MHz/24MHz and 19.5 Mpixel/s respectively. The spectral range of the sensor is 290nm to 1100nm. Two-dimensional images of the retina are recorded and registered to produce a spectral (i.e. third dimension is colour) cube while assuring patient comfort. The image capture time of the HRC is 80ms. A 2x2 binning mode was used with an effective pixel resolution of 696x520 pixels.

4.2.4 Gas Delivery System (RespirAct™, Thornhill Research Inc., Toronto, Canada)

The gas delivery system employed in the study was made up of a sequential re-breathing gas delivery circuit (Hi-Ox80, Viaya Healthcare, Yoruba Linda, CA). The circuit which was attached to participants

via a facemask was made up of a commercial 3-valve oxygen delivery system with a rebreathing bag on the exhalation port. Participants breathed previously exhaled gas from the rebreathing bag when the contents of the fresh gas reservoir were depleted. The circuit was in turn connected to an automated gas flow controller (RespirAct™, Thornhill Research Inc. Toronto, Canada) and blender that has been primarily developed and employed for the purposes of gas provocation by the Fisher laboratory at University of Toronto for over a decade. Similarly, Hudson laboratory have contributed to the development of the instrument from the beginning and have used it for over a decade. The device enables the precise control of the partial end tidal pressures of oxygen ($P_{ET}O_2$) and carbon dioxide ($P_{ET}CO_2$) by modulating the inspired portion of oxygen and carbon dioxide, it is possible to accurately and repeatedly generate stable controlled and safe levels of hypoxia and hyperoxia. This technique uniquely targets exact pre-determined PO_2 levels and sustains them while maintaining isocapnia over the pre-determined phase duration irrespective of the individuals' respiratory rate. $P_{ET}O_2$ and $P_{ET}CO_2$ accurately measures PaO_2 and $PaCO_2$ respectively when breathing using the RespirAct™ sequential re-breathing gas delivery system^{150, 197}. The benefits of using this technique include the avoidance of under or overshooting the desired $P_{ET}O_2$ and $P_{ET}CO_2$ hence the consistency of data is improved. Also, safety improves since the risk of overshooting the target end-tidal gases into dangerous levels are eliminated providing improved, sustained safety and comfort for participants. Participants' systemic SO_2 levels were carefully and continuously monitored while using this device. If the subject is uncomfortable, deemed at risk in any way the experiment was immediately terminated and 100% O_2 was administered.

Healthy young participants underwent spectral imaging of the retina and ONH for a series of stepped hypoxic and hyperoxic stimuli by varying the inspired portion of oxygen. For the *hypoxic provocation*, the study necessitates the use of a hypoxic stimulus of a $P_{ET}O_2$ of 50mmHg to provide effective dissociation of hemoglobin, which would be detectable at the level of retina. $P_{ET}O_2$ was varied between baseline/normoxia and 50, 60 and 80mmHg. An end-tidal O_2 of 50 mmHg is commonly used in

physiological studies. For the hyperoxic provocation, $P_{ET}O_2$ steps of 200, 300 and 400mmHg were used to provide adequate vasoconstriction of the retinal arterioles.

4.2.5 RTVue Doppler FD-OCT

Once the Doppler scans are acquired, they are integrated together with a 3D disk scan exported as raw data from the RTVue instrument using a custom made transfer output software. The data was then converted with ReVue software (Optovue Inc.) into a format compatible with the DOCTORC software (version 2.1.1.4); which is used for assessment and identification of candidate vessel locations and vessel boundaries by an initial automated assessment. Retinal vessels are also identified as either arterioles or venules based on the Doppler signal ¹⁴⁷.

Doppler scans are then registered with the OCT projection image, infrared scanning laser ophthalmoscopy (SLO) image. A human grader is then able to manually grade the Doppler signals by correlating vessels seen on the Doppler FD-OCT cross sectional B-scans with those visible on the en-face images ¹⁴⁷. A colour fundus image is required to verify the automatic vessel assessment location and identification of arterioles/venules by DOCTORC (Fig 4.1). The grading procedure may include adjusting vessel locations and size, matching corresponding vessels on the two concentric rings, adding missing vessels, deleting extraneous vessels, verifying the classification of the vessel type and allocating a confidence score ranging from 0 to 5 to reflect the graders certainty of accuracy of grading. The confidence score is allocated based on several factors such as Doppler signal strength of the vessel, vessel size agreement between the two concentric rings and clarity of vessel boundaries ¹⁴⁷. With completion of grading, DOCTORC software then computes blood flow results and automatically exports them into a folder specified per subject.

4.2.3 Study Procedure

Participants were seated for 10 minutes to allow stabilization of their hemodynamic parameters (heart rate and blood pressure) during which time they underwent a period of air-breathing. Medical tape (Tegaderm;

3M Health Care, St. Paul, MN) was used to tightly seal the facemask to the participants face – The facemask was connected to the RespirAct™ sequential re-breathing gas delivery system. At the end of this stabilization period, pulse rate, resting blood pressure, retinal blood SO₂, SPO₂ and TRBF baseline measurements were taken at normoxia. Participants then underwent the further phases of the gas provocation protocol. In each phase of the provocation (hyperoxia and hypoxia), retinal blood SO₂ and TRBF was measured with the HRC and Doppler FD-OCT systems during the last 5 minutes of the phase. Pulse rate, SPO₂ and blood pressure rate was also monitored concurrently every 2.5 minutes using a rapid response critical care gas analyzer (Cardiicap 5, Datex-Ohmeda, Helsinki, Finland) and transmitted electronically to a data acquisition system (S5 Collect, Datex-Ohmeda, USA). A period of 15 minutes was allowed for the individual's metabolic measures to return to baseline in between provocation challenges and about 5 minutes between every specific provocation. During testing, the conditions in the lab was kept stable at an absolute pressure of 101.325 kPa (14.696 psi, 1 atm) and a temperature of 20 °C (293.15 K, 68 °F). The study procedure is depicted diagrammatically in Appendix B and C.

4.2.4 Statistical Analysis

4.2.5.1 Measuring ODR with the HRC Device

Retinal blood oximetry measurements were made in one major retinal arteriole and venule pair in the superonasal quadrant 1-2 disc diameters away from the ONH. The analysis was done by comparing the reflected light intensity within a vessel to the intensity of light in the adjacent retina at isobestic (oxygen insensitive) and oxygen sensitive wavelengths. The Image J line tool was used to accurately determine the x, y coordinate of the selected point on the retina for blood SO₂ measurements (Fig 3.1). A line (three times the width of the vessel) was drawn perpendicular to the blood vessel and with customized macros using Image J (NIH) software. The value of maximum intensity of light reflected from the adjacent retinal background and the minimum value on the vessel measurement site (vessel intensity) are used to calculate OD and ODRs. This method of calculating ODR was adopted from Beach and co-workers (1999)⁹ due to the current absence of a better algorithm.

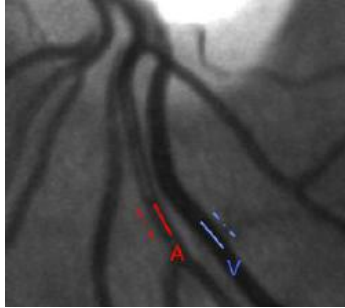


Figure 4.4.1 The intensity of light reflected from the vessel is compared to that of the adjacent retina for both arterioles and venules

$$OD = \log\left(\frac{I_0}{I}\right) \dots\dots\dots 18$$

Where, I_0 is the intensity of light within the vessel

I is the intensity of light of the adjacent retina

$$ODR = \frac{OD_{os}}{OD_i} \dots\dots\dots 19$$

Where, OD_{os} is the optical density at an oxygen sensitive wavelength and

OD_i is the optical density at an isosbestic (oxygen insensitive) wavelength

Image processing techniques were carried out with the PHySpec V1.17.0 software on the acquired images so as to normalize and remove artifacts by subtraction of a normalisation and beam dump cube. The optic disk and superonasal regions of the fundus were then selected with the rectangle tool. The image cubes were then registered using of a cross-correlation technique, with the 586nm image as reference. All other structures in the images were aligned to the coordinates of the reference image. Images were rotated and translated while comparing to the reference image for maximum cross-correlation. Image correction was done to stabilize and remove eye movement artifacts from image cubes.

The 605/586 wavelength combination which was found in the previous study to have the least variability of three wavelength combinations (605/586, 600/569 and 610/548) with our device, was used in the current study. Systemic SO_2 (SPO_2) values for all 10 participants were compared for consistency of results. Data for six participants were subsequently excluded due to inconsistencies. The Mean ODR for arterioles and venules was then computed for the 4 selected participants and used to calculate retinal blood SO_2 at baseline in arterioles and venules according to the equation:

$$SO_2 = a + k \cdot ODR \dots \dots \dots 20$$

Boxplots of retinal blood SO_2 in venules (SvO_2) and arterioles (SaO_2) were subsequently formed to compare the two parameters.

TRBF (ul/min), SaO_2 (%) and SvO_2 (%) was then determined for each step of $P_{ET}O_2$ (BL1, 200, 300, 400, BL2, 80, 60 and 50 mmHg) and grouped for all ten participants recruited. Separate retinal SO_2 equations were determined in arterioles and venules per provocation step. To investigate the relationship between TRBF, SaO_2 and SvO_2 with $P_{ET}O_2$, mean values of TRBF, SaO_2 and SvO_2 were computed per participant and per each of the 8 provocation steps. These- values (8 per participant) were then grouped together for each of the three parameters (80 data points in all per parameter). TRBF was then plotted against retinal SO_2 separately for arterioles and venules in scatterplots to determine the correlation between each parameter with the Pearson's correlation coefficient (r) and p-values ($\alpha = 0.05$) were determined for the correlation. Statistica software (StatSoft, Inc., Tulsa, OK, USA) version 11.0 and Microsoft Excel 2010 was used for analyzing the data. Significance was pegged at $p < 0.05$. Due to the small sample population employed, all outliers were included in the correlation analysis.

4.3 Results

4.3.1 HRC Systemic SO_2 Data for n=9

The systemic SO_2 values for each individual for the HRC and Doppler FD-OCT are shown in Tables 4.1 and 4.2, respectively.

Subject ID#	Systemic SO_2							
	$P_{ET}O_2$, 400 mmHg	$P_{ET}O_2$, 300 mmHg	$P_{ET}O_2$, 200 mmHg	BL1	BL2	$P_{ET}O_2$, 80 mmHg	$P_{ET}O_2$, 60 mmHg	$P_{ET}O_2$, 50 mmHg
02	100	99	100	98	99	97	93	91
03	99	99	98	97	99	94	90	86
04	97	98	97	97	97	94	92	89
05	99	99	99	100	100	99	93	87
06	99	99	99	97	99	92	88	88
07	99	99	98	99	99	95	90	90
08	99	99	99	99	99	98	93	89
09	100	100	100	100	100	96	92	70
10	100	100	100	100	100	97	90	84
Mean	98.56	98.89	99.11	99.11	99.11	95.78	91.22	86.00

SD	1.33	1.05	0.60	0.93	0.93	2.22	1.79	6.36
-----------	------	------	------	------	------	------	------	------

Table 4.1 Systemic SO₂ per P_{ET}O₂ for n=9 during HRC measurements.

4.3.1 RtVue Systemic SO₂ Data for n=9

Subject ID#	Systemic SO₂							
	P_{ET}O₂, 400 mmHg	P_{ET}O₂, 300 mmHg	P_{ET}O₂, 200 mmHg	BL1	BL2	P_{ET}O₂, 80 mmHg	P_{ET}O₂, 60 mmHg	P_{ET}O₂, 50 mmHg
02	99	98	98	98	99	99	100	99
03	100	99	99	99	99	99	100	100
04	99	99	99	100	99	99	100	100
05	100	98	99	100	99	99	100	100
06	100	98	98	98	99	99	100	99
07	97	94	97	97	97	96	99	97
08	95	95	92	92	92	92	95	91
09	80	86	88	88	89	89	91	85
10	99	98	98	98	99	99	100	99
Mean	98.89	99.44	99.44	99.44	99.00	96.78	92.44	86.67
SD	0.78	0.53	0.53	0.73	0.87	1.30	2.30	3.32

Table 4.2 Systemic SO₂ per P_{ET}O₂ for n=9 during Rtvue measurements

4.3.2 Quantification of Retinal Blood SO₂ at baseline with 605/586 Wavelength Combination

The mean retinal blood SO₂ value at baseline in arterioles for 4 participants was 95.19% ± 31.04% and venules was 53.89% ± 17.24%, p = 0.115 (Table 4.3). The baseline ODR and retinal SO₂ values for arterioles and venules are shown in Figure 4.1

Subject ID#	ODR in Arterioles	ODR in Venules	SaO ₂ (%)	SvO ₂ (%)
04	0.624	0.530	105.419	68.730
05	0.488	0.514	52.518	62.554
06	0.601	0.429	96.598	29.467
09	0.677	0.494	126.227	54.794
Mean	0.5975	0.4917	95.190	53.89
SD	0.079	0.0442	31.042	17.25

Table 4.3 ODR and retinal SO₂ baseline measurements for 4 participants in venules and arterioles

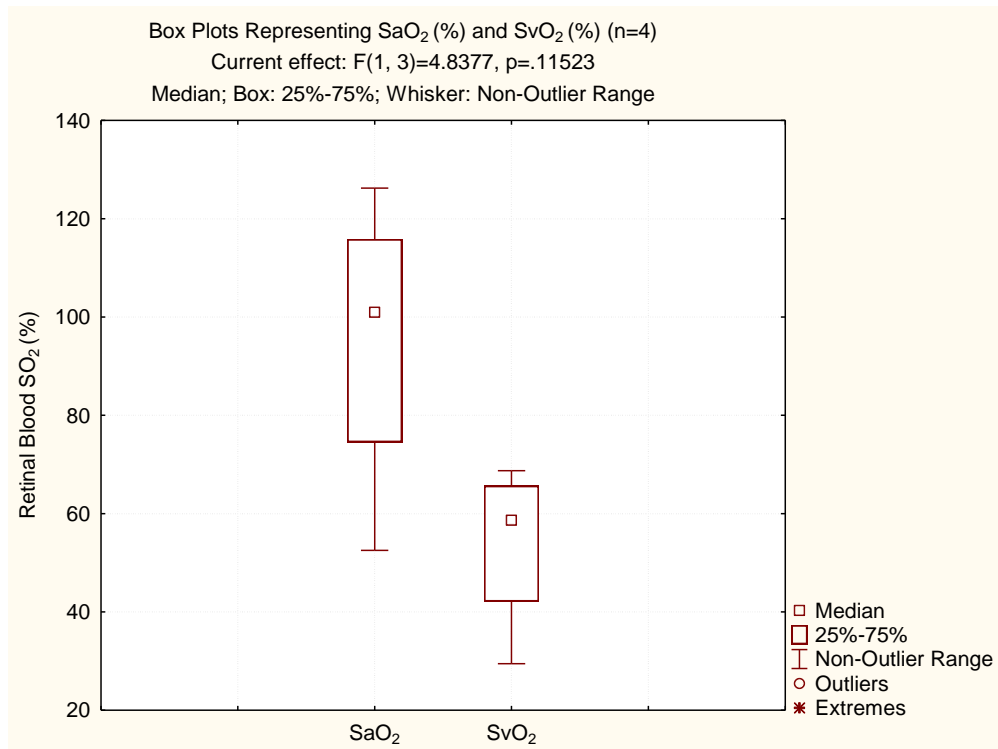


Figure 4.2 Box plots representing baseline retinal SO₂ values for 4 participants.

4.3.2 Relationship between Retinal Blood SO₂ and Retinal Blood Flow

There was a negative linear relationship between retinal blood SO₂ and TRBF values in the 10 participants studied. The Pearson's correlation coefficient (r) between TRBF and SaO₂ was $r = -0.354$ and $p = 0.001$. The Pearson's correlation coefficient (r) between TRBF and SvO₂ was $r = -0.295$, $p = 0.008$ (Table 4.4). The Mean (\pm SD) of TRBF and retinal blood SO₂ values for 10 participants are shown in Figure 4.2 and 4.3.

SUBJECT ID#	Mean \pm SD		
	TRBF (μ l/min)	SvO ₂ (%)	SaO ₂ (%)
01	30.11 \pm 6.49	-0.84 \pm 33.77	72.14 \pm 6.53

02	20.70±7.71	106.49±35.16	101.16±27.83
03	15.03±6.77	145.05±41.73	112.96±16.07
04	19.79±4.83	58.30±20.09	92.227±13.91
05	23.22±8.22	43.10±19.43	76.58±19.56
06	25.99±6.72	38.46±21.76	85.75±6.98
07	21.72±5.40	-21.13±27.28	78.62±12.76
08	21.84±4.63	5.39±27.13	93.75±10.90
09	20.96±2.44	60.05±18.45	115.92±14.37
10	19.79±2.93	105.14±10.93	120.85±18.89

Table 4.4 Table showing mean ±SD TRBF and retinal SO₂ values in arterioles and venules for each of 10 participants.

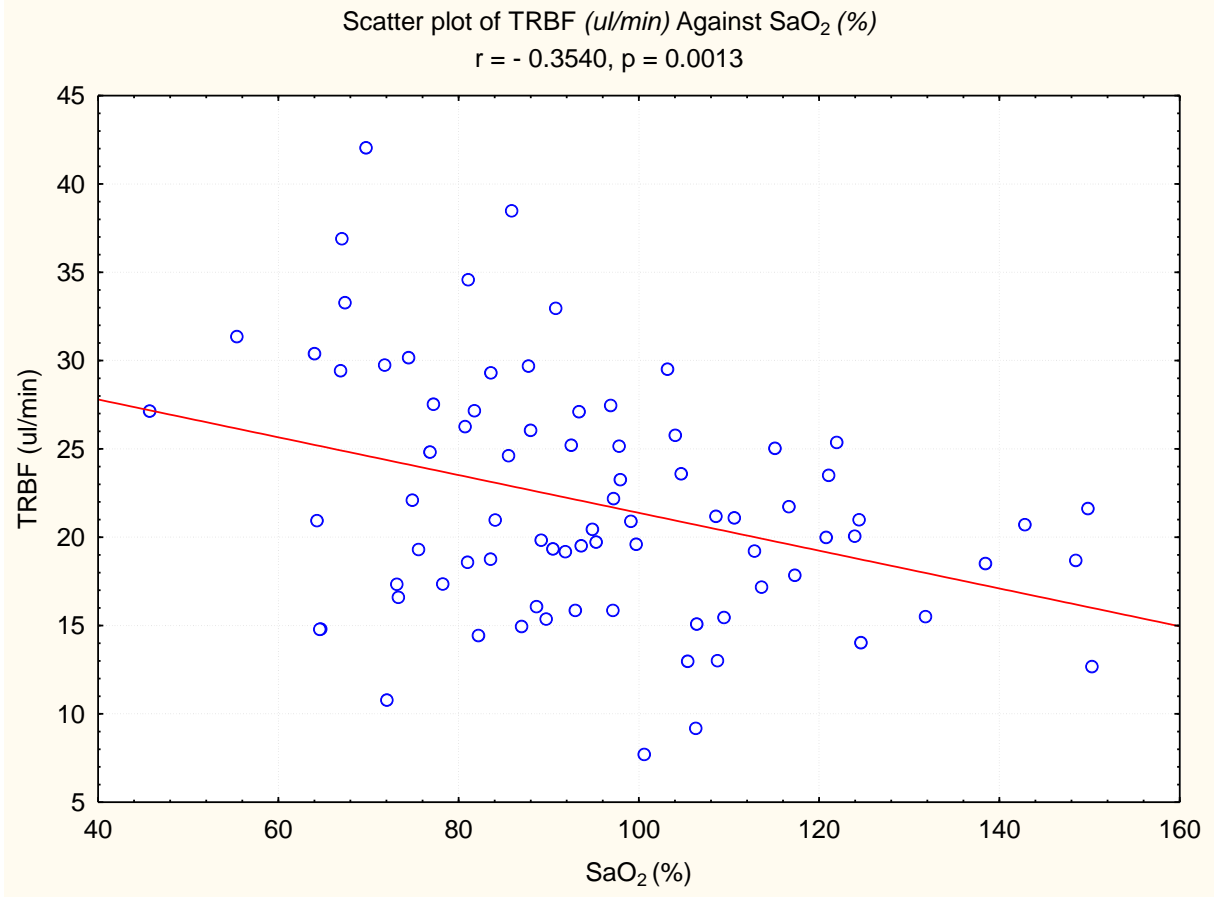


Figure 4.3 Scatter plot of TRBF against SaO₂ across all 8 provocation steps (n=10)

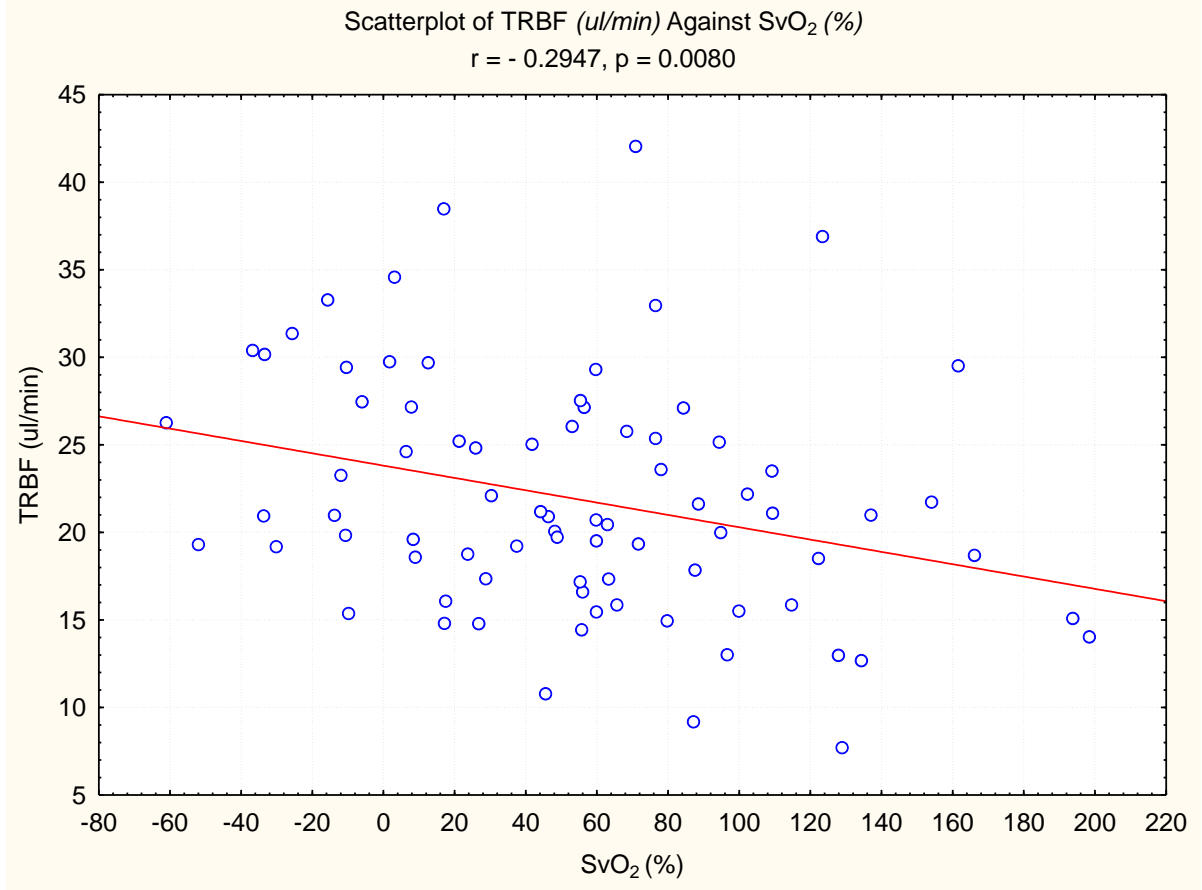


Figure 4.4 Scatter plot of TRBF against SaO₂ across all 8 provocation steps (n=10)

4.4.0 Discussion and Conclusion

4.4.1 Quantification of retinal blood SO₂ at baseline

The mean \pm SD absolute value of retinal blood SO₂ in the arterioles (SaO₂) was found to be 95.19% \pm 31.04% and was 53.89% \pm 17.24% in the venules (SvO₂). These absolute values (SaO₂ and SvO₂) at baseline for the 4 participants fell within the range expected and described in the literature ^{9, 153, 168}. The difference between the two parameters were not statistically significant (p=0.12). The lack of significance was believed to be due to the presence of significant variation in the retinal SO₂ values (and overlap of the two parameters), especially in the arterioles, and also the small sample size utilised. However, the magnitude of the difference between the two parameters was high and consistent with the low flow, high oxygen exchange vascular system typical of the retinal vascular system.

Calibration was performed with separate SO₂ equations per provocation step. Retinal blood SO₂ calculated showed considerable high inter-subject variability and unrealistic calculated retinal SO₂ values such as values beyond the physiological range (0-100%) i.e. above 100% and some calculated negative values. Similar high inter-subject variability (especially in SvO₂) have been reported by Mordant and co-workers (2011) who also used a hyperspectral imaging technique similar to the one used in this study ¹⁵⁷. Hardarson and co-workers (2012) in their study on diabetic patients found a retinal blood SO₂ 93 \pm 4% in the retinal arterioles of healthy volunteers at normoxia and 58 \pm 6% in venules (mean \pm SD, n=31) ¹⁸⁶. Another study by the same group 16 participants found that retinal SaO₂ measured 96% \pm 9% (mean \pm SD) during normoxia. In a study by Beach and co-workers in 1999, SvO₂ in ten participants was observed at normoxia and corrected for choroidal pigmentation. Mean SvO₂ was reported as 55% \pm 3.39% (SE) with a range of 26% among subjects at normoxia ⁹. Geirsdottir and co-workers (2012) determined the retinal SO₂ in 120 healthy individuals with the Oxymap T1 retinal oximeter. SaO₂ was 92.2% \pm 3.7% and SvO₂ was reported as 55.6% \pm 6.3% ¹⁵³ at normoxia.

4.4.2 Relationship between Retinal SO₂ and Retinal Blood Flow

TRBF was found in this study to relate inversely with SaO₂ and SvO₂ with a Pearson's correlation coefficient of $r = -0.354$ and $p = 0.001$ for arterioles. Similarly, an $r = -0.295$ and $p=0.008$ was determined for the relationship between TRBF and SvO₂. The inverse relationship reported was consistent with current literature^{3,3,207}.

Very few studies have looked at both blood flow and retinal SO₂ concurrently. Hammer and co-workers (2011) in their experiment used laser Doppler velocimetry to determine an increased blood velocity and vessel diameters during flicker stimulation. In addition, arteriolar and venous retinal SO₂ was determined using dual wavelength (548nm and 610nm) optical oximetry fundus images. SaO₂ remained constant at 98%-99%, with an increase in SvO₂ from $60\% \pm 5.7\%$ to $64\% \pm 5.9\%$ ($P<0.0005$) under flicker stimulation. The diameter of central retinal arteries and veins increased significantly from $193 \pm 20\mu\text{m}$ to a maximum of $202 \pm 19\mu\text{m}$ ($P<0.001$); $5.6\% \pm 4.9\%$ and from $228 \pm 20\mu\text{m}$ to $242 \pm 17\mu\text{m}$ ($P<0.001$); $7.6\% \pm 3.4\%$, respectively, suggesting an increase in retinal blood velocity¹⁷³. A relatively old but relevant study by Sebag and co-workers in 1989 looked at optic atrophy and the effects it had on retinal blood flow and SO₂¹⁵⁴. Retinal SaO₂ for temporal and nasal regions of affected eyes was determined by retinal vessel oximetry. In this study, arteriovenous SO₂ values were $12\% \pm 9\%$ higher in eyes affected by optic atrophy in 7 participants. Arteriovenous blood flow measured with LDV was $48\% \pm 20\%$ lower in 4 participants also with optic atrophy. Retinal blood flow rates in temporal retinal arterioles of affected eyes were found to be $23.5\mu\text{l}/\text{min}$ and $12.3\mu\text{l}/\text{min}$ for the fellow and affected eyes, respectively. The average percent difference was -48% , reflecting a significant reduction in blood flow in the affected eyes ($P = 0.017$)¹⁵⁴. Frayser and co-workers (1974) also looked at retinal blood flow and SO₂. Retinal blood flow was measured in otherwise normal volunteers who had been at an altitude 17,500ft for 5-9 days. Retinal blood flow doubled that normally observed at sea level at SaO₂ of $70 \pm 3\%$. RBF after 9 days at the altitude was $331\text{ml}/100\text{g}\cdot\text{min}^{-1}$ ^{208,208}.

4.3.3 Summary

Vasoconstriction of retinal vessels occurs in hyperoxia which in turn reduces blood flow. The reduction in blood flow permits increased oxygen extraction and thus a decrease in retinal SO_2 . Despite this fact however, it is believed that possibly the dissociation of HbO_2 is considerably reduced due to the high concentration of dissolved oxygen in hyperoxia resulting in an increased retinal SO_2 . Dissolved oxygen in the choroidal circulation also further adds to the high concentration of oxygen in the retina in hyperoxia, as oxygen in the choroidal blood diffuses into the retina in larger amounts than in hypoxia ^{11, 220-222}. Retinal SO_2 increases in hyperoxia are, however, generally restricted as a result of Hb being almost 100% saturated at normoxia ¹⁶⁸. Retinal blood SO_2 generally increases (non-linearly) with increasing oxygen tension (PO_2) up to about 100mmHg from where it plateaus as shown in the oxygen dissociation curve previously described (Fig 1.4).

Inter-subject variation of especially retinal SO_2 parameters in this pilot study may be due to several inherent factors due to the lack of an automated algorithm and thus, the use of a manual analysis methodology adopted from Beach and co-workers (1999). For example, the effect of cursor placement of the researcher is believed to have played a major role in the analysis. Additionally, choroidal pigmentation was not compensated for in this study which included people of Black, Asian, Middle Eastern and White backgrounds. Choroidal pigmentation varies among individuals and races, which significantly affects the variation in SaO_2 among participants ⁹. Vessel diameters have also been reported previously to have influence on measurements of hemoglobin SO_2 and need to be compensated for in future studies ⁹. Also, artifacts from eye movement, reflections from the RPE, the iris and uneven illumination due to vessels closer to the periphery of captured images is believed to have had some effect on our retinal blood SO_2 results. Additional limitations which may have also affected TRBF estimates in this study lay in the possibility of leakage in the seal between the participants face and the breathing mask used and participant's refusal to breathe deeply which may have resulted in inadequate targeting of end tidal values.

To overcome some of these problems the average OD of 6 images (3 9-cubed images and 3 21-cubed images) per participant and per provocation step were used. Participants were made as comfortable as possible and were also instructed to keep as still as possible while fundus images were taken. The participants were also given short breaks in between fundus photos to blink and stretch. Other difficulties were, however, inevitable due to technicalities of our prototype and the manual analysis method. Finally, due to a smaller sample size all outliers were included in the correlation analysis which could have weakened the association.

The mean \pm SD of retinal blood SO_2 in the arterioles (SaO_2), $95.19\% \pm 31.04\%$ and in the venules (SvO_2), $53.89\% \pm 17.24\%$ fell within the range expected and described in the literature. The magnitude of the difference between the SaO_2 and SvO_2 was consistent with the literature and appropriate for a low flow, high oxygen exchange vascular system typical of the inner retinal vascular system. TRBF was found in this study to relate inversely with SaO_2 and SvO_2 . The inverse relationship reported was consistent with current literature.

5 Conclusion

In Chapter 3, the 605/586 wavelength combination out of all the 3 wavelength combinations (605/586, 600/569 and 610/548) considered in the study showed the overall least variability when measuring ODR of retinal vessels close to the optic disk with our prototype HRC device.

The least variability of the wavelength combinations, that is the 605/586 nm, presupposed that it was the most reliable of the three wavelength combinations considered for measuring ODR with the prototype HRC used in the study.

In Chapter 4, the absolute mean retinal blood SO_2 at normoxia in the arterioles (SaO_2) and venules (SvO_2) fell within the range described in the literature. The magnitude of the difference between the SaO_2 and SvO_2 (~ 40%) was also consistent with the literature. This magnitude was appropriate for a low flow, high oxygen exchange vascular system typical of the inner retinal vascular system.

Using group data, rather than individual data for each study participant, TRBF was found to relate inversely with SaO_2 ($r = -0.354$ and $p = 0.001$) and SvO_2 ($r = -0.295$ and $p=0.008$). This relationship between TRBF and SaO_2 and SvO_2 , was as expected based upon data derived primarily from animal models. This study is ground-breaking and unique, in that, it is the first study to concomitantly measure both retinal blood SO_2 and TRBF in human participants. Individual data showed extensive variability and noise, thus limiting the strength of the association between TRBF and SaO_2 and SvO_2 .

5.1 Future Directions

5.1.2 *Corrections for pigmentation, vessel size, eye movement artifacts and unwanted reflections*

Choroidal pigmentation varies among individuals and races, which will significantly affect the variation in retinal SO_2 values among participants {{1082 Beach 1999;}}. Choroidal pigmentation should be compensated for in future studies in order to calculate ODRs for SO_2 measurements. This could be possible with the use of an in vitro model comprising of capillary tubes; similar to that of Lemailet and co-workers (2009) to measure phantom optical properties {{998 Lemailet,P. 2009;}}. This in vitro model could be used to model retinal vessels and the fundus environment so as to provide similar artifacts that arise from choroidal pigmentation, eye movement, etc. and thus calibrate and provide algorithms/correction factors that could be incorporated into the SO_2 equations.

Vessel diameters have also been reported previously to have an influence on measurements of hemoglobin SO_2 and need to be corrected {{1082 Beach 1999;}}. Future studies should look at measuring vessel diameters to evaluate the change in retinal blood SO_2 over a series of differing vascular reactivity conditions. This change in vascular reactivity may also be compared to that related to TRBF changes. Finally, algorithms designed to compensate for eye movement artifacts and unwanted reflections should be included in future studies so as to elicit the true SO_2 from ODR results acquired from the reflectance profile.

5.1.3 *Further Criteria for Selection of Wavelength Combinations for Retinal Oximetry*

A critically important specification for reliable and optimal measurements of optical density in spectral analysis techniques such as retinal oximetry is the choice of specific wavelengths. Despite this, there has not been any well-defined standard model reported as yet for the determination of the most consistent and reliable wavelength pairs for retinal oximetry.

Criteria that may be considered in the choice of wavelength combinations might include the absorbance characteristics of individual wavelengths. That is, the difference in absorbance between each wavelength pair and the mean absorption of light per wavelength combination should be investigated. Also, absorption differences between vessels (arterioles/venules) and adjacent tissue may be of interest. Reflections from blood vessels and tissue (fundus) diminish as the amount of light absorbed by the tissue/vessel increases.

5.1.1 Quantification of Retinal Blood SO_2 in Diseased Retinae

Failure of the autoregulatory system and VR of the retinal vascular system has been implicated in the pathogenesis of several major ocular diseases such as retinopathy of prematurity (ROP), age-related macular degeneration (ARMD), diabetic retinopathy (DR) and glaucoma {{1194 HICKAM 1963; 1337 Wangsa 2003; 1240 Olafsdottir,O.B. 2011; 820 Harris 2003;}}. While limited studies have been conducted by other research groups using snapshot techniques (which bleach the photopigments) {{1308 Hardarson,S.H. 2012; 835 Hardarson,S.H. 2011; 1240 Olafsdottir,O.B. 2011; 1241 Traustason,S. 2009;}}, there are yet no investigations to determine differences in retinal blood SO_2 in diseased retinae with the HRC system, so as to provide further validation data for the apparatus.

Letters of Copyright Permission

Nature

NATURE PUBLISHING GROUP LICENSE TERMS AND CONDITIONS

Jul 23, 2013

This is a License Agreement between Afua Oteng-Amoako ("You") and Nature Publishing Group ("Nature Publishing Group") provided by Copyright Clearance Center ("CCC"). The license consists of your order details, the terms and conditions provided by Nature Publishing Group, and the payment terms and conditions.

All payments must be made in full to CCC. For payment instructions, please see information listed at the bottom of this form.

License Number	XXXXXXXXXX
License date	Jul 22, 2013
Licensed content publisher	Nature Publishing Group
Licensed content publication	Eye
Licensed content title	Spectral imaging of the retina
Licensed content author	D J Mordant, I Al-Abboud, G Muyo, A Gorman, A Sallam et al.
Licensed content date	Mar 1, 2011
Volume number	25
Issue number	3
Type of Use	reuse in a thesis/dissertation
Requestor type	academic/educational
Format	print and electronic
Portion	figures/tables/illustrations
Number of figures/tables/illustrations	2
High-res required	no

Figures	Fig 1, Fig 3
Author of this NPG article	no
Your reference number	None
Title of your thesis / dissertation	Effect of Change in PETO2 on Total Retinal Blood Flow and Oxygen Saturation in the Major Vessels of Healthy Participants
Expected completion date	Aug 2013
Estimated size (number of pages)	100
Total	0.00 USD

Terms and Conditions

Terms and Conditions for Permissions

Nature Publishing Group hereby grants you a non-exclusive license to reproduce this material for this purpose, and for no other use, subject to the conditions below:

1. NPG warrants that it has, to the best of its knowledge, the rights to license reuse of this material. However, you should ensure that the material you are requesting is original to Nature Publishing Group and does not carry the copyright of another entity (as credited in the published version). If the credit line on any part of the material you have requested indicates that it was reprinted or adapted by NPG with permission from another source, then you should also seek permission from that source to reuse the material.
2. Permission granted free of charge for material in print is also usually granted for any electronic version of that work, provided that the material is incidental to the work as a whole and that the electronic version is essentially equivalent to, or substitutes for, the print version. Where print permission has been granted for a fee, separate permission must be obtained for any additional, electronic re-use (unless, as in the case of a full paper, this has already been accounted for during your initial request in the calculation of a print run). NB: In all cases, web-based use of

full-text articles must be authorized separately through the 'Use on a Web Site' option when requesting permission.

3. Permission granted for a first edition does not apply to second and subsequent editions and for editions in other languages (except for signatories to the STM Permissions Guidelines, or where the first edition permission was granted for free).

4. Nature Publishing Group's permission must be acknowledged next to the figure, table or abstract in print. In electronic form, this acknowledgement must be visible at the same time as the figure/table/abstract, and must be hyperlinked to the journal's homepage.

5. The credit line should read:

Reprinted by permission from Macmillan Publishers Ltd: [JOURNAL NAME] (reference citation), copyright (year of publication)

For AOP papers, the credit line should read:

Reprinted by permission from Macmillan Publishers Ltd: [JOURNAL NAME], advance online publication, day month year (doi: 10.1038/sj.[JOURNAL ACRONYM].XXXXX)

Note: For republication from the *British Journal of Cancer*, the following credit lines apply.

Reprinted by permission from Macmillan Publishers Ltd on behalf of Cancer Research UK:

[JOURNAL NAME] (reference citation), copyright (year of publication) For AOP papers, the credit line should read:

Reprinted by permission from Macmillan Publishers Ltd on behalf of Cancer Research UK:

[JOURNAL NAME], advance online publication, day month year (doi: 10.1038/sj.[JOURNAL ACRONYM].XXXXX)

6. Adaptations of single figures do not require NPG approval. However, the adaptation should be credited as follows:

Adapted by permission from Macmillan Publishers Ltd: [JOURNAL NAME] (reference citation), copyright (year of publication)

Note: For adaptation from the *British Journal of Cancer*, the following credit line applies.

Adapted by permission from Macmillan Publishers Ltd on behalf of Cancer Research UK:

[JOURNAL NAME] (reference citation), copyright (year of publication)

7. Translations of 401 words up to a whole article require NPG approval. Please visit <http://www.macmillanmedicalcommunications.com> for more information. Translations of up to a 400 words do not require NPG approval. The translation should be credited as follows:

Translated by permission from Macmillan Publishers Ltd: [JOURNAL NAME] (reference citation), copyright (year of publication).

Note: For translation from the *British Journal of Cancer*, the following credit line applies.

Translated by permission from Macmillan Publishers Ltd on behalf of Cancer Research UK:

[JOURNAL NAME] (reference citation), copyright (year of publication)

We are certain that all parties will benefit from this agreement and wish you the best in the use of this material. Thank you.

Special Terms: v1.1

If you would like to pay for this license now, please remit this license along with your payment made payable to "COPYRIGHT CLEARANCE CENTER" otherwise you will be invoiced within 48 hours of the license date. Payment should be in the form of a check or money order referencing your account number and this invoice number RLNK501071926.

Once you receive your invoice for this order, you may pay your invoice by credit card. Please follow instructions provided at that time.

Make Payment To:

Copyright Clearance Center

Dept 001

P.O. Box 843006

Boston, MA 02284-3006

For suggestions or comments regarding this order, contact RightsLink Customer Support:

customercare@copyright.com or +1-877-622-5543 (toll free in the US) or +1-978-646-2777.

Gratis licenses (referencing \$0 in the Total field) are free. Please retain this printable license for your reference. No payment is required.

REFERENCES

1. Garhöfer G, Resch H, Sacu S, et al. Effect of regular smoking on flicker induced retinal vasodilatation in healthy subjects. *Microvasc Res.* 2011;82(3):351-355.
2. Gilmore ED, Hudson C, Preiss D, Fisher J. Retinal arteriolar diameter, blood velocity, and blood flow response to an isocapnic hyperoxic provocation. *American Journal of Physiology - Heart and Circulatory Physiology.* 2005;288(6 57-6):H2912-H2917.
3. Luksch A, Garhöfer G, Imhof A, et al. Effect of inhalation of different mixtures of O₂ and CO₂ on retinal blood flow. *Br J Ophthalmol.* 2002;86(10):1143-1147.
4. Venkataraman ST, Hudson C, Fisher JA, Rodrigues L, Mardimae A, Flanagan JG. Retinal arteriolar and capillary vascular reactivity in response to isoxic hypercapnia. *Exp Eye Res.* 2008;87(6):535-542. doi: 10.1016/j.exer.2008.08.020.
5. Beach JM, Tiedeman JS, Hopkins M, Sabharwal Y. Multi-spectral fundus imaging for early detection of diabetic retinopathy. *Proc SPIE Int Soc Opt Eng.* 1999;3603:114-121.
6. Macrae RA. Spectral transmission and scattering properties of red blood cells. *Journal of the Optical Society of America A: Optics and Image Science, and Vision.* 1961;51:1366-1372.
7. Hammer M, Schweitzer D, Michel B, Thamm E, Kolb A. Single scattering by red blood cells. *Appl Opt.* 1998;37(31):7410-7418.
8. Borovoi AG, Naats EI, Oppel UG. Scattering of light by a red blood cell. *J Biomed Opt.* 1998;3(3):364-372.
9. Beach JM, Schwenzer KJ, Srinivas S, Kim D, Tiedeman JS. Oximetry of retinal vessels by dual-wavelength imaging: Calibration and influence of pigmentation. *J Appl Physiol.* 1999;86(2):748-758.

10. Olafsdottir OB, Hardarson SH, Gottfredsdottir MS, Harris A, Stefánsson E. Retinal oximetry in primary open-angle glaucoma. *Invest Ophthalmol Vis Sci*. 2011;52(9):6409-6413.
11. Wangsa-Wirawan ND, Linsenmeier RA. Retinal oxygen: Fundamental and clinical aspects. *Arch Ophthalmol*. 2003;121(4):547-557.
12. Hickam JB, Frayser R, Ross JC. A study of retinal venous blood oxygen saturation in human subjects by photographic means. *Circulation*. 1963;27:375-385.
13. Harris A, Dinn RB, Kagemann L, Rechtman E. A review of methods for human retinal oximetry. *Ophthalmic Surgery Lasers and Imaging*. 2003;34(2):152-164.
14. Funk RHW. Blood supply of the retina. *Ophthalmic Res*. 1997;29(5):320-325.
15. Wu DM, Kawamura H, Sakagami K, Kobayashi M, Puro DG. Cholinergic regulation of pericyte-containing retinal microvessels. *American Journal of Physiology - Heart and Circulatory Physiology*. 2003;284(6 53-6):H2083-H2090.
16. Chakravarthy U, Gardiner TA. Endothelium-derived agents in pericyte function/dysfunction. *Prog Retin Eye Res*. 1999;18(4):511-527.
17. Hickam JB, Sieker HO, Frayser R. Studies of retinal circulation and A-V oxygen difference in man. *Trans Am Clin Climatol Assoc*. 1959;71:34-44.
18. Delori FC. Noninvasive technique for oximetry of blood in retinal vessels. *Appl Opt*. 1988;27(6):1113-1125.
19. Alm A, Bill A. Ocular and optic nerve blood flow at normal and increased intraocular pressures in monkeys (*macaca irus*): A study with radioactively labelled microspheres including flow determinations in brain and some other tissues. *Exp Eye Res*. 1973;15(1):15-29.

20. Guyton AC, Hall JE. *Textbook of Medical Physiology*. 11th ed. Philadelphia: Elsevier Inc.; 2006.
21. Foulds WS. The choroidal circulation and retinal metabolism -- an overview. *Eye*. 1990;4(2):243-248.
22. Delaey C, Van De Voorde J. Regulatory mechanisms in the retinal and choroidal circulation. *Ophthalmic Res*. 2000;32(6):249-256.
23. Alm A, Bill A. The oxygen supply to the retina. I. effects of changes in intraocular and arterial blood pressures, and in arterial P O₂ and P CO₂ on the oxygen tension in the vitreous body of the cat. *Acta Physiol Scand*. 1972;84(2):261-274.
24. Hayreh SS. The cilio-retinal arteries. *Br J Ophthalmol*. 1963;47:71-89.
25. Olver JM. Functional anatomy of the choroidal circulation: Methyl methacrylate casting of human choroid. *Eye*. 1990;4(2):262-272.
26. Weiter JJ, Ernest JT. Anatomy of the choroidal vasculature. *Am J Ophthalmol*. 1974;78(4):583-590.
27. Singh Hayreh S. Segmental nature of the choroidal vasculature. *Br J Ophthalmol*. 1975;59(11):631-648.
28. Cringle SJ, Yu D-, Yu PK, Su E-. Intraretinal oxygen consumption in the rat in vivo. *Invest Ophthalmol Visual Sci*. 2002;43(6):1922-1927.
29. Schweitzer D, Thamm E, Hammer M, Kraft J. A new method for the measurement of oxygen saturation at the human ocular fundus. *Int Ophthalmol*. 2001;23(4-6):347-353.
30. Schweitzer D, Hammer M, Kraft J, Thamm E, Konigsdorffer E, Strobel J. In vivo measurement of the oxygen saturation of retinal vessels in healthy volunteers. *IEEE Trans Biomed Eng*. 1999;46(12):1454-1465.

31. Alm A, Bill A. The oxygen supply to the retina. II. effects of high intraocular pressure and of increased arterial carbon dioxide tension on uveal and retinal blood flow in cats. A study with radioactively labelled microspheres including flow determinations in brain and some other tissues. *Acta Physiol Scand*. 1972;84(3):306-319.
32. Kiel JW. *The Ocular Circulation*. Morgan & Claypool; 2011.
33. Field DT, Williams CM, Butler LT. Consumption of cocoa flavanols results in an acute improvement in visual and cognitive functions. *Physiology and Behavior*. 2011;103(3-4):255-260.
34. Dumskyj MJ, Aldington SJ, Doré CJ, Kohner EM. The accurate assessment of changes in retinal vessel diameter using multiple frame electrocardiograph synchronised fundus photography. *Curr Eye Res*. 1996;15(6):625-632.
35. Dumskyj MJ, Eriksen JE, Doré CJ, Kohner EM. Autoregulation in the human retinal circulation: Assessment using isometric exercise, laser doppler velocimetry, and computer-assisted image analysis. *Microvasc Res*. 1996;51(3):378-392.
36. Harris A, Arend O, Bohnke K, Kroepfl E, Danis R, Martin B. Retinal blood flow during dynamic exercise. *Graefe's Archive for Clinical and Experimental Ophthalmology*. 1996;234(7):440-444.
37. Robinson F, Riva CE, Grunwald JE, Petrig BL, Sinclair SH. Retinal blood flow autoregulation in response to an acute increase in blood pressure. *Invest Ophthalmol Visual Sci*. 1986;27(5):722-726.
38. Chen H, Hudson C, Atallah S, McLeod D. The acute effect of smoking on retinal blood flow: An assessment with the heidelberg retina flowmeter. *Invest Ophthalmol Visual Sci*. 1996;37(3).
39. Morgado PB, Chen HC, Patel V, Herbert L, Kohner EM. The acute effect of smoking on retinal blood flow in subjects with and without diabetes. *Ophthalmology*. 1994;101(7):1220-1226.

40. Dhasmana D, Herbert L, Patel V, Chen HC, Jones M, Kohner EM. The effect of acute ethanol consumption on the human retinal circulation: A study in diabetic and non-diabetic subjects. *Eur J Ophthalmol*. 1994;4(3):144-150.
41. Kojima S. Ethanol consumption and ocular circulation. *Folia Ophthalmol Jap*. 2006;57(5):336-341.
42. McGahon MK, Dash DP, Arora A, et al. Diabetes downregulates large-conductance Ca²⁺-activated potassium β 1 channel subunit in retinal arteriolar smooth muscle. *Circ Res*. 2007;100(5):703-711.
43. West SG. Effect of diet on vascular reactivity: An emerging marker for vascular risk. *Curr Atheroscler Rep*. 2001;3(6):446-455.
44. Antcliff RJ, Marshall J. The pathogenesis of edema in diabetic maculopathy. *Semin Ophthalmol*. 1999;14(4):223-232.
45. Patel V, Rassam S, Newsom R, Wiek J, Kohner E. Retinal blood flow in diabetic retinopathy. *Br Med J*. 1992;305(6855):678-683.
46. Schmetterer L, Wolzt M. Ocular blood flow and associated functional deviations in diabetic retinopathy. *Diabetologia*. 1999;42(4):387-405.
47. Weigert G, Luksch A, Maár N, Sacu S, Schmetterer L, Garhöfer G. Effects of vitamin C on hyperoxia-induced reduction of retinal blood flow. *Microvasc Res*. 2009;77(3):256-259.
48. Hademenos GJ, Massoud TF. *The Physics of Cerebrovascular Diseases*. New York: Springer-Verlag New York, Inc.; 1998.
49. Glucksberg MR, Dunn R. Direct measurement of retinal microvascular pressures in the live, anesthetized cat. *Microvasc Res*. 1993;45(2):158-165.

50. Harris A, Kagemann L, Cioffi GA. Assessment of human ocular hemodynamics. *Surv Ophthalmol*. 1998;42(6):509-533.
51. Riva CE, Sinclair SH, Grunwald JE. Autoregulation of retinal circulation in response to decrease of perfusion pressure. *Invest Ophthalmol Visual Sci*. 1981;21(1 II):34-38.
52. Chen G, Zhao L, Liu Y, Liao F, Han D, Zhou H. Regulation of blood viscosity in disease prevention and treatment. *Chinese Science Bulletin*. 2012;57(16):1946-1952.
53. Stoltz JF, Donner M. New trends in clinical hemorheology: An introduction to the concept of the hemorheological profile. *Schweizerische medizinische Wochenschrift. Supplementum*. 1991;43:41-49.
54. Jayalalitha G, Deviha VS, Uthayakumar R. Fractal model of the blood vessel in cardiovascular system. *Proceedings of the 15th International Conference on Advanced Computing and Communications, ADCOM 2007*. 2007:175-182.
55. Guyton AC. Long-term regulation of the circulation. In: Reeve EBG, Ed, Guyton AC, Ed, Colorado. University. Medical Center, National Research Council (U.S.). Committee on Shock, eds. *Physical Bases of Circulatory Transport; Regulation and Exchange*. Edited by E.B. Reeve (and) Arthur C. Guyton. Philadelphia, Saunders, 1967; Philadelphia, Saunders, 1967; 1967.
56. Johnson PC. Autoregulation of blood flow : Proceedings of an international symposium held June 10, 11, 12 1963. 1964.
57. Delaey C, Van De Voorde J. Pressure-induced myogenic responses in isolated bovine retinal arteries. *Invest Ophthalmol Visual Sci*. 2000;41(7):1871-1875.
58. Pillunat LE, Anderson DR, Knighton RW, Joos KM, Feuer WJ. Autoregulation of human optic nerve head circulation in response to increased intraocular pressure. *Exp Eye Res*. 1997;64(5):737-744.

59. Riva CE, Hero M, Titze P, Petrig B. Autoregulation of human optic nerve head blood flow in response to acute changes in ocular perfusion pressure. *Graefes Archive for Clinical and Experimental Ophthalmology*. 1997;235(10):618-626.
60. Riva CE, Pournaras CJ, Tsacopoulos M. Regulation of local oxygen tension and blood flow in the inner retina during hyperoxia. *J Appl Physiol*. 1986;61(2):592-598.
61. Eperon G, Johnson M, David NJ. The effect of arterial PO₂ on relative retinal blood flow in monkeys. *Investigative Ophthalmology & Visual Science*. 1975;14(5):342-352.
62. Kiss B, Polska E, Dorner G, et al. Retinal blood flow during hyperoxia in humans revisited: Concerted results using different measurement techniques. *Microvasc Res*. 2002;64(1):75-85.
63. Fallon TJ, Maxwell D, Kohner EM. Retinal vascular autoregulation in conditions of hyperoxia and hypoxia using the blue field entoptic phenomenon. *Ophthalmology*. 1985;92(5):701-705.
64. Jean-Louis S, Lovasik JV, Kergoat H. Systemic hyperoxia and retinal vasomotor responses. *Invest Ophthalmol Visual Sci*. 2005;46(5):1714-1720.
65. Riva CE, Grunwald JE, Sinclair SH. Laser doppler velocimetry study of the effect of pure oxygen breathing on retinal blood flow. *Invest Ophthalmol Visual Sci*. 1983;24(1):47-51.
66. Langhans M, Michelson G, Groh MJM. Effect of breathing 100% oxygen on retinal and optic nerve head capillary blood flow in smokers and non-smokers. *Br J Ophthalmol*. 1997;81(5):365-369.
67. Brazitikos PD, Pournaras CJ, Munoz J-, Tsacopoulos M. Microinjection of L-lactate in the preretinal vitreous induces segmental vasodilation in the inner retina of miniature pigs. *Invest Ophthalmol Visual Sci*. 1993;34(5):1744-1752.

68. Pournaras C, Tsacopoulos M, Chauis Ph. Studies on the role of prostaglandins in the regulation of retinal blood flow. *Exp Eye Res.* 1978;26(6):687-697.
69. Nagaoka T, Sakamoto T, Mori F, Sato E, Yoshida A. The effect of nitric oxide on retinal blood flow during hypoxia in cats. *Invest Ophthalmol Visual Sci.* 2002;43(9):3037-3044.
70. Pournaras CJ, Rungger-Brändle E, Riva CE, Hardarson SH, Stefansson E. Regulation of retinal blood flow in health and disease. *Prog Retin Eye Res.* 2008;27(3):284-330.
71. Muir E, Hamkin EW. **A clinical approach to the interpretation of arterial blood gases.** *Acute Care Perspectives.* 2002;11(1):5-14.
72. Allen K. Four-step method of interpreting arterial blood gas analysis. *Nurs Times.* 2005;101(1):42-45.
73. Forstermann U, Hertting G, Neufang B. The role of endothelial and non-endothelial prostaglandins in the relaxation of isolated blood vessels of the rabbit induced by acetylcholine and bradykinin. *Br J Pharmacol.* 1986;87(3):521-532.
74. Haefliger IO, Flammer J, Bény J-, Lüscher TF. Endothelium-dependent vasoactive modulation in the ophthalmic circulation. *Prog Retin Eye Res.* 2001;20(2):209-225.
75. Palmer RMJ, Ashton DS, Moncada S. Vascular endothelial cells synthesize nitric oxide from L-arginine. *Nature.* 1988;333(6174):664-666.
76. Haefliger IO, Flammer J, Luscher TF. Nitric oxide and endothelin-1 are important regulators of human ophthalmic artery. *Invest Ophthalmol Visual Sci.* 1992;33(7):2340-2343.
77. Benedito S, Prieto D, Nielsen PJ, Berg Nyborg NC. Role of the endothelium in acetylcholine-induced relaxation and spontaneous tone of bovine isolated retinal small arteries. *Exp Eye Res.* 1991;52(5):575-579.

78. Haefliger IO, Meyer P, Flammer J, Lüscher TF. The vascular endothelium as a regulator of the ocular circulation: A new concept in ophthalmology?. *Surv Ophthalmol*. 1994;39(2):123-132.
79. Benedito S, Prieto D, Nielsen PJ, Nyborg NCB. Histamine induces endothelium-dependent relaxation of bovine retinal arteries. *Invest Ophthalmol Visual Sci*. 1991;32(1):32-38.
80. De Mey JG, Vanhoutte PMV. Anoxia and endothelium-dependent reactivity of the canine femoral artery. *J Physiol (Lond)*. 1983;Vol. 335:65-74.
81. Pohl U, Holtz J, Busse R, Bassenge E. Crucial role of endothelium in the vasodilator response to increased flow in vivo. *Hypertension*. 1986;8(1):37-44.
82. Gilmore ED. *Retinal blood flow and vascular reactivity in diabetic retinopathy*. [Doctor of Philosophy]. University of Waterloo; 2006.
83. Moncada S, Vane JR. Pharmacology and endogenous roles of prostaglandin endoperoxides, thromboxane A₂, and prostacyclin. *Pharmacol Rev*. 1978;30(3):293-331.
84. Chesterman CN. Vascular endothelium, haemostasis and thrombosis. *Blood Rev*. 1988;2(2):88-94.
85. Inoue A, Yanagisawa M, Kimura S, et al. The human endothelin family: Three structurally and pharmacologically distinct isopeptides predicted by three separate genes. *Proc Natl Acad Sci U S A*. 1989;86(8):2863-2867.
86. Withrington PG, De Nucci G, Vane JR. Endothelin-1 causes vasoconstriction and vasodilation in the blood perfused liver of the dog. *J Cardiovasc Pharmacol*. 1989;13(SUPPL. 5):S209-S210.
87. Schaller BJ. The role of endothelin in stroke: Experimental data and underlying pathophysiology. *Archives of Medical Science*. 2006;2(3):146-158.

88. Arai H, Hori S, Aramori I, Ohkubo H, Nakanishi S. Cloning and expression of a cDNA encoding an endothelin receptor. *Nature*. 1990;348(6303):730-732.
89. Harris A, Arend O, Wolf S, Cantor LB, Martin BJ. CO₂ dependence of retinal arterial and capillary blood velocity. *Acta Ophthalmol Scand*. 1995;73(5):421-424.
90. Mather KJ, Lteif A, Steinberg HO, Baron AD. Interactions between endothelin and nitric oxide in the regulation of vascular tone in obesity and diabetes. *Diabetes*. 2004;53(8):2060-2066.
91. Morawietz H, Talanow R, Szibor M, et al. Regulation of the endothelin system by shear stress in human endothelial cells. *J Physiol (Lond)*. 2000;525(3):761-770.
92. Schmetterer L, Findl O, Strenn K, et al. Effects of endothelin-1 (ET-1) on ocular hemodynamics. *Curr Eye Res*. 1997;16(7):687-692.
93. Haefliger IO, Flammer J, Luscher TF. Heterogeneity of endothelium-dependent regulation in ophthalmic and ciliary arteries. *Invest Ophthalmol Visual Sci*. 1993;34(5):1722-1730.
94. Meyer P, Flammer J, Luscher TF. Endothelium-dependent regulation of the ophthalmic microcirculation in the perfused porcine eye: Role of nitric oxide and endothelins. *Invest Ophthalmol Visual Sci*. 1993;34(13):3614-3621.
95. Kurihara H, Yazaki Y. Regulation of vascular tone. In: Haber E., ed. *Molecular Cardiovascular Medicine*. Scientific American, Inc.; 1995:275-288.
96. Orgül S, Gugleta K, Flammer J. Physiology of perfusion as it relates to the optic nerve head. *Surv Ophthalmol*. 1999;43(6 SUPPL.):S17-S26.
97. Huang D, Swanson EA, Lin CP, et al. Optical coherence tomography. *Science*. 1991;254(5035):1178-1181.

98. Huang D, Swanson EA, Lin CP, et al. Optical coherence tomography. *Science*. 1991;254(5035):1178-1181.
99. Drexler W, Morgner U, Kärtner FX, et al. In vivo ultrahigh-resolution optical coherence tomography. *Opt Lett*. 1999;24(17):1221-1223.
100. Boppart SA, Bouma BE, Pitris C, Tearney GJ, Fujimoto JG, Brezinski ME. Forward-imaging instruments for optical coherence tomography. *Opt Lett*. 1997;22(21):1618-1620.
101. Tearney GJ, Bouma BE, Fujimoto JG. High-speed phase- and group-delay scanning with a grating-based phase control delay line. *Opt Lett*. 1997;22(23):1811-1813.
102. Hee MR, Baumal CR, Puliafito CA, et al. Optical coherence tomography of age-related macular degeneration and choroidal neovascularization. *Ophthalmology*. 1996;103(8):1260-1270.
103. Hee MR, Puliafito CA, Wong C, et al. Optical coherence tomography of macular holes. *Ophthalmology*. 1995;102(5):748-756.
104. Puliafito CA, Hee MR, Lin CP, et al. Imaging of macular diseases with optical coherence tomography. *Ophthalmology*. 1995;102(2):217-229.
105. Schuman JS, Hee MR, Arya AV, et al. Optical coherence tomography: A new tool for glaucoma diagnosis. *Curr Opin Ophthalmol*. 1995;6(2):89-95.
106. Schuman JS, Hee MR, Puliafito CA, et al. Quantification of nerve fiber layer thickness in normal and glaucomatous eyes using optical coherence tomography: A pilot study. *Arch Ophthalmol*. 1995;113(5):586-596.
107. Li T, May RG, Wang A, Claus RO. Optical scanning extrinsic fabry-perot interferometer for absolute microdisplacement measurement. *Appl Opt*. 1997;36(34):8858-8861.

108. Fercher AF, Hitzenberger CK, Kamp G, El-Zaiat SY. Measurement of intraocular distances by backscattering spectral interferometry. *Opt Commun*. 1995;117(1-2):43-48.
109. Tomlins PH, Wang RK. Theory, developments and applications of optical coherence tomography. *J Phys D*. 2005;38(15):2519-2535.
110. Ramos JLB, Li Y, Huang D. Clinical and research applications of anterior segment optical coherence tomography - A review. *Clinical and Experimental Ophthalmology*. 2009;37(1):81-89.
111. Sakata LM, DeLeon-Ortega J, Sakata V, Girkin CA. Optical coherence tomography of the retina and optic nerve - A review. *Clinical and Experimental Ophthalmology*. 2009;37(1):90-99.
112. Huang D. OCT terminology - demystified!. *Ophthalmology Management*. PentaVision. 2009
113. Choma MA, Sarunic MV, Yang C, Izatt JA. Sensitivity advantage of swept source and fourier domain optical coherence tomography. *Optics Express*. 2003;11(18):2183-2189.
114. Leitgeb R, Hitzenberger CK, Fercher AF. Performance of fourier domain vs. time domain optical coherence tomography. *Optics Express*. 2003;11(8):889-894.
115. Riva CE, Grunwald JE, Sinclair SH, Petrig BL. Blood velocity and volumetric flow rate in human retinal vessels. *Invest Ophthalmol Visual Sci*. 1985;26(8):1124-1132.
116. Bill A. Quantitative determination of uveal blood flow in rabbits. *Acta Physiol Scand*. 1962;55:101-110.
117. Pournaras CJ, Riva CE. Retinal blood flow evaluation. *Ophthalmologica*. 2013;229(2):61-74.
118. Riva CE, Alm A, Pournaras CJ. Ocular circulation. In: *Adler's Physiology of the Eye, 11th Edition*. 11th ed. Elsevier; 2011:243-266.

119. Delori FC, Fitch KA, Feke GT, Deupree DM, Weiter JJ. Evaluation of micrometric and microdensitometric methods for measuring the width of retinal vessel images on fundus photographs. *Graefes Archive for Clinical and Experimental Ophthalmology*. 1988;226(4):393-399.
120. Rassam SMB, Patel V, Brinchmann-Hansen O, Engvold O, Kohner EM. Accurate vessel width measurement from fundus photographs: A new concept. *Br J Ophthalmol*. 1994;78(1):24-29.
121. Pache M, Nagel E, Flammer J. Reproducibility of measurements with the retinal vessel analyzer under optimal conditions. *Klin Monatsbl Augenheilkd*. 2002;219(7):523-527.
122. Nagel E, Münch K, Vilser W. Measurement of the diameter of segments of retinal branch vessels in digital fundus images - an experimental study of the method and reproducibility. *Klin Monatsbl Augenheilkd*. 2001;218(9):616-620.
123. Garhofer G, Bek T, Boehm AG, et al. Use of the retinal vessel analyzer in ocular blood flow research. *Acta Ophthalmol*. 2010;88(7):717-722.
124. Riva CE, Feke GT, Ben-Sira I. Fluorescein dye-dilution technique and retinal circulation. *Am J Physiol*. 1978;234(3):H315-322.
125. Riva CE, Ben Sira I. Injection method for ocular hemodynamic studies in man. *Invest Ophthalmol*. 1974;13(1):77-79.
126. MEIER P, ZIERLER KL. On the theory of the indicator-dilution method for measurement of blood flow and volume. *J Appl Physiol*. 1954;6(12):731-744.
127. Wolf S, Arend O, Reim M. Measurement of retinal hemodynamics with scanning laser ophthalmoscopy: Reference values and variation. *Surv Ophthalmol*. 1994;38(SUPPL. 1):S95-S100.
128. Kohner EM. The problems of retinal blood flow in diabetes. *Diabetes*. 1976;25(SUP.2):839-844.

129. Riva CE, Petrig BL. Retinal blood flow: Laser doppler velocimetry and blue field simulation technique. In: Masters BR, ed. *Noninvasive Diagnostic Techniques in Ophthalmology*. New York: New York : Springer-Verlag; 1990:390.
130. Loebel M, Riva CE. Macular circulation and the flying corpuscles phenomenon. *Ophthalmology*. 1978;85(9):911-917.
131. Martin JA, Roorda A. Direct and noninvasive assessment of parafoveal capillary leukocyte velocity. *Ophthalmology*. 2005;112(12):2219-2224.
132. Goodman JW. Statistical properties of laser speckle patterns. In: New York: Springer-Verlag, ed. *Laser Speckle and Related Phenomenon*. ; 1875:9-75.
133. Fujii H, Nohira K, Yamamoto Y, Ikawa H, Ohura T. Evaluation of blood flow by laser speckle image sensing part 1. *Applied Optics*. 1987;26(24).
134. Briers JD, Fercher AF. Retinal blood-flow visualization by means of laser speckle photography. *Invest Ophthalmol Visual Sci*. 1982;22(2):255-259.
135. Tamaki Y, Araie M, Kawamoto E, Eguchi S, Fujii H. Noncontact, two-dimensional measurement of retinal microcirculation using laser speckle phenomenon. *Invest Ophthalmol Visual Sci*. 1994;35(11):3825-3834.
136. Strenn K, Menapace R, Rainer G, Findl O, Wolzt M, Schmetterer L. Reproducibility and sensitivity of scanning laser doppler flowmetry during graded changes in Po₂. *Br J Ophthalmol*. 1997;81(5):360-364.
137. Riva CE, Grunwald JE, Sinclair SH, O'Keefe K. Fundus camera based retinal LDV. *Appl Opt*. 1981;20(1):117-120.

138. Riva CE, Grunwald JE, Sinclair SH, O'Keefe K. Fundus camera based retinal LDV. *Appl Opt.* 1981;20(1):117-120.
139. Wang Y, Lu A, Gil-Flamer J, Tan O, Izatt JA, Huang D. Measurement of total blood flow in the normal human retina using doppler fourier-domain optical coherence tomography. *Br J Ophthalmol.* 2009;93(5):634-637.
140. Arend O, Remky A, Cantor LB, Harris A. Altitudinal visual field asymmetry is coupled with altered retinal circulation in patients with normal pressure glaucoma. *Br J Ophthalmol.* 2000;84(9):1008-1012.
141. Riva CE, Grunwald JE, Sinclair SH, Petrig BL. Blood velocity and volumetric flow rate in human retinal vessels. *Invest Ophthalmol Visual Sci.* 1985;26(8):1124-1132.
142. Sehi M, Tsui E, Cheng R, et al. Relative magnitude of vascular reactivity in the major arterioles of the retina. *Microvasc Res.* 2012;83(2):200-204.
143. Williamson TH, Harris A. Color doppler ultrasound imaging of the eye and orbit. *Surv Ophthalmol.* 1996;40(4):255-267.
144. Izatt JA, Kulkarni MD, Yazdanfar S, Barton JK, Welch AJ. In vivo bidirectional color doppler flow imaging of picoliter blood volumes using optical coherence tomography. *Opt Lett.* 1997;22(18):1439-1441.
145. Zhao Y, Chen Z, Saxer C, Xiang S, De Boer JF, Nelson JS. Phase-resolved optical coherence tomography and optical doppler tomography for imaging blood flow in human skin with fast scanning speed and high velocity sensitivity. *Opt Lett.* 2000;25(2):114-116.
146. Wang Y, Bower BA, Izatt JA, Tan O, Huang D. Retinal blood flow measurement by circumpapillary fourier domain doppler optical coherence tomography. *J Biomed Opt.* 2008;13(6).

147. Konduru RK, Tan O, Nittala MG, Huang D, Sadda SR. Reproducibility of retinal blood flow measurements derived from semi-automated doppler OCT analysis. *Ophthalmic Surgery Lasers and Imaging*. 2012;43(1):25-31.
148. Riva CE, Harino S, Petrig BL, Shonat RD. Laser doppler flowmetry in the optic nerve. *Exp Eye Res*. 1992;55(3):499-506.
149. Michelson G. Principle, validity, and reliability of scanning laser doppler flowmetry. *J Glaucoma*. 1996;5(2):99-105.
150. *Medical Physiology*. Philadelphia: Philadelphia : Lippincott Williams & Wilkins; 2003.
151. Bengtsson J, Bake B, Johansson Å, Bengtson JP. End-tidal to arterial oxygen tension difference as an oxygenation index. *Acta Anaesthesiol Scand*. 2001;45(3):357-363.
152. Kent M. *The Oxford Dictionary of Sports Science & Medicine*. 3rd ed. Oxford University Press; 2006.
153. Geirsdottir A, Palsson O, Hardarson SH, Olafsdottir OB, Kristjansdottir JV, Stefánsson E. Retinal vessel oxygen saturation in healthy individuals. *Invest Ophthalmol Vis Sci*. 2012;53(9):5433-5442.
154. Sebag J, Delori FC, Feke GT, Weiter JJ. Effects of optic atrophy on retinal blood flow and oxygen saturation in humans. *Arch Ophthalmol*. 1989;107(2):222-226.
155. Assendelft OWV, Thomas CC. *Spectrophotometry of Haemoglobin Derivatives*. III ed. Springfield, IL: ; 1970.
156. Alabboud I. *Human retinal oxymetry using hyperspectral imaging*. [Doctor of Philosophy]. Heriot Watt University; 2009.
157. Mordant DJ, Al-Abboud I, Muyo G, et al. Spectral imaging of the retina. *Eye*. 2011;25(3):309-320.

158. Tremper KK, Barker SJ. Pulse oximetry. *Anesthesiology*. 1989;70(1):98-108.
159. Kagemann J, Larry E., Wollstein G, Wojtkowski M, et al. Spectral oximetry assessed with high-speed ultra-high-resolution optical coherence tomography. *J Biomed Opt*. 2007;12(4):041212. doi: 10.1117/12.773029.
160. Schweitzer D, Guenther S, Scibor M, Hammer M. Spectrometric investigations in ocular hypertension and early stages of primary open angle glaucoma and of low tension glaucoma - multisubstance analysis. *Int Ophthalmol*. 1992;16(4-5):251-257.
161. Smith MH, R.deiminghoff K, Hillman LW, Chipman RA. Oxygen saturation measurements of blood in retinal vessels during blood loss. *J Biomed Opt*. 1998;3(3):296-303.
162. Johnson WR, Wilson DW, Fink W, Humayun M, Bearman G. Snapshot hyperspectral imaging in ophthalmology. *J Biomed Opt*. 2007;12(1).
163. Yoneya S, Saito T, Nishiyama Y, et al. Retinal oxygen saturation levels in patients with central retinal vein occlusion. *Ophthalmology*. 2002;109(8):1521-1526.
164. Pittman RN, Duling BR. A new method for the measurement of percent oxyhemoglobin. *J Appl Physiol*. 1975;38(2):315-320.
165. Pittman RN, Duling BR. Measurement of percent oxyhemoglobin in the microvasculature. *J Appl Physiol*. 1975;38(2):321-327.
166. Khoobehi B, Beach JM, Kawano H. Hyperspectral imaging for measurement of oxygen saturation in the optic nerve head. *Invest Ophthalmol Visual Sci*. 2004;45(5):1464-1472.
167. Beach JM, Ning J, Khoobehi B. Hyperspectral algorithm for mapping tissue oxygen saturation. *Proceedings of the 7th Nordic Signal Processing Symposium, NORSIG 2006*. 2007:142-145.

168. Hardarson SH, Harris A, Karlsson RA, et al. Automatic retinal oximetry. *Invest Ophthalmol Visual Sci*. 2006;47(11):5011-5016.
169. Gloster J. Fundus oximetry. *Exp Eye Res*. 1967;6(3):187-212.
170. Delori FC, Gragoudas ES, Francisco R, Pruett RC. Monochromatic ophthalmoscopy and fundus photography. the normal fundus. *Arch Ophthalmol*. 1977;95(5):861-868.
171. Harvey AR, Lawlor J, McNaught AI, Williams JW, Fletcher-Holmes DW. Hyperspectral imaging for the detection of retinal diseases. *Proceedings of SPIE - The International Society for Optical Engineering*. 2002;4816:325-335.
172. Photon etc. www.photonetc.com/EN/APPLICATIONA/Health/Retinal_Imaging-78. Accessed 09/26, 2012.
173. Hammer M, Vilser W, Riemer T, et al. Retinal venous oxygen saturation increases by flicker light stimulation. *Invest Ophthalmol Visual Sci*. 2011;52(1):274-277.
174. Becker HF, Polo O, Mcnamara SG, Berthon-Jones M, Sullivan CE. Effect of different levels of hyperoxia on breathing in healthy subjects. *J Appl Physiol*. 1996;81(4):1683-1690.
175. Siesky B, Harris A, Kagemann L, et al. Ocular blood flow and oxygen delivery to the retina in primary open-angle glaucoma patients: The addition of dorzolamide to timolol monotherapy. *Acta Ophthalmol*. 2010;88(1):142-149.
176. Chung HS, Harris A, Kagemann L, Martin B. Peripapillary retinal blood flow in normal tension glaucoma. *Br J Ophthalmol*. 1999;83(4):466-469.

177. Harris A, Arend O, Kopecky K, et al. Physiological perturbation of ocular and cerebral blood flow as measured by scanning laser ophthalmoscopy and color doppler imaging. *Surv Ophthalmol.* 1994;38(SUPPL. 1):S81-S86.
178. Drexler W, Fujimoto JG. State-of-the-art retinal optical coherence tomography. *Prog Retin Eye Res.* 2008;27(1):45-88.
179. Slessarev M, Han J, Mardimae A, et al. Prospective targeting and control of end-tidal CO₂ and O₂ concentrations. *J Physiol (Lond)*. 2007;581(3):1207-1219.
180. Fong AY, Wachman E. Hyperspectral imaging for the life sciences. *Biophoton Int.* 2008;15(3):38-41.
181. Kagemann L, Harris A, Chung HS, Evans D, Buck S, Martin B. Heidelberg retinal flowmetry: Factors affecting blood flow measurement. *Br J Ophthalmol.* 1998;82(2):131-136.
182. Laing RA, Cohen AJ, Friedman E. Photographic measurements of retinal blood oxygen saturation: Falling saturation rabbit experiments. *Invest Ophthalmol.* 1975;14(8):606-610.
183. Crittin M, Schmidt H, Riva CE. Hemoglobin oxygen saturation (So₂) in the human ocular fundus measured by reflectance oximetry: Preliminary data in retinal veins. *Klin Monatsbl Augenheilkd.* 2002;219(4):289-291.
184. Hardarson SH, Stefánsson E. Oxygen saturation in branch retinal vein occlusion. *Acta Ophthalmol.* 2011.
185. Schweitzer D, Lasch A, Van Der Vorst S, et al. Change of retinal oxygen saturation in healthy subjects and in early stages of diabetic retinopathy during breathing of 100% oxygen. *Klin Monatsbl Augenheilkd.* 2007;224(5):402-410.

186. Hardarson SH, Stefánsson E. Retinal oxygen saturation is altered in diabetic retinopathy. *Br J Ophthalmol*. 2012;96(4):560-563.
187. Hammer M, Vilser W, Riemer T, et al. Diabetic patients with retinopathy show increased retinal venous oxygen saturation. *Graefe's Archive for Clinical and Experimental Ophthalmology*. 2009;247(8):1025-1030.
188. Michelson G, Scibor M. Intravascular oxygen saturation in retinal vessels in normal subjects and open-angle glaucoma subjects. *Acta Ophthalmol Scand*. 2006;84(3):289-295. doi: 10.1111/j.1600-0420.2005.00631.x.
189. Traustason S, Hardarson SH, Gottfredsdottir MS, et al. Dorzolamide-timolol combination and retinal vessel oxygen saturation in patients with glaucoma or ocular hypertension. *Br J Ophthalmol*. 2009;93(8):1064-1067.
190. Smith MH. Optimum wavelength combinations for retinal vessel oximetry. *Appl Opt*. 1999;38(1):258-267.
191. Delori FC, P., Delori FC, Pflibsen KP. Spectral reflectance of the human ocular fundus. *Appl Opt*. ;28(6):1061.
192. Van Norren D, Tiemeijer LF. Spectral reflectance of the human eye. *Vision Res*. 1986;26(2):313-320.
193. Palkovits S, Lasta M, Boltz A, et al. Measurement of retinal oxygen saturation in patients with chronic obstructive pulmonary disease. *Invest Ophthalmol Visual Sci*. 2013;54(2):1008-1013.
194. Cohen AJ, Laing RA. Multiple scattering analysis of retinal blood oximetry. *IEEE Transactions on Biomedical Engineering*. 1976;23(5):391-400.

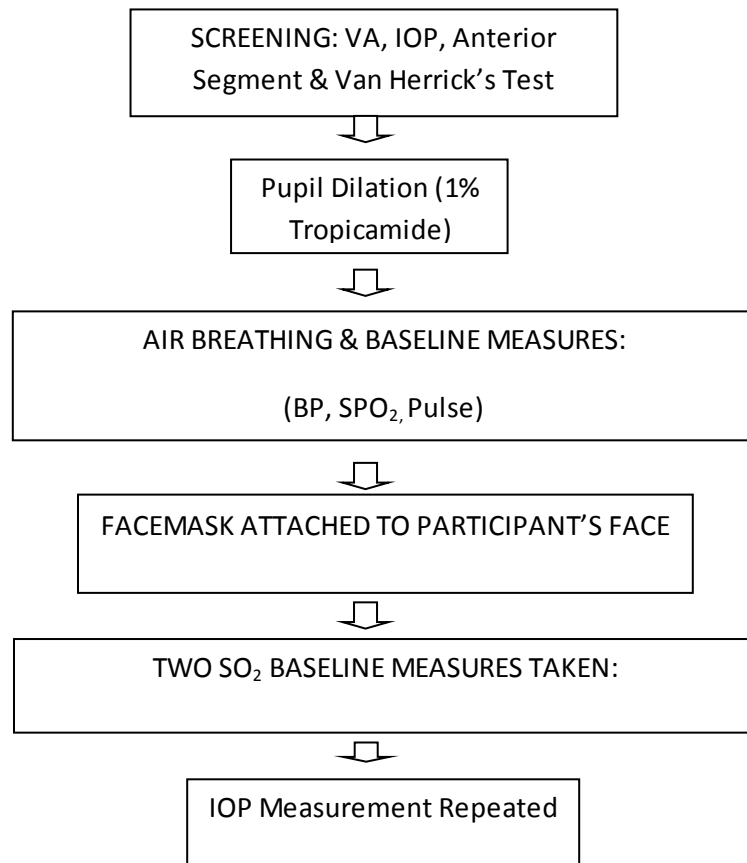
195. Tiedeman JS, Kirk SE, Srinivas S, Beach JM. Retinal oxygen consumption during hyperglycemia in patients with diabetes without retinopathy. *Ophthalmology*. 1998;105(1):31-36.
196. Geeraets WJ, Berry ER. Ocular spectral characteristics as related to hazards from lasers and other light sources. *Am J Ophthalmol*. 1968;66(1):15-20.
197. Sehi M, Tsui E, Cheng R, et al. Relative magnitude of vascular reactivity in the major arterioles of the retina. *Microvasc Res*. 2012;83(2):200-204.
198. Slessarev M, Somogyi R, Preiss D, Vesely A, Sasano H, Fisher JA. Efficiency of oxygen administration: Sequential gas delivery versus "flow into a cone" methods. *Crit Care Med*. 2006;34(3):829-834.
199. Hardarson SH, Basit S, Jonsdottir TE, et al. Oxygen saturation in human retinal vessels is higher in dark than in light. *Invest Ophthalmol Visual Sci*. 2009;50(5):2308-2311.
200. Traustason S, Jensen AS, Arvidsson HS, Munch IC, Sondergaard L, Larsen M. Retinal oxygen saturation in patients with systemic hypoxemia. *Investigative ophthalmology & visual science*. 2011;52(8):5064-5067.
201. Traustason S, Kiilgaard JF, Karlsson RA, Hardarson SH, Stefansson E, la Cour M. Spectrophotometric retinal oximetry in pigs. *Invest Ophthalmol Visual Sci*. 2013;54(4):2746-2751.
202. Kristjansdottir JV, Hardarson SH, Harvey AR, Olafsdottir OB, Eliasdottir TS, Stefansson E. Choroidal oximetry with a noninvasive spectrophotometric oximeter. *Invest Ophthalmol Visual Sci*. 2013;54(5):3234-3239.
203. Hammer M, Vilser W, Riemer T, Schweitzer D. Retinal vessel oximetry-calibration, compensation for vessel diameter and fundus pigmentation, and reproducibility. *J Biomed Opt*. 2008;13(5).

204. Lasta M, Palkovits S, Boltz A, et al. Reproducibility of retinal vessel oxygen saturation measurements in healthy young subjects. *Acta Ophthalmol.* 2012;90(8):e616-e620.
205. Shahidi AM, Patel SR, Flanagan JG, Hudson C. Regional variation in human retinal vessel oxygen saturation. *Exp Eye Res.* 2013;113(0):143-147. doi: <http://dx.doi.org/10.1016/j.exer.2013.06.001>.
206. *Understanding Continuous Mixed Venous Oxygen Saturation Monitoring with the Swan-Ganz Oximetry TD System.* 2nd ed. Edwards Lifesciences; 2002.
207. Harris A, Arend O, Kopecky K, et al. Physiological perturbation of ocular and cerebral blood flow as measured by scanning laser ophthalmoscopy and color doppler imaging. *Surv Ophthalmol.* 1994;38(SUPPL. 1):S81-S86.
208. Frayser R, Gray GW, Houston CS. Control of the retinal circulation at altitude. *J Appl Physiol.* 1974;37(3):302-304.
209. la Cour M, Kiilgaard JF, Eysteinnsson T, et al. Optic nerve oxygen tension: Effects of intraocular pressure and dorzolamide. *Br J Ophthalmol.* 2000;84(9):1045-1049.
210. Bach Pedersen D, Koch Jensen P, la Cour M, et al. Carbonic anhydrase inhibition increases retinal oxygen tension and dilates retinal vessels. *Graefe's Archive for Clinical and Experimental Ophthalmology.* 2005;243(2):163-168.
211. Siesky B, Harris A, Cantor LB, et al. A comparative study of the effects of brinzolamide and dorzolamide on retinal oxygen saturation and ocular microcirculation in patients with primary open-angle glaucoma. *Br J Ophthalmol.* 2008;92(4):500-504.
212. Wang Y, Bower BA, Izatt JA, Tan O, Huang D. In vivo total retinal blood flow measurement by fourier domain doppler optical coherence tomography. *J Biomed Opt.* 2007;12(4).

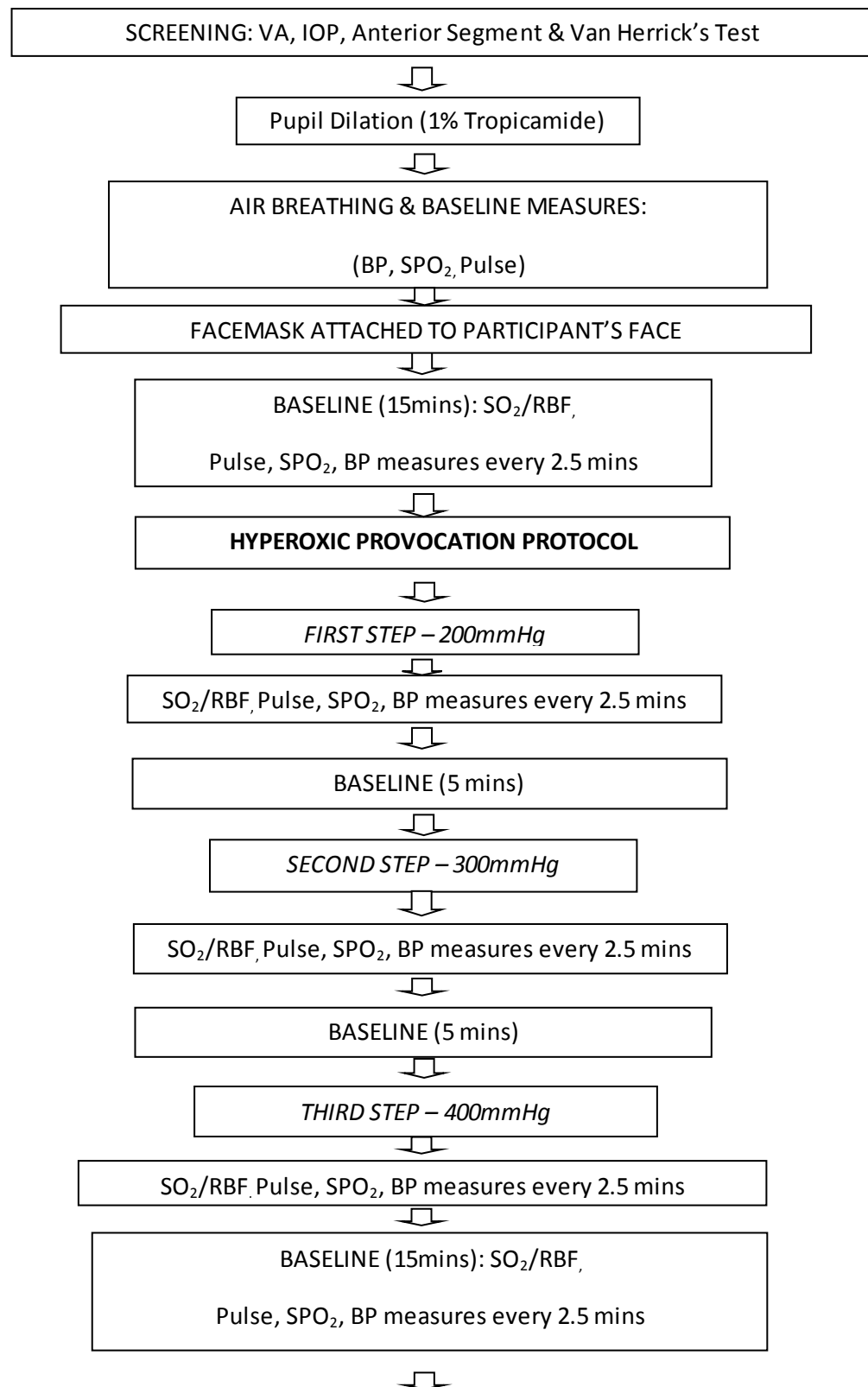
213. Wang Y, Bower BA, Izatt JA, Tan O, Huang D. Retinal blood flow measurement by circumpapillary fourier domain doppler optical coherence tomography. *J Biomed Opt.* 2008;13(6).
214. Wang Y, Fawzi A, Tan O, Gil-Flamer J, Huang D. Retinal blood flow detection in diabetic patients by doppler fourier domain optical coherence tomography. *Optics Express.* 2009;17(5):4061-4073.
215. Wang Y, Fawzi AA, Varma R, et al. Pilot study of optical coherence tomography measurement of retinal blood flow in retinal and optic nerve disease s. *Invest Ophthalmol Visual Sci.* 2011;52(2):840-845.
216. Werkmeister RM, Dragostinoff N, Palkovits S, et al. Measurement of absolute blood flow velocity and blood flow in the human retina by dual-beam bidirectional doppler fourier-domain optical coherence tomography. *Invest Ophthalmol Visual Sci.* 2012;53(10):6062-6071.
217. Wehbe H, Ruggeri M, Jiao S, Gregori G, Puliafito CA, Zhao W. Automatic retinal blood flow calculation using spectral domain optical coherence tomography. *Optics Express.* 2007;15(23):15193-15206.
218. Leitgeb RA, Schmetterer L, Drexler W, Fercher AF, Zawadzki RJ, Bajraszewski T. Real-time assessment of retinal blood flow with ultrafast acquisition by color doppler fourier domain optical coherence tomography. *Optics Express.* 2003;11(23):3116-3121.
219. Tan O, Wang Y, Konduru RK, Zhang X, Sadda SR, Huang D. Doppler optical coherence tomography of retinal circulation. *Journal of Visualized Experiments.* 2012(67).
220. Linsenmeier RA, Yancey CM. Effects of hyperoxia on the oxygen distribution in the intact cat retina. *Invest Ophthalmol Visual Sci.* 1989;30(4):612-618.
221. Pournaras CJ, Riva CE, Tsacopoulos M, Strommer K. Diffusion of O₂ in the retina of anesthetized miniature pigs in normoxia and hyperoxia. *Exp Eye Res.* 1989;49(3):347-360.

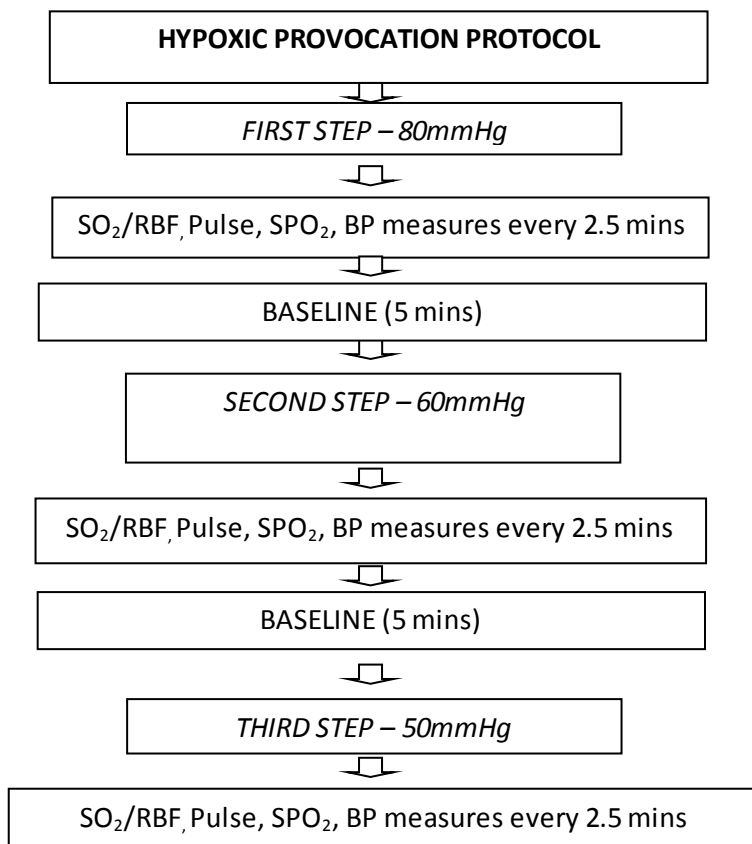
222. Wolbarsht ML, Stefansson E, Landers 3rd. MB. Retinal oxygenation from the choroid in hyperoxia.
Exp Biol. 1987;47(1):49-52.

Appendix A: Optical Density Ratio (ODR) Variability with the Image Replicating Imaging Spectrometer (IRIS) Hyperspectral Retinal Camera (Photon etc. Inc. Montreal). Flow Chart of Procedures



Appendix B: Total Retinal Blood Flow and ODR with Gas Provocation Challenge in Healthy Participants. Flow Chart of Procedures





* Both provocation challenge protocols would be run for the HRC (SO₂) followed by the Doppler OCT (RBF). To allow for P_{ET}O₂ of 50mmHg to be reached, gas tanks would need to be changed; as such, both SO₂ and RBF will be taken with the HRC and Doppler OCT at the same time at this stage

Appendix C: Hyperoxia and Hypoxia Protocols

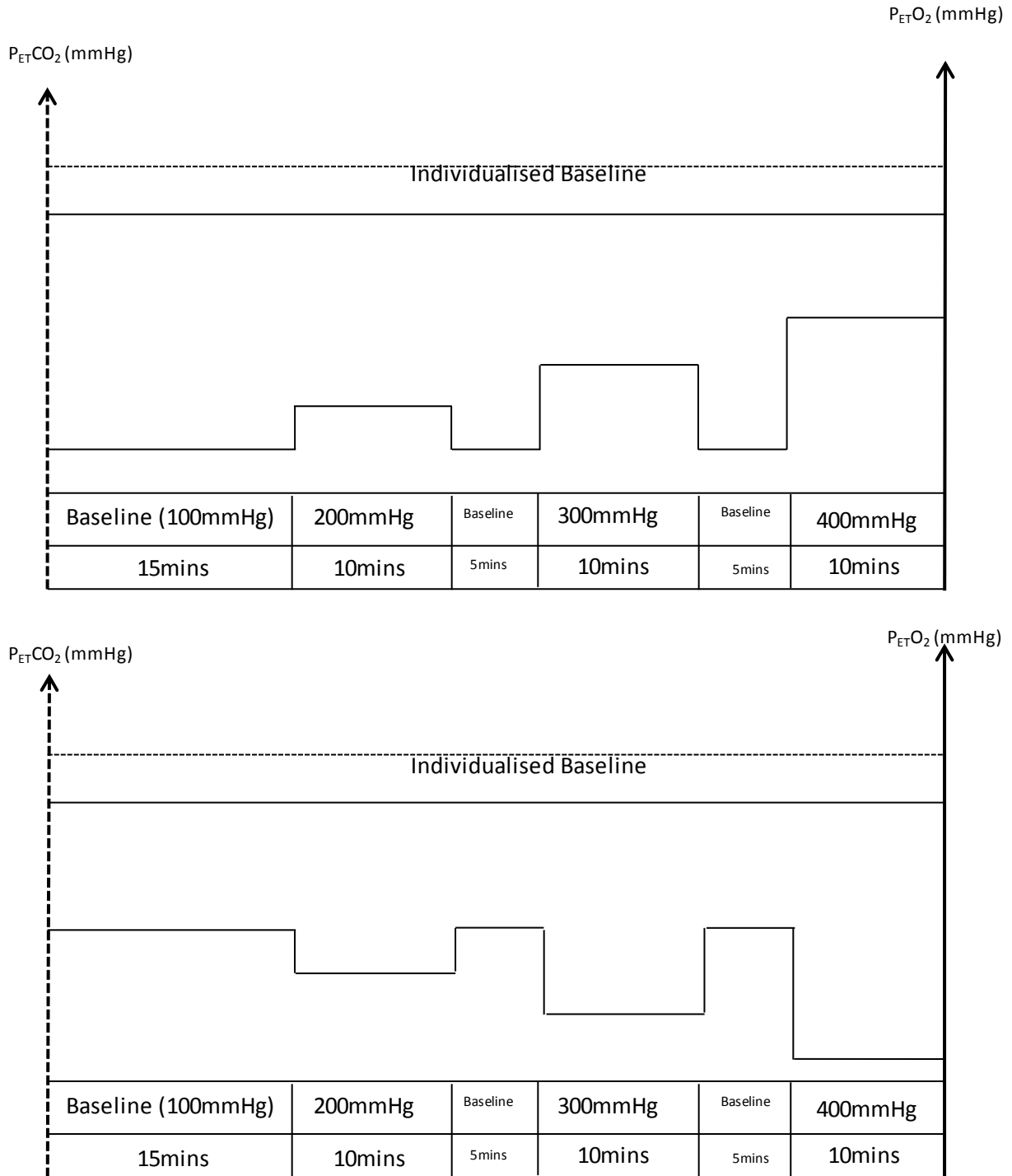


Figure 1.0 Hyperoxia protocol; $P_{ET}O_2$ of 100, 200, 300 and 400mmHg (Above) and hypoxia protocol; $P_{ET}O_2$ of 100, 80, 60 and 50mmHg (below) protocols. Three repeat measurements of TRBF and SO_2 were taken at each $P_{ET}O_2$ step.